Master's thesis

NTNU
Norwegian University of Science and Technology
Faculty of Medicine and Health Sciences
Department of Clinical and Molecular Medicine

Kamilla Isaksen Stortjønnli

Exploring drug resistance mechanisms in Multiple Myeloma - Focusing on the role of immunoglobulin kappa light chain and protein secretion

Master's thesis in Molecular Medicine
Supervisor: Kristine Misund and Ida Johansson
May 2019

NTNU
Norwegian University of Science and Technology

Kamilla Isaksen Stortjønnli

Exploring drug resistance mechanisms in Multiple Myeloma - Focusing on the role of immunoglobulin kappa light chain and protein secretion

Master's thesis in Molecular Medicine
Supervisor: Kristine Misund and Ida Johansson
May 2019

Norwegian University of Science and Technology
Faculty of Medicine and Health Sciences
Department of Clinical and Molecular Medicine

NTNU
Norwegian University of
Science and Technology

Abstract

Multiple myeloma (MM) is a type of cancer arising in the bone marrow affecting the immunoglobulin (Ig) producing plasma cells. This causes an uncontrolled proliferation of a single plasma cell clone and an overproduction of monoclonal Igs. MM is considered a rare type of cancer however it is one of the most common haematological malignancies and only about 50% of MM patients will survive 5 years or more. Which isotype of Ig that is produced varies among MM patients, with about 25% producing the IgA isotype and up to 20% of MM patients only producing the light chains of Igs, either as the kappa (IgK) or the lambda isotype. In the last two decades, introduction of novel treatment strategies such as proteasome inhibitors (PIs) have proven to be effective in MM therapy, providing good clinical results and longer survival of MM patients. Despite these advantages, intrinsic and acquired resistance against MM treatment have become a major challenge that eventually cause MM patients to relapse. MM is thus considered as an incurable cancer, and research trying to find new treatment strategies and to identify mechanisms of drug resistance are well under progress but are yet to be found. In this thesis, we first investigated the cytotoxic effects of targeting both the ubiquitin-proteasome system and autophagy in AMO-1 cells by using the autophagy inhibitor hydroxychloroquine (HCQ) in combination with the PIs, carfilzomib (CFZ) and bortezomib (BZ). We found significantly synergistic cytotoxicity in AMO-1 cells treated with the HCQ-CFZ-combination and that HCQ seemed to somewhat reverse CFZ resistance in CFZ adapted AMO-1 cells. No synergistic cytotoxic effects were seen for the HCQ-BZ combination. These results suggest an HCQ-CFZ-combination as a potential MM therapy strategy. MM patients only producing Ig light chains are often affected by renal failure due to free Ig light chains being secreted by the MM cells and lead to poorer prognosis. Thus, understanding how these Ig light chains are secreted is of great meaning and may also represent a novel resistance mechanism in MM. The autophagy receptor SQSTM1 has shown to be involved in the generation of protein aggregates of proteins marked for degradation, thus we investigated if SQSTM1 could have a role in the release of IgK from MM cells. In INA-6 cells, we found that SQSTM1 seemed to be released together with IgK in dense protein structures, most likely protein aggregates. However, it could not be proved that IgK release was SQSTM1-dependent. The protein expression level of IgK, SQSTM1 and the drug efflux pump MDR1 was detected in PI adapted MM cells and the results provides an insight to the complexity of drug resistance where PI adapted MM cell lines seemed to adapt differently to the PIs both between cell lines, but also depending on the PI used.

Acknowledgement

This master's thesis was conducted at the Centre for Myeloma Research, Department of Clinical and Molecular Medicine, Norwegian university of Science and Technology.

I would like to express my greatest appreciation to my supervisor, Kristine Misund, for her unblemished teaching and guidance during the planning and development of this thesis. I would also like to give a special thanks to my co-supervisor, Ida Johansson, for excellent help and patient guidance during this work. They have both been of great support and the willingness to generously give their time has been very much appreciated.

I also want to express my appreciation to the members of the myeloma and CEMIR group and I am very grateful for the assistance provided by Sonja Andersen, Unni Nonstad and Hanne Hella in the laboratory. Lastly, I would like to thank Geir Bjørkøy for the time and knowledge he has shared.

Kamilla Isaksen Stortjønnli

Kamilla Isaksen Stortjønnli Trondheim, May 2019

List of abbreviations

ABCB1	ATP-binding cassette sub-family B member 1
AID	Activation induced cytidine deaminase
ASCT	Autologous stem cell transplantation
ATF6	Activating transcription factor 6
Atg	Autophagy-related genes
ATP	Adenosine triphosphate
BafA1	Bafilomycin A1
BB	Binding buffer
BiP	Binding immunoglobulin protein
BM	Bone marrow
bp	Base pair
BSA	Bovine Serum Albumin
BZ	Bortezomib
ccdB	Control of cell death B
CCND1	Cyclin D1 gene
CCND3	Cyclin D3 gene
cDNA	Complementary DNA
CFZ	Carfilzomib
CHOP	CCAAT-enhancer-binding protein homologous protein
CMA	Chaperone-mediated autophagy
CmR	Chloramphenicol resistance
CNV	Copy number variants
CP	Core particle
C_q/C_t	Quantification cycle
CRISPR	Clustered Regularly Interspaced Short Palindromic Repeats
CSR	Class switch recombination
DMEM	Dulbecco's Modified Eagle Medium
DNA	Deoxyribonucleic acid
DTT	Dithiothreitol
DUB	Deubiquitinating enzyme
E1	Ubiquitin-activating enzyme
E2	Ubiquitin-conjugating enzyme
E3	Ubiquitin-ligating enzyme
EDTA	Ethylenediaminetetraacetic acid
ElF2	Eukaryotic Initiation Factor 2
EP-tube	Eppendorf tube
ER	Endoplasmic reticulum
ERAD	ER-associated degradation
Fab region	Fragment antigen binding region
Fc region	Fragment crystallizable region
FCS	Fetal calf serum
FDA	US Food and Drug Administration

FDC	Follicular dendritic cell
FITC	Fluorescein isothiocyanate
FLC	Free light chain
GABARAP	Gamma-amonibutyrate receptor-associated protein
GADD34	Growth arrest and DNA damage-inducible protein 34
GAPDH	Glyceraldehyde 3-phosphate dehydrogenase
GFP	Green fluorescent protein
gRNA	Guide RNA
HCQ	Hydroxychloroquine
HEK293T	Human Embryonic Kidney 293T
Ig	Immunoglobulin
IgH	Immunoglobulin heavy chain
IgK	Immunoglobulin kappa light chain
IMiDs	Immunomodulatory drugs
IL	Interleukin
IRE1	Inositol-requiring enzyme 1
JNK pathway	c-Jun N-terminal kinase pathway
kDa	Kilodaltons
KIR	Keap-interacting region
KO	Knockout
LAMP-2A	Lysosome-associated membrane protein 2
LB	Lysogeny broth
LDS	Lithium dodecyl sulphate
LIR	LC3 interacting region
MAP1LC3	Microtubule-associated proteins 1 light chain 3
MAPK	Mitogen-activated protein kinase
MDR1	Multidrug resistance transporter 1
MGUS	Monoclonal gammopathy of uncertain significance
MM	Multiple myeloma
MMSET/FGFR3	Multiple myeloma SET domain/Fibroblast growth factor receptor 3
MOPS	3-(N-morpholino) propanesulfonic acid
MQ-water	Milli-Q-Water
mRNA	Messenger RNA
NBR1	Next to BRCA1 gene 1 protein
NDP52	Nuclear domain 10 protein 52
NF-κB	Nuclear factor-κappa B
NP-40	Nonidet P40
NFE2L2	Nuclear Erythroid-Related factor 2
OPTN	Optineurin
PB1	Phox/Bem1
PBS	Phosphate-buffered saline
PC	Plasma cell
PCR	Polymerase Chain Reaction
PE	Phosphatidylethanolamine

PERK	Protein kinase RNA (PKR)-like ER kinase
PI	Proteasome inhibitor
PI/complete	Complete® protease inhibitor
PIC	Phosphatase inhibitor cocktail
PS	Phosphatidylserines
PSMB5	Proteasome subunit beta type-5
qRT-PCR	Quantitative real-time PCR
RIP	Receptor interacting protein
RLU	Relative luciferase units
RNA	Ribonucleic acid
RP	Regulatory particle
RPMI	Roswell Park Memorial Institute
S1P/S2P	Site-1&2 protease
SD	Standard deviation
SDS-PAGE	Sodium dodecyl sulphate–polyacrylamide gel electrophoresis
SEM	Standard Error of the Mean
SHM	Somatic hypermutation
SLC	Surrogate light chain
SMM	Smouldering multiple myeloma
SOC	Super Optimal broth with Catabolite repression
SQSTM1	Sequestosome 1
SV40	Simian Virus 40
TAE	Tris Acetate EDTA
TB domain	TRAF6-binding domain
TBS	Tris-buffered saline
TE buffer	Tris-EDTA buffer
T_{FH}-cell	Follicular helper T-cell
TRAF6	TNF receptor associated factor 6
TX100	TritonX-100
UBA	Ubiquitin binding adaptor
UPR	Unfolded protein response
UPS	Ubiquitin-proteasome system
V-ATPase	Vacuolic H^+-ATPase
V(D)J recombination	Variable-(diversity)-joining recombination
WB	Western blot
WT	Wild type
XBP1	X-box binding protein 1
ZnF	Zinc finger

Table of content

1.0 Introduction

1.1 General features, epidemiology and oncogenesis of Multiple Myeloma

Multiple myeloma (MM) is a type of cancer arising in the bone marrow (BM) affecting the immunoglobulin (Ig) producing plasma cells (PC). This entails an uncontrolled proliferation of one PC clone in the BM characterized by an overproduction of monoclonal Igs [1]. MM is often developed from monoclonal gammopathy of uncertain significance (MGUS) which is a non-cancerous presence of <3 g/dl serum M-protein (monoclonal Ig) and <10% clonal PCs in the BM with no other symptoms. The condition is mostly discovered incidentally and the annual risk of progressing to MM is 1%. Smoldering multiple myeloma (SMM) is also an asymptomatic disorder considered as a transitional phase from MGUS to symptomatic MM. SMM is characterized by a higher risk of progression to MM with an annual risk of 10% the first five years after diagnosis and is defined by a serum M-protein level of ≥3 g/dl and/or 10-60% clonal PC in the BM. Symptomatic MM is determined by the presence of one or more of the myeloma-related symptoms and/or myeloma-defining events, ≥10% clonal BM PCs or biopsy-proven bony or extramedullary plasmacytoma. The myeloma-related symptoms are characterized by end-organ damage such as renal insufficiency, anaemia, hypercalcemia and bone lesions [2, 3].

1.1.1 Epidemiology

Although considered a rare type of cancer, MM is one of the most common haematological malignancies and have an estimated number of 30 700 new cases in 2018 that accounts for about 1,8% of all new cancer cases in the U.S. [4]. According to the Cancer Registry of Norway, there was a total of 429 new cases of MM in 2016 which accounts for about 1,3% of all new cases of cancer that same year [5]. Of all the patients diagnosed with MM, only about 50% survive 5 years or more. The median age at diagnosis is 69 years, with 37% being younger than 65 years, 30% between 65 and 74 years and 33% are older than 74 years. MM is highly rare for people under 35 years of age and accounts for only 0,5% of new cases [4].

1.1.2 Oncogenesis

MM results from a series of chromosomal alterations that accumulate during B-cell maturation, as reviewed in [6-8]. Primary genetic events leading to MM can be divided into hyperdiploid and non-hyperdiploid subtypes. Hyperdiploidy is observed in about 55% of MM patients and is characterized by trisomies of the odd number chromosomes 3, 5, 7, 9, 11, 15, 19, and 21. Non-hyperdiploidy, is observed in 40-50% of MM patients and is characterized by translocations involving the region encoding the *Ig heavy chain (IgH)* gene on chromosome 14. The most common translocations in MM, t(4;14), t(6;14), t(11;14), t(14;16) and t(14;20), cause an overexpression of specific oncogenes (*Multiple myeloma SET domain/Fibroblast growth factor receptor 3 (MMSET/FGFR3), Cyclin D3 gene (CCND3), Cyclin D1 gene (CCND1), Transcription factor Maf, and MafB*, respectively) now under the control of the *IgH* enhancer. Secondary genetic events such as copy-number variations (CNV), translocations involving the proto-oncogene *Myc*, and somatic mutations affecting mitogen-activated protein kinase (MAPK), nuclear factor-κB (NF-κB), and deoxyribonucleic acid (DNA)-repair pathways are observed in MM, and are expected to be involved tumour progression [6-8].

1.1.3 Treatments in Multiple Myeloma

In MM there are several treatment strategies which are composed to fight MM in the best possible way and that also takes into account the age and disease stage of the patient [9]. In this section, some of the most common treatments, such as chemotherapy, stem cell transplantation, steroids, immunomodulatory drugs (IMiDs) and proteasome inhibitors (PIs) will be briefly introduced.

A common cancer treatment is chemotherapy which uses cytotoxic drugs to destroy cells that are in the process of dividing [10]. Since cancer cells proliferate more rapidly than normal cells, the cancer cells are more affected. In MM, chemotherapy is often used as a preparation for stem cell transplantation [9, 10]. The most common type of stem cell transplantation is an autologous stem cell transplantation (ASCT) which uses stem cells harvested from the patient's own blood [11]. ASCT has proven effective as the median overall survival of MM patients was prolonged by 1 year [9].

Steroids, more specific corticosteroids, are used in MM therapy in all stages of the disease for its numerous abilities in killing MM cells, decreasing inflammation, relieving pain and

reducing side-effects caused by other forms of treatment. The most commonly used steroids in MM therapy are dexamethasone and prednisone [10].

Over the past two decades, the outcome for MM patients have dramatically approved. Among the new treatments emerging in the early 2000's was the IMiDs, thalidomide, lenalidomide and pomalidomide. IMiDs are part of the initial therapy of MM and have multiple anti-cancerous effects. These include disruption of the plasma cell microenvironment in the BM, anti-inflammatory and cytotoxic effects [10, 12]. Another type of drug among the new treatments emerging in the early 2000's, that has greatly improved the clinical outcome of MM patients, are PIs. PIs are used throughout all stages of MM and are also included in the initial therapy of MM patients [9, 10]. Thus, PIs have become a cornerstone in MM therapy. The two PIs, carfilzomib (CFZ) and bortezomib (BZ), have been used in this thesis and are further described in section 1.5 Proteasome inhibitors in Multiple Myeloma therapy.

Despite good clinical effects and significant improvement of MM patient survival, patients who initially respond well to treatment will eventually relapse and develop resistance against the drugs used in MM therapy [13]. Thus, MM is considered an incurable disease.

1.2 Immunoglobulins – Structure and molecular genetics

In response of foreign antigens, the humoral immunity will initiate the production and secretion of highly diverse and specific immunoglobulins (Ig), also known as antibodies. The Igs can neutralize microbial toxins, prevent entry and spread of antigens and trigger effector mechanisms, such as the complement system and opsonisation, that will eliminate the intruding microbe. Igs are produced by a differentiated form of B-cells (also known as B-lymphocytes) and are produced both as membrane bound and secreted Igs. Plasma cells, a differentiated form of B-cells, are the ones affected in MM and they produce the secreted form of Igs. MM plasma cells produce an abundant amount of Igs and knowing how they are structurally composed and how they can be produced, in such a diverse and specified manner toward a given antigen, is of great value [14]. The production of Igs is described in section 1.3.1 B-cell development – From pro-B-cell to immature B-cell.

1.2.1 Immunoglobulin structure

Igs share a common structure but exhibit highly diverse variability on the region that binds to the antigen. The core structure, similar for all Igs, is composed of two identical heavy chains and two identical light chains assembled in a symmetric Y-shaped structure (Figure 1). Both the light and heavy chains are constructed of so-called Ig domains, where the heavy chain have a series of four Ig domains and the light chain have a series of two Ig domains. The Ig domains are homologous structures that contain a two-layered ß-sheet held together by a disulphide bridge where each layer is composed of three to five antiparallel polypeptide chains. Each light and heavy chain have a variable (V) N-terminal end and a constant (C) C-terminal end. The heavy chains have one variable (V_H) Ig domain and three or four constant (C_H) Ig domains, and the light chains have one variable (V_L) Ig domain and one constant (C_L) Ig domain (Figure 1). Variable Ig domains are named so because of their varying amino acid sequence between Igs generated by different B-cell clones. The variable Ig domain and first constant Ig domain of the heavy chain (V_H and C_{H1}) and the adjoining variable Ig domain and constant Ig domain of the light chain form the antigen-binding site, also called fragment antigen binding (Fab) region. The constant region Ig domains does not participate in antigen recognition. The C_H Ig domains interact with other molecules and immune cells, thereby helping to mediate the effector functions of the Ig. This part of the Ig is called the fragment crystallizable (Fc) region [14].

Igs are divided into distinct classes due to structural differences of their C_H regions. The five different isotypes are named by giving the different C_H chains their own Greek letter; IgA contains α heavy chains; IgD, δ; IgE, ε; IgG, γ; IgM, μ. Each isotype is related to a distinct effector function. The light chains are also divided into isotypes, called κ (kappa) and λ (lambda), based on differences in the C_L region. Each Ig has either two identical κ light chains or two identical λ light chains. Normally, humans have about 60% Igs containing κ light chains and about 40% Igs containing λ light chains, but the ratio can shift in patients with B-cell tumours, such as for MM patients, where the malignant cells derive from a single B-cell clone, all with the same light chain [14].

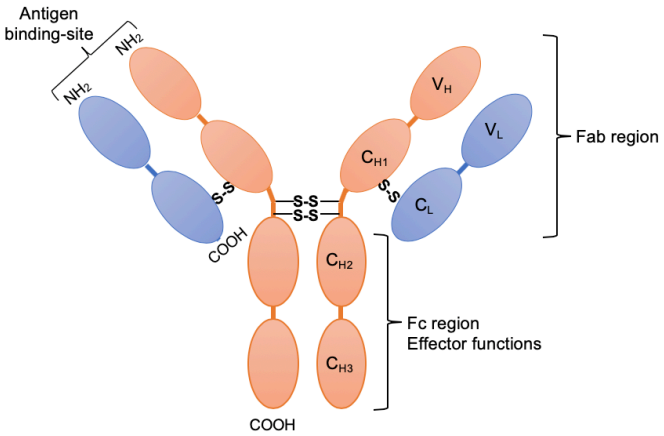

***Figure 1**: **Illustration of the immunoglobulin (Ig) structure**. The core structure is composed of two identical heavy chains and two identical light chains assembled in a symmetric Y-shaped structure. The two heavy chains and the heavy and light chains are held together by a disulphide bridge. The heavy chain is composed of four Ig domains and the light chain is composed of two Ig domains, where each chain has a variable (V) N-terminal end and a constant (C) C-terminal end. V_H, C_{H1} and the adjoining V_L and C_L form the antigen-binding site, also called fragment antigen binding (Fab) region, although the constant Ig domains does not participate in antigen recognition. C_{H3} and C_{H4} mediates the effector functions of the Ig and is called the fragment crystallizable (Fc) region.*

1.2.2 Immunoglobulins in Multiple Myeloma

The human immune system normally generates several clones of PCs producing its specific Ig (polyclonal), but during the pathogenesis of MM one single PC clone gets a growth advantage and will take over the BM so that only one specific Ig will be produced (monoclonal). As a result of this, MM patients will each have its single-clone of PCs producing and secreting its specific monoclonal Ig. In 55% of the cases, the monoclonal Ig is of IgG isotype, 25% of IgA isotype and 15-20% of MM patients will only produce the light chain of Igs, also known as free light chains (FLC) [15, 16].

Renal failure is a common clinical manifestation in MM patients with a prevalence ranging from 20-50%. The cause is most often due to toxic effects of the abundant amounts of FLC accumulation in renal structures such as glomeruli and tubuli. Glomerulopathies is caused by the deposition of FLC or monoclonal Ig (seen in light chain amyloidosis and light chain deposition disease) and, the most common one, cast nephropathy is the forming of FLC into insoluble casts leading to acute renal injury [17]. MM patents producing FLC seem to more frequently be affected by renal failure, bone disease, and light chain amyloidosis and the prognosis of these patients appears to be poorer than patients producing the monoclonal IgG or IgA variant [18]. However, treatment of renal failure has shown to improve the survival of MM patients [17].

1.3 Biology and development of plasma cells

Plasma cells (PCs) differentiate from B-cells in the BM into specialized cells synthesising and secreting Igs to defeat hostile antigens. B-cells are mainly BM-derived lymphocytes that play an important role in the adaptive immune system providing the humoral immunity through Ig secretion. Mature B-cells, located in the periphery, are divided into subsets depending on what progenitor stem cells they derive from and what function they serve. In a naïve state (before antigen encounter) mature B-cells produce both membrane-associated IgD and IgM that have the same Ig specificity. However, upon antigen encounter, these cells also have the ability to acquire functional competence by going through somatic hypermutation (SHM) and class switch recombination (CSR) prior to further development into an Ig secreting PC, as described later [19, 20].

1.3.1 B-cell development – From pro-B-cell to immature B-cell

Before developing into mature B-cells, BM progenitors that initially have no Ig expression develop into IgM-expressing immature B-cells. Igs are made up of multiple gene segments and the gene segments encoding the variable regions of both heavy and light chain are joined together by a process known as somatic recombination to generate the final variable region exon. The variable heavy chain (V_H) region is constructed from the joining of three gene segments, *V (variable)*, *D (diversity)* and *J (joining),* and the variable light chain (V_L) region is constructed from the joining of two gene segments, *V* and *J*. There are multiple segments for *V*, *D* and *J* and the joining of these are known as *V(D)J* recombination (Figure 2). Due to the presence of several segments for *V*, *D* and *J*, the diversity of the antibody repertoire can be in the millions. *V(D)J* recombination follows the B-cell development from pro-B-cell to an IgM-expression immature B-cell (Figure 3) and is controlled by several checkpoints that determine if the prior developmental steps have been successful [20-23].

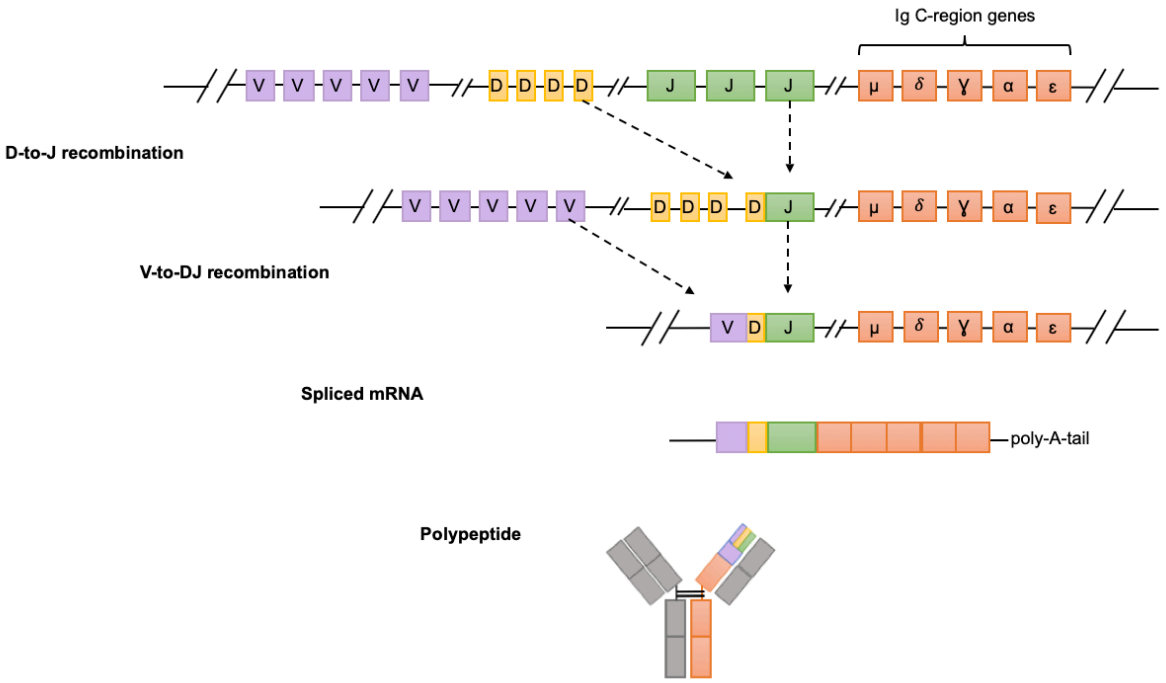

***Figure 2**: **Illustrating somatic (V(D)J) recombination of the immunoglobulin (Ig) heavy chain,** starting with the germline DNA containing several segments of the genes for variable (V), diversity (D) and joining (J). First a D and J segment is joined together before the DJ-joined segment are joined with a V segment. The V and C region exon is transcribed and spliced in order to form the mRNA that is lastly translated into a polypeptide chain.*

The first developmental steps are antigen independent and take place in the BM starting with Ig V_H region recombination in an early pro-B-cell, where a D_H gene segment is joined to a J_H gene segment, on both alleles (Figure 2 and Figure 3). Following is the pre-B-I-cell stage recombining a random V_H gene segment to the already recombined DJ_H-sequence on only one of the alleles (Figure 2 and Figure 3). The VDJ_H rearranged genes is here checked, and if the rearrangement is proven non-productive the sister allele will try to make a productive VDJ_H gene-rearrangement. If the new gene is not productive the pre-B-I-cell will undergo apoptosis, but if successful, the pre-B-I-cell will proceed its development to a pre-B-II-cell and expression of a pre-B-receptor (Figure 3). After *V(D)J* recombination, the variable region exon is transcribed, and the ribonucleic acid (RNA) transcript is spliced. Here, the VDJ_H segment will be joined together with a $C\mu$ gene from the heavy chain constant region (Figure 2) to produce and express IgM heavy chains on the cell surface with surrogate light chains (SLC) and Ig α/Ig β (required to initiate signals into the B-cell). If the IgM heavy chain is able to bind to stromal cells and initiate signalling through Ig α/Ig β this leads to an allelic exclusion thereby inhibiting any further heavy chain rearrangements [20-23].

The pre-B-receptor will return into the pre-B-II-cell and the recombination of Ig V_L region is initiated. The V_L exon is composed of a single V_L-to-J_L gene segment joining of the Ig kappa light chain (IgK) alleles. If not succeeded, the lambda light chain alleles will try to make a productive V_L-J_L recombination. When a productive V_L-J_L recombination is acquired and expressed, it is ready to be assembled with the IgM heavy chain into IgM expressed in the cell surface of an immature B-cell [20-22].

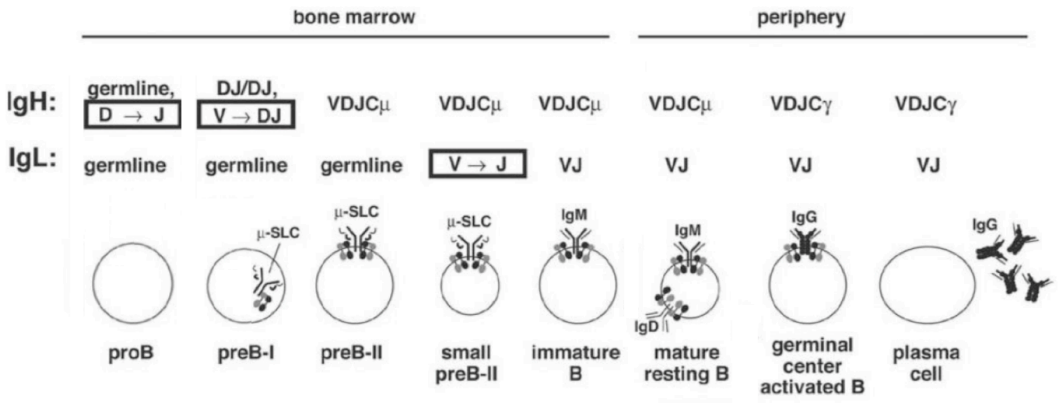

***Figure 3**: **Illustration of the simultaneous steps of B-cell developmental and immunoglobulin (Ig) gene recombination**. B-cell development starts in the bone marrow (BM) with a pro-B cell and D_H-J_H recombination. The cell will progress to the pre-B-I cell stage recombining a random V_H-gene to the already recombined DJ_H-genes. Next is the pre-B-II-cell stage and expression of a pre-B-receptor composed of IgM, surrogate light chain (SLC) and signalling complex Ig α/Ig β that will inhibit further heavy chain rearrangements if the heavy chain and signalling complex is functional. Following is the stage where the small pre-B-II-cell will perform a V_L-J_L recombination of the light chain leading to an immature B-cell producing membrane bound IgM. After going through selection processes in the BM and periphery, the immature B-cells will develop into mature resting B-cells (also called naïve B-cells) expressing both membrane-bound IgM and IgD. When encountering a foreign antigen, the mature resting B-cells will go into germinal centre where the cells go through somatic hypermutation (SHM) and class switch recombination (CSR) to further development into an Ig secreting plasma cell. Figure is adopted and edited from [24].*

1.3.2 B-cell tolerance – From immature B-cell to mature B-cell

Before proceeding to the next developmental step where the immature B-cell progress to a mature resting B-cell, the immature B-cell has to undergo a series of selection processes. This in to ensure that the immature B-cell is non-reactive to self-molecules in the BM or self-antigens in the periphery. The B-cells that survive this selection migrate to follicles where a positive selection is performed for the immature B-cells that are able to bind to foreign antigens. These now called mature resting B-cells (Figure 3), also called naïve B-cells, will in addition to IgM express a second cell surface antibody, IgD, that share the same antigen specificity. The selection processes are described in further detail in referred sources [22, 25, 26].

1.3.3 B-cell activation – From mature B-cell to Ig secreting plasma cell

In response to foreign antigens, the B-cells have to generate Igs of high specificity and high affinity, including the right isotype to fit the needed effector functions in order to fight the infection in the most effective manner. In the process of achieving this, the mature B-cells go through a complicated process of SHM, T-cell dependent selection and CSR, and finally differentiation into a Ig producing PC (Figure 3 and Figure 4).

Mature B-cells are activated by an antigen-interaction in secondary lymphoid organs (lymph node, spleen). Some of the activated B-cells will here differentiate into short lived Ig secreting PC, often secreting IgM as a primary humoral response. Activated B-cells will move into the dark zone of a germinal centre where they become centroblasts through SHM and simultaneous proliferation (Figure 4A). SHM is driven by an intracellular enzyme called activation induced cytidine deaminase (AID) which induce the producing of point mutations in the *V*-region of Igs. These point mutations can either increase or decrease the antigen affinity and specificity, resulting in a positive selection of Igs with the highest affinity against the antigen and differentiation into centrocytes (Figure 4B). This selection takes place in the light zone of the germinal centre by follicular dendritic cells (FDC) and follicular helper T-cells (T_{FH}-cells) that present the same antigen that activated the mature B-cell [23, 27].

Next for the centrocyte is CSR where the cell changes its Ig isotype, and thus effector function, while keeping the same antigen specificity (Figure 4C). CSR is not a random process and is dictated by cytokines secreted from activating helper T-cells. The process of CSR is explained in detail in referred sources [23, 27]. After CSR, the maturation-process from an activated mature B-cell has ended with an Ig secreting PC ready to attack the antigen (Figure 3). These long-lived PCs, mainly located in the BM, are the cells affected in MM. Some of the cells however will differentiate into a memory B-cell instead of a PC, which allow the body to neutralize the same antigen at an earlier stage in case of reinfection (Figure 4D).

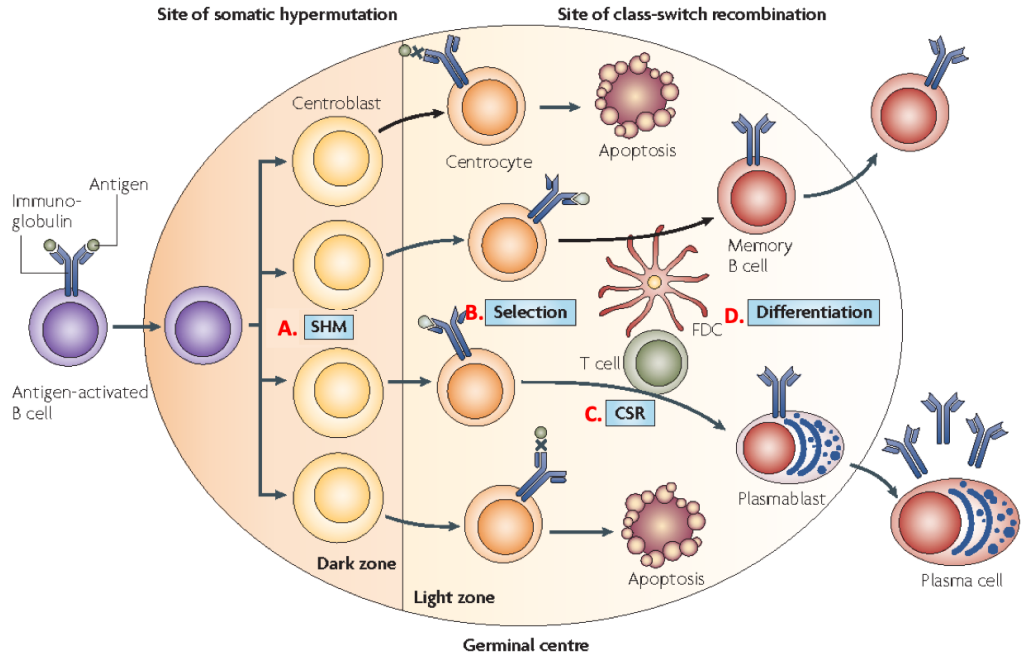

***Figure 4**: **Illustration of a germinal centre and the development of long-lived immunoglobulin (Ig) secreting plasma cell**. **A.** A mature resting B-cell will be activated by an antigen encounter and migrate to the dark zone of a germinal centre. Here it will differentiate into a centroblasts through somatic hypermutation (SHM) and proliferation. **B.** The centroblasts will migrate to the light zone and differentiate into centrocytes. Follicular dendritic cells (FDC) and folicullar helper T-cells (T_{FH}-cells) will present the same activating antigen to the cells and positively select the ones with the highest antigen affinity. The rest will undergo apoptosis. **C.** The positively selected centrocytes will go through class switch recombination (CSR) and **D.** lastly differentiation into an Ig secreting plasma cell or a memory B-cells. Figure is adopted and edited from [28].*

1.4 Protein degradation systems

As mentioned, MM cells produce abundant amount of Igs. This overproduction will also generate a lot of non-functional Igs that needs to be eliminated in order to deal with the stressful environment that a cancer cell endure. Normal cells are dependent on functional protein degradation systems in order to maintain cellular homeostasis, but the degradation systems also play an important role for MM cells by promoting cancer cell survival and proliferation. The following sections will introduce different types of protein degradation systems considered essential for MM cells.

1.4.1 The Ubiquitin-proteasome system and the proteasome

The proteasome is an adenosine triphosphate (ATP)-dependent complex responsible of degrading non-functional intracellular proteins. In order to distinguish between proteins to be degraded or not, proteins destined for degradation is covalently tagged with a key molecule, ubiquitin, which polymerizes on the protein and work as a degradation signal [29].

The proteasome is constructed by two subcomplexes: catalytic core particle (CP), also known as 20S proteasome, and one or two proteasome activating complex(es), called 19S regulatory particle(s) (RP) (Figure 5). The 19S RP has to be bound to either one or both ends of the 20S proteasome in order to form an enzymatically active proteasome. The assembly of the proteasome subcomplexes can generate either of the two major proteasomes: the 26S proteasome having only one 19S RP attached to one of the ends and the 30S proteasome having 19S RP attached on both ends. The 20S CP of the proteasome is a barrel shaped structure with proteolytic functions and the 19S RP has the role of recognizing, unfolding and translocating the ubiquitinated proteins into the 20S CP [29].

The 20S CP is constructed of heptametrical rings stacked on top of each other, containing two inner β-rings and two outer α-rings. The α-rings work as a gate controlling the substrate passage and opens up in the presence of an activator. In the β-ring, only three of the seven β-subunits (β1, β2, β5) contain different proteolytic active sites responsible for protein degradation, resulting in six proteolytic active β-subunits in a single proteasome [29].

This ubiquitin-proteasome system (UPS), which include the actions of E1 (ubiquitin-activating), E2 (ubiquitin-conjugating) and E3 (ubiquitin-ligating) enzymes, gives rise to the ability to select, transport and proteolytically brake down intracellular substrates for i.e. recycling. Ubiquitination of proteins is also a reversible reaction due to the presence of cysteine-proteases and metalloprotease deubiquitinating enzymes (DUBs). By degrading structurally abnormal and short-lived regulatory proteins, the UPS controls many basic cellular processes such as signal transduction, immune responses, metabolism, cell cycle progression, cell death, protein quality control and development [29].

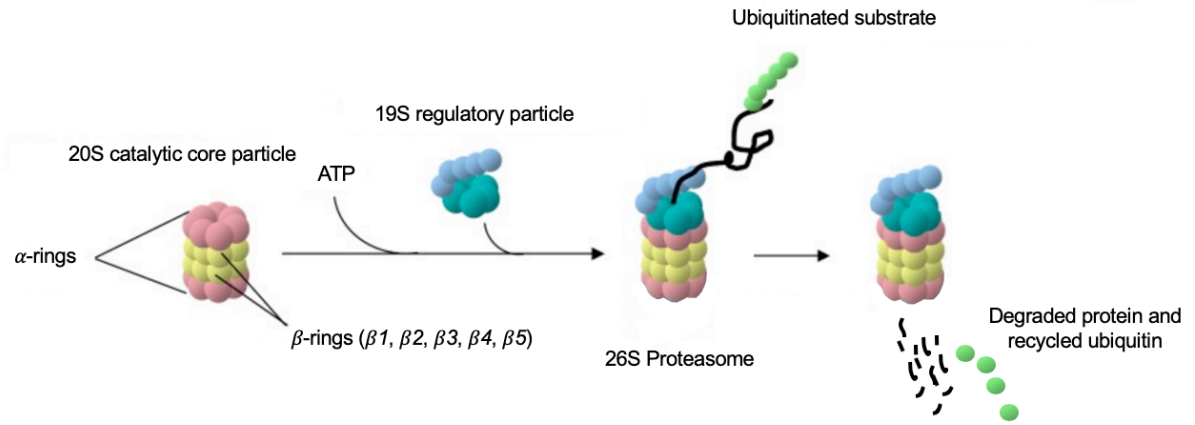

***Figure 5**: **Illustration of proteasome structure and protein degradation.** The 20S core particle (CP), consisting of two inner β-rings and two outer α-rings, and the terminal 19S regulatory particle (RP) constitute the enzymatically active proteasome. Ubiquitinated proteins are recognized, unfolded and transported by the 19S RP into the 20S CP where the protein is degraded, and the ubiquitin is recycled. The illustration is adopted and edited from [30].*

1.4.2 Autophagy

Another important protein degradation process in human cells are autophagy. There are three different types of autophagy: Chaperone-mediated autophagy (CMA), micro-autophagy and macro-autophagy. However, this thesis will focus on macro-autophagy, hereafter referred to as autophagy. Autophagy is defined by the sequestering of cytoplasmic components destined for degradation by ubiquitination, such as proteins and organelles (also known as cargo), by an isolation membrane (phagophore). It is still unclear where this isolation membrane originate from, but possible sources are the endoplasmic reticulum (ER), the golgi asparagus, mitochondria and endosomes [31]. Further, the double membraned phagophore will enclose to form an autophagosome that subsequently fuses with a lysosome for degradation of the cargo using the proteolytic properties of lysosomes (Figure 6) [30, 32].

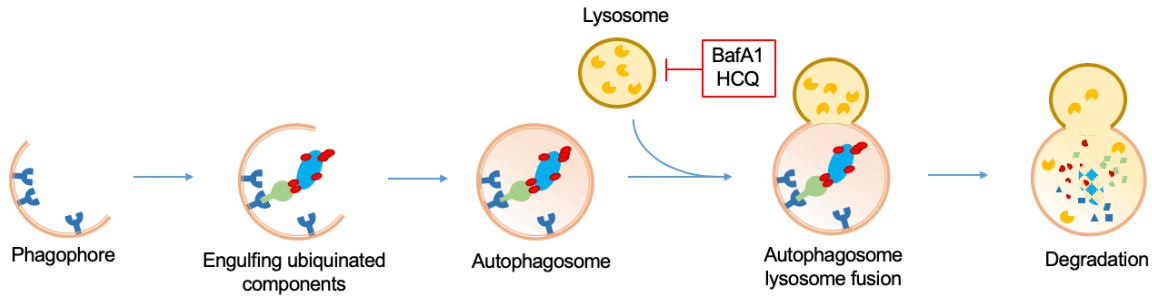

***Figure 6**: **Illustration of autophagic degradation of ubiquitinated cargo.** Ubiquitinated cargo is bound by autophagy adaptor proteins which subsequently bind to a receptor on the phagophore. The phagophore will elongate and close to form an autophagosome. Finally, a lysosome will fuse with the autophagosome in order to degrade the content. Autophagy inhibitors, such as bafilomycin A1 (BafA1) and hydroxychloroquine (HCQ), can prevent autophagosome-lysosome fusion and thus cargo degradation.*

Autophagy occur at a basal level but is further induced due to diverse types of stress or starvation. The components of which autophagy eliminates can for example be parts of the cytosol, organelles such as the mitochondria, protein aggregates or intracellular pathogens [32, 33].

Autophagy-related genes (Atg), controlling the formation and turnover of the autophagosome, was discovered by Dr. Yoshimori Ohsumi and led to him being awarded the Nobel Prize in Physiology or Medicine in 2016 [30, 34]. Needed for autophagosome formation are two conserved, ubiquitin-like protein conjugation systems, Atg12-Atg5- and the Atg8-phosphatidylethanolamine (PE) conjugation systems [35]. At least seven mammalian homologues of Atg8 have been identified and can be subdivided into two groups containing three microtubule-associated proteins 1 light chain 3 (MAP1LC3A, -B and -C) isoforms and four gamma-aminobutyrate receptor-associated protein (GABARAP) and GABARAP-like proteins (GATE-16/GABARAPL2) [36]. After synthesis, pro-MAP1LC3, hereafter referred to as LC3, is cleaved at its C-terminal end by Atg4, exposing a glycine residue, resulting in the cytosolic form of LC3 called LC3-I. After a subsequent activation by Atg7 and conjugation of PE to the C-terminal end, LC3-I is transformed into the membrane bound form, LC3-II. After autophagosome formation, LC3-II is located on both the inner and outer side of the membrane, where LC3-II on the outer side is released to the cytosol and the inner LC3-II is degraded together with the autophagosomal cargo thus working as an autophagy marker [30, 37].

Autophagy was originally viewed as a non-specific process, but a selective form of autophagy has also been acknowledged. LC3-II, in addition of being needed for autophagosome formation, is also involved in selective autophagy by recognizing adaptor proteins like sequestosome 1 (SQSTM1) (also known as p62), next to BRCA1 gene 1 protein (NBR1), nuclear domain 10 protein 52 (NDP52) and optineurin (OPTN) which binds to and transports ubiquitinated proteins to the autophagosome by direct binding to LC3-II for degradation (Figure 7) [38, 39].

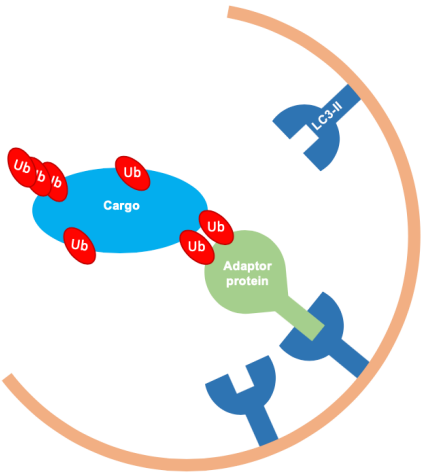

***Figure 7**: **Closer view of the components interacting in selective autophagy**. Ubiquitinated cargo is bound by autophagy adaptor proteins which transport the complex to LC3-II on the autophagosomal membrane.*

Of the several LC3-II binding adaptor proteins, SQSTM1 is the most studied and function in critical roles in autophagy, protein aggregation and cell signalling [40]. SQSTM1 is composed of six domains with different interacting partners (Figure 8). The LC3 interacting region (LIR) domain recognizes and binds to LC3-II on the autophagosomal membrane while C-terminal ubiquitin binding adaptor (UBA) binds to ubiquitin, allowing ubiquitinated substrates to be incorporated into the autophagosome. SQSTM1 also have the ability to polymerize using its N-terminal Phox/Bem1 (PB1) domain which is considered an essential function in the collection of ubiquitinated cargo, protein aggregation and transport of this complex to the autophagosome [30, 38].

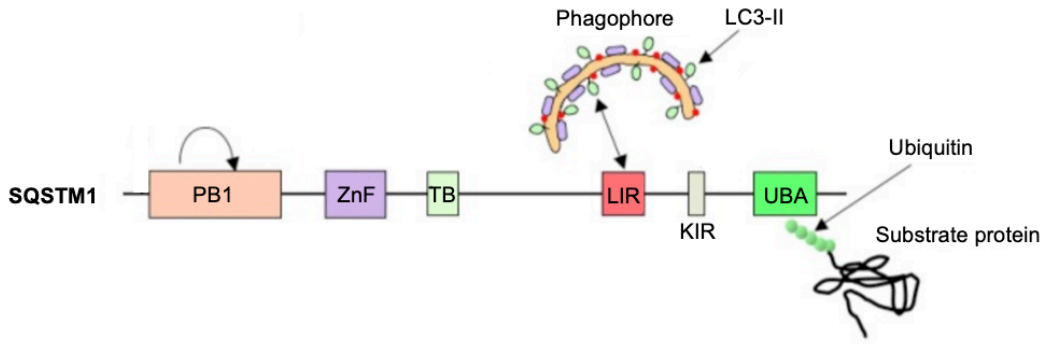

***Figure 8**: **Structure of SQSTM1 which include six different domains.** The N-terminal Phox/Bem1 (PB1) domain is involved in polymerization of SQSTM1, ZnF (Zinc Finger) allows binding of receptor interacting protein (RIP), the TNF receptor associated factor 6 (TRAF6)-binding (TB) domain allows TRAF6-binding, LIR interacts with LC3-II of the autophagosomal membrane, Keap-interacting region (KIR) acts as a Keap1-binding domain and lastly the ubiquitin binding adaptor (UBA) domain which interacts with ubiquitin. This figure is adopted and edited from [30].*

Although the autophagic pathway is essential in order to maintain cellular homeostasis, research on this field has revealed a contextual role of autophagy. In normal cells, autophagy work as a tumour supressor, eliminating damaged organelles and protein aggregates which otherwise could promote tumorigenesis and genomic instability. Conversely, once cancer is established, an increase in autophagic flux will enable cancer cell survival by reducing the sensitivity towards cell-intrinsic and microenvironmental stimuli that would normally promote apoptosis [41].

1.4.2.1 Autophagy inhibitors

Autophagy inhibitors are used in research to help understand the regulation of autophagy in human diseases and can provide insight into the application of autophagy-targeted therapy. bafilomycin A1 (BafA1) is a well-known autophagy inhibitor specifically inhibiting the vacuolic H^+-ATPase (V-ATPase) on lysosomes. V-ATPase contribute to the acidification of lysosomes by an ATP-dependent pumping of protons into the lysosome. Inhibition of lysosome acidification will prevent degradation of cargo in autophagosomes thus inhibiting autophagic flux. BafA1 is also suggested to inhibit autophagosome-lysosome fusion, but the specific mechanism is still uncertain. Although seen as a possible candidate in cancer therapy, BafA1 is not approved by the US Food and Drug Administration (FDA) for clinical trials due to secondary adverse effects on normal cells [42, 43].

Hydroxychloroquine (HCQ) is an FDA approved drug initially used in treatment of certain types of malaria and autoimmune diseases such as systemic lupus erythematosus and inflammatory arthritis, but anti-cancer effects have later been revealed. The most common approach in cancer therapy is the property of functioning as an autophagy inhibitor, making it the only one clinically approved. HCQ function as an autophagy inhibitor by preventing the lysosome from degrading the cargo engulfed by the autophagosome. The exact mechanism is not fully understood, but HCQ is suggested to work as a week base that gets transported and trapped inside the lysosome thus de-acidifying the lysosome [44, 45].

1.5 Proteasome inhibitors in Multiple Myeloma therapy

Proteasome inhibitors (PIs) has shown good clinical effects in MM therapy [46], presumably due to the fact that MM cells are highly dependent on well-functioning protein degradation systems to obtain cellular homeostasis. Thus, by inhibiting the proteasomes, the PIs aim to induce cytotoxic effects in MM cells by increasing the protein folding burden.

1.5.1 Bortezomib

Bortezomib (BZ) was the first PI introduced and was approved by the FDA in 2003 for the use in relapsed and/or refractory MM patients [47]. Since then, the use of BZ has expanded to newly diagnosed MM patients and disease maintenance and is now considered as a backbone in MM therapy [48]. BZ is a reversible PI binding and blocking the proteolytic activity of the ß5, and partly the ß1 and ß2, subunit located on the 26S proteasome (Figure 5). The inhibitory effects of BZ on the proteasome, although not fully understood, has proven effective for many patients and result in cancer cell death. On the other hand, only about 35% of MM patients are sensitive to BZ [49], meaning that more than half of the patients have an innate resistance towards BZ. In addition, patients initially sensitive to BZ also tend to develop an acquired resistance and relapse after long-term treatment [49]. As an attempt to overcome drug resistance, a second generation of PIs, such as carfilzomib, ixazomib, marizomib and oprozomib, was developed with the aim of improving the anti-tumour function by increasing the inhibitory efficacy of the proteasome [49, 50].

1.5.2 Carfilzomib

Carfilzomib (CFZ) was first approved by the FDA in 2012 for the use in relapsed and/or refractor MM patients [51]. CFZ is an PI that binds irreversibly to the proteasome and was developed to deliver a more sustained inhibition than BZ by specifically binding and inhibiting the proteolytic subunit, ß5, of the proteasome with higher affinity. This irreversible inhibition of the ß5 subunit lead to the requirement of new subunit synthesis and proteasome assembly for restoration of proteasome activity. CFZ also exerts inhibition of the ß1 and ß2 subunits, but with low affinity. The novel mechanisms of CFZ proved to be effective for some patients with innate and acquired resistance to BZ, but in time MM patients developed further drug resistance [51, 52].

1.6 Proteasome inhibitor resistance

Today, PI's therapeutic effects on MM patients are impeded by the presence of drug resistance and the search for understanding underlying resistance mechanisms are well under progress. An overview of some suggested mechanisms will be presented in this section.

1.6.1 ß5 subunit point mutation and overexpression

Research of prolonged *in vitro* BZ exposure in leukaemia and MM cell lines has led to the observation of point mutations in the *proteasome subunit beta type-5* (*PSMB5)* gene encoding the β5 subunit. These point mutations, resulting in amino acid substitutions, were located in close proximity to the binding pocket of BZ in the β5 subunit and disrupts the binding of BZ, thus suggested as a possible cause of BZ resistance in MM patients [53, 54]. However, such mutations have not been found in MM patients [53, 55]. In addition, an overexpression of the β5 subunit has been observed in BZ resistant cancer cell lines and is proposed as a compensatory mechanism for the impaired catalytic activity of the mutant proteasomes caused by the β5 subunit mutations [53-55].

1.6.2 MDR1 overexpression

As mutations in the β5 subunit of proteasomes is yet to be found in patient myeloma cells, there must be other mechanisms causing PI resistance. A mechanism suggested to cause resistance against CFZ in MM patients is the multidrug resistance protein 1 (MDR1) encoded by the *ATP-binding cassette sub-family B member 1 (ABCB1)* gene. MDR1 is located in the cell membrane where it has the ability to pump foreign substances, such as drugs, out of the cells [56]. Overexpression of MDR1 was found to be the most significant change in a CFZ adapted MM cell line, AMO-1, and have the ability to reduce CFZ induced cytotoxicity through drug efflux. When inhibiting the MDR1 with the already established MDR1 inhibitory drugs, nelfinavir and lopinavir, the cytotoxic effect of BZ and CFZ was shown to be re-established in CFZ adapted MM cells [54, 57].

1.6.3 Autophagy induction

Autophagy serve an important role during MM in order to maintain the resident pool of BM long-lived PCs and to ensure sustainable Ig production [58-60]. SQSTM1 was also pointed out as an important mediator in this interplay. When treating MM cell lines with PIs, it has been shown to lead to increased production of SQSTM1-positive protein aggregates, thus

autophagy is believed to function as a possible compensatory mechanism to PI resistance and UPS insufficiency [59, 61]. It has been shown that autophagy is upregulated as a response to PI treatment in MM cell lines, suggesting that it may have a role in survival mechanisms against MM therapy [62]. This opens a new path of attempting to overcome drug resistance by combining PIs and autophagy inhibitors which has been shown effective *in vitro* with CFZ and HCQ in several MM cell lines and primary MM cells [59, 61, 63].

1.7 ER-stress and the Unfolded Protein Response

In eukaryotic cells, the endoplasmic reticulum (ER) is an essential organelle responsible for the synthesis, folding, sorting and transportation of proteins. ER-stress is a state in which the cells enter when the amount of unfolded or misfolded proteins exceed the capacity of the ER chaperone and folding machinery [64, 65]. Under normal conditions, up to about 30% of newly synthesized proteins are degraded due to misfolding [66]. MM cells, that are known to produce abundant amounts of Igs, are hence assumed to have a very high amount of misfolded proteins that in turn induce ER-stress. ER-stress lead to the induction of the so-called unfolded protein response (UPR), which can serve both as a tumour supporter and a tumour supressor. As a tumour supporter, promoting cancer cell survival, UPR works as a homeostatic corrector aiming to lower the ER stress levels by either increasing the ER chaperone and folding machinery or by activating the ER-associated degradation (ERAD) pathway. The ERAD pathway will recognize unfolded or misfolded proteins in the ER and tag them with ubiquitin which lead to subsequent degradation by the proteasome. On the other hand, if the intensity of ER-stress is too high and the UPR-induced mechanisms fail to relieve ER-stress, UPR will function as a tumour supressor and induce cancer cell death by activation of apoptosis [64, 65].

ER-stress activates three branches of UPR signalling. Each pathway is activated by the dissociation of the binding immunoglobulin protein (BiP) from its respective signalling protein (Inositol-requiring enzyme 1α (IRE1α), protein kinase RNA (PKR)-like ER kinase (PERK) and activating transcription factor 6 (ATF6)) and induce different UPR responses as shown in Figure 9.

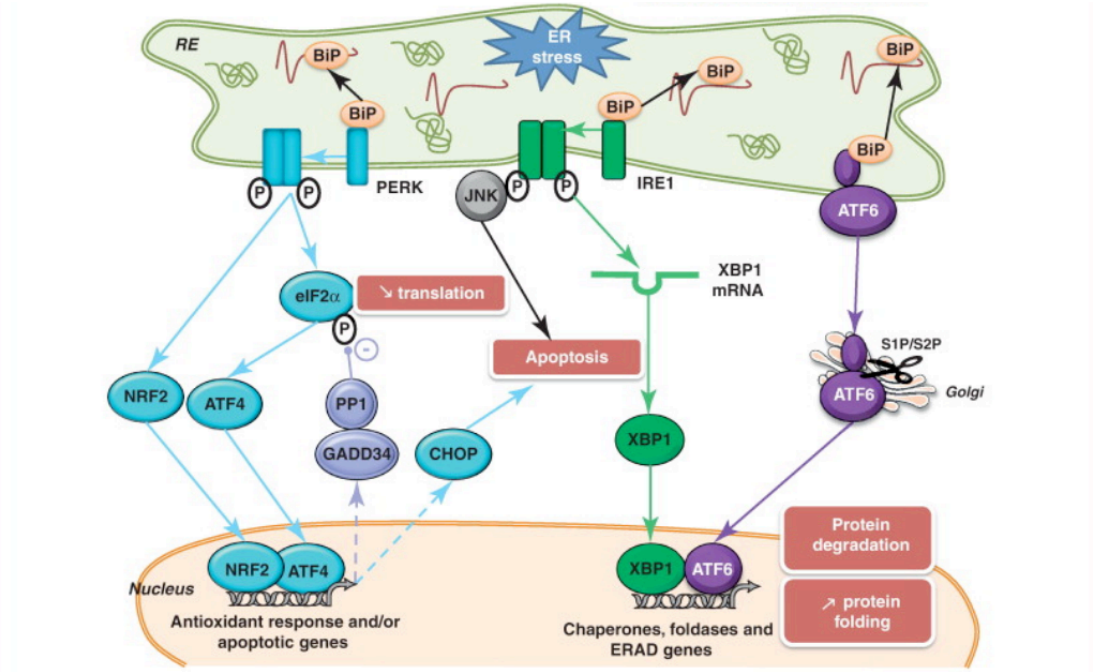

***Figure 9**: **The endoplasmic reticulum (ER) stress pathways**. Upon Binding immunoglobulin protein (BiP) dissociation Protein kinase RNA (PKR)-like ER kinase (PERK) will dimerize, autophosphorylate and subsequently lead to phosphorylation of eukaryotic initiation factor 2 (elF2α). This will lead to a decrease in global protein synthesis. p-elF2α will also promote expression of Activating transcription factor 4 (ATF4), resulting in an activation of the pro-apoptotic transcriptional factor CCAAT-enhancer-binding protein homologous protein (CHOP) and Growth arrest and DNA damage-inducible protein 34 (GADD34) which will dephosphorylate elF2α. In addition, PERK activates nuclear erythroid-related factor 2 (NFE2L2, also called NRF2), which result in expression of genes containing antioxidant response elements. Similar to PERK, Inositol-requiring enzyme 1α (IRE1α) will dimerize/oligomerize and autophosphorylate, activating two different pathways. One will lead to the activation of the pro-apoptotic c-Jun N-terminal kinase (JNK) pathway and the other will catalyse X-box binding protein 1 (XBP1) mRNA splicing, allowing the XBP1 protein to promote several genes involved in UPR and ERAD. Activating transcription factor 6 (ATF6), the last of the three UPR pathway branches, will translocate from the ER upon activation to the golgi apparatus. In the golgi apparatus, ATF6 is cleaved by Site-1&2 protease (S1P/S2P), creating an active transcription factor that mediates expression of several components important for protein folding, degradation and ER expansion [64, 65]. The illustration is adopted and edited from [67].*

As mentioned, ERAD is critical in trying to reduce ER-stress through ubiquitination of proteins in the ER and transporting them to proteasomes for degradation. This process can serve as a tumour supporter but the use of PIs in MM therapy, targeting ERAD, have proved to work against this tumour-promoting process. However, in addition to ERAD, ER stress is also assumed to have the ability to activate autophagy as a secondary protein degradation pathway in cases when ER stress capacity is exceeded [64, 68, 69].

2.0 Aim of study

The overall goal in this study is to investigate molecular mechanisms involved in the drug resistance development against the proteasome inhibitors (PIs), carfilzomib (CFZ) and bortezomib (BZ), used in treatment against multiple myeloma (MM). Previously obtained results in the myeloma group have shown that the autophagy inhibitor hydroxychloroquine (HCQ) potentiates the cytotoxic effect of CFZ in INA-6 cells and that HCQ has the ability to reverse the resistance against CFZ in CFZ adapted INA-6 cells [61]. It is therefore of interest to investigate the combinatory effect of HCQ and PIs in another MM cell line, AMO-1. PI adapted INA-6 cell lines have also been found to significantly modify their basal expression level of immunoglobulin kappa light chain (IgK) and the autophagy receptor sequestosome 1 (SQSTM1) [70, 71], thus we want to investigate if the expression level of IgK and SQSTM1 also has been changed in the PI adapted AMO-1 cell line. SQSTM1 have been shown to be involved in the binding and sequestering of ubiquitinated cargo, i.e. dysfunctional IgK, into protein aggregates for degradation by autophagy [30]. Unpublished results obtained by the myeloma group has shown that IgK and SQSTM1 are released from INA-6 cells after autophagic and proteasome inhibition (Appendix 8.7A). As many MM patients develop renal insufficiencies due to free immunoglobulin light chains being secreted by MM cells [18], we want to investigate if SQSTM1 could have a role in the release of IgK from MM cells which could represent a possible mechanism involved in drug resistance. Based on this, the more specific aims of the study are:

1. Determining the cytotoxic effect of targeting both arms of protein degradation, the ubiquitin-proteasome system and autophagy, in the PI adapted MM cell line, AMO-1.
2. To investigate the role of IgK in drug sensitivity using INA-6 IgK knockout cells.
3. To investigate the levels of IgK and SQSTM1 in the PI adapted MM cell line AMO-1.
4. To investigate whether protein aggregates are released from the MM cells in an SQSTM1-dependent manner as an alternative way of developing drug resistance.
5. To investigate possible drug resistance mechanisms in MM cells such as the drug efflux pump MDR1 and endoplasmic reticulum-stress.

3.0 Materials and Methods

3.1 Cell line and cell culturing

3.1.1 INA-6 cell lines

INA-6 cells are MM cells derived from a MM patient and are a common cell line used in research. INA-6 cells are IL-6 dependent suspension cells that express high levels of IgK [72]. In this thesis, different types of INA-6 cell lines were used, such as IgK knockout (KO) cell lines including two IgK control cell lines (IgK Ctr 1 and Ctr 2) expressing normal IgK levels, a SQSTM1 knockout (KO) cell line and INA-6 cell lines adapted to CFZ and BZ. The five IgK KO cell clones and the two IgK control cell clones were made by a former master's student, Roy Abhijeet, using Clustered Regularly Interspaced Short Palindromic Repeats (CRISPR)/Cas9 technology and single cell cloning [71]. The SQSTM1 KO #3-2 cell line was made by Dr. Toril Holien also by using CRISPR/Cas9 technology and single cell cloning.

The CFZ and BZ adapted INA-6 cells were established by Dr. Kristine Misund. The cells were cultivated in medium containing an initial dose of 3 nM of CFZ or BZ and were introduced to an increasing drug concentration of 1 nM/month to a final dose of 10 nM after 6 months. The cells were then cultured in 10 nM of CFZ and BZ for 3 months, followed by 4 weeks of drug free cultivation. These cells are referred to as INA-6-CFZR and INA-6-BZR. A control cell line was made by growing the cells under the same conditions without the drugs and is referred to as INA-6 wild type (WT).

The INA-6 cell lines were cultured in Roswell park memorial Institute (RPMI)-1640 medium (Sigma Aldrich, #R8758) containing the antibiotics L-glutamine (2 mmol/l, Sigma Aldrich #56-85-9) and gentamycin (40 µg/mL Sanofi-Aventis), 10% fetal calf serum (FCS) (Gibco™, #10270106) and IL-6 (1 ng/ml) (Biosource, #1003). This medium is further referred to as INA-6 medium. The INA-6 cell lines were cultured at 37˚C in a 5% CO_2 atmosphere and culture medium was replenished twice weekly.

3.1.2 AMO-1 cell lines

AMO-1 is a MM cell line that predominantly produce IgA with kappa light chain [73]. AMO-1 cells are suspension cells and are not IL-6 dependent. CFZ and BZ adapted AMO-1 cell lines (referred to as AMO-1-CFZR and AMO-1-BZR) and control cell line, AMO-1-WT,

were a kind gift from Prof. Dr. med. Christoph Driessen, Le, Switzerland. The PI adapted AMO-1 cell lines were replenished twice a week and cultivated in RPMI-1640 medium containing the antibiotic L-glutamine (2 mmol/l), 10% FCS and 90 nM of CFZ or BZ.

3.2 Cell counting

Cells were counted using the Z2 Beckman Coulter counter (Life sciences, #6605700) which measures the size and counts the cells using the Coulter Principle. INA-6 and AMO-1 cells were quantified by counting structures between 10 and 19 µm. 20 µl of the cell suspension was added to 10 ml of ISOTON II Diluent (Beckman Coulter Life Sciences, #8546719) and measured twice. The average was used to calculate the number of cells/ml of the cell suspension.

3.3 Cell treatment

In this thesis, several drugs were used to treat the cells. The two PIs used were CFZ (Active Biochemicals, #A1098) and BZ (Selleck Chemicals, #S1013) and the drugs used to inhibit autophagy were hydroxychloroquine (HCQ) (Sigma Aldrich) and bafilomycin A1 (BafA1) (Sigma Aldrich, #B1793). Thapsigargin (Sigma Aldrich, #T9033) was used as a positive control for ER-stress.

3.4 Cell Viability Assay

To assess the cell viability and apoptosis after drug treatment, two different assays were used. CellTiter Glo® assay measures the amount of ATP produced by living cells and Annexin V/Propidium iodide staining assay measures uptake of Annexin V- Fluorescein isothiocyanate (FITC) and propidium iodide by apoptotic cells measured by flow cytometry.

3.4.1 CellTiter Glo® Assay

CellTiter Glo® Luminescent Cell Viability Assay (Promega, #G9242) measures the metabolic activity in a cell culture by quantifying the presence of ATP produced by living cells. Although not a viability assay, this assay gives an indication of how many viable cells are present. To measure the presence of ATP produced by living cells, a reagent mixture, CellTiter Glo ® Reagent, is added containing components lysing the cells and the enzyme luciferase that produce bioluminescence in an ATP-dependent reaction. When the CellTiter Glo® Reagent is added to the cell culture, the cells are lysed, and ATP leaks out to engage in

the luciferase reaction. The amount of luminescence signal produced is proportional to the amount of ATP present. The protocol for this assay was collected from Promega [74].

Protocol

Cells were seeded (30 000 cells/well) (50 µl) in a 96-well opaque-walled multi plate (Corning Costar® plate, #3610). The cells were stimulated with drugs (50 µl) and incubated at 37˚C, 5% CO_2 for 4 or 24 h. When there was 30 minutes left of incubation-time, both the cells and the CellTiter Glo® Reagent (premade CellTiter Glo buffer diluted 1:1 with substrate) were equilibrated to room temperature. After incubation, 70 µl of the CellTiter Glo® Reagent was added to each well, mixed for 2 min to induce cell lysis and incubated at room temperature for 10 min to let the luciferase reaction run. The plate was, after incubation, recorded using VICTOR^3 ™ 1420 Multilabel counter (PerkinElmer, Waltham, Massachusetts, USA), measuring the amount of luminescent light emitting from each sample. The result was given as luciferase units in each well that was converted to relative luciferase units (RLU) in percentage where the control was set to 100%.

3.4.2 Annexin V/Propidium iodide Staining Assay

While CellTiter Glo® assay only detects the ATP-levels produced by living cells, not separating between cell death and inhibited proliferation, Annexin V/Propidium iodide staining assay can distinguish between living, apoptotic and late apoptotic/necrotic cells, thus providing more detailed information about cell viability. In addition of a binding buffer (BB) containing components necessary for proper staining, the Annexin V/Propidium iodide staining protocol includes a fluorescein isothiocyanate (FITC) conjugated form of Annexin V with a green colour and a red fluorescent DNA-intercalating agent, propidium iodide.

During the early stages of apoptosis most cells will alter their organization of plasma membrane phospholipids by placing the normally cytoplasmic faced phosphatidylserines (PSs) on the extracellular surface of the plasma membrane. Annexin V binds these PSs that are exposed on the surface in a calcium-dependent manner thereby marking the apoptotic cells. However, due to membrane decomposition during necrosis, Annexin V will also bind to intracellular PSs in necrotic cells. Therefore, in order to distinguish between apoptotic and necrotic cells, propidium iodide is added. Propidium iodide intercalates into DNA and do not have the ability to pass through the plasma membrane. As a result of that, propidium iodide usually is excluded from viable and apoptotic cells and can be used to identify necrotic cells.

To sum up, viable cells will remain unstained due to no PS exposure and no membrane-disintegration, apoptotic cells will be Annexin V positive because of PS exposure and propidium iodide negative due to no membrane-disintegration. Lastly, necrotic/late apoptotic cells will stain positive for both Annexin V and propidium iodide due to PS exposure and membrane disintegration.

Protocol

Cells (60 000 cells/ml) were seeded (100 µl) in a 96-well plate, stimulated with drugs (100 µl) in duplicates and incubated at 37˚C for 4 h or 24 h. All the steps after incubation were performed on ice. After incubation, the cells were transferred to cold flow-tubes, washed 1x in cold phosphate-buffered saline (PBS) and spun down (4˚C, 1500 rpm, 5 min) before decanting and dissolving the sample pellet.

To stain the cells, Annexin-V-FITC kit including BB and PI (Tau technologies, #A700) was used. BB was diluted 1:10 in deionized water with a total volume that would give 300 µl/sample before adding Annexin V (0,25 µl/sample) to the BB mix. 300 µl of the BB and Annexin V mixture was added to each sample. The samples were then mixed and incubated on ice protected from light for 30 min. After incubation, propidium iodide (2 µl/sample) and BB (50 µl/sample) were mixed and added to the samples shortly before they were analysed on BD LSR II Flowcytometer (BD, Bioscience, USA). Results from the flow cytometry were analysed in a software called FlowJo performed by a technician in the myeloma group, thus concluding the amount of viable, apoptotic and necrotic cells in each sample. Final results are given as % viable cells.

3.5 Protein isolation

Cells were harvested, spun down (4˚C, 1500 rpm, 8 min) and washed 1x with cold PBS. The cells were then lysed using an 8 M Urea lysis buffer (30-40 µl for 1 million cells) or TritonX-100 (TX100) lysis buffer (Appendix 8.1 and 8.2), vortexed 3x15 seconds with 30 seconds of rest on ice in between and lastly incubated on a shaker (4˚C, 1500 rpm, 30-60 min). After shaking, the lysates were spun down (4˚C, 13 000 rpm, 15 min) and the supernatant was transferred to a new tube before proteins of interest were examined by western blotting. The protein extracts were stored at -80˚C.

3.6 Measuring protein concentration with BioRad Protein Assay

The protein concentration for each sample protein extract had to be measured using the BioRad Protein Assay and adjusted to equal concentrations. Adjusting the samples to an equal concentration before detection was important in order to compare the level of protein detected between samples and to use as similar protein amount as possible from each sample in the western blot gel electrophoresis. The reagent used for this assay was prepared by diluting BioRad Protein Assay Reagent concentrate (BioRad, #500-0006) 1:5 in Milli-Q (MQ)-water. The BioRad Reagent was protected from light due to light sensitivity. The samples were diluted 1:1000 in BioRad Reagent, with duplicates for each condition, and the blank consisted of the lysis buffer diluted 1:1000 in BioRad Reagent. The reagent-sample mix was incubated for 10 minutes in room temperature, protected from light, before the absorbance was measured on a spectrophotometer (Genesys20, 595 nm). The average from each duplicate was used to calculate the protein concentration using the formula below. The constant (C = 21) used in this equation is based on a previously performed standard curve prepared from serial dilutions with a known concentration of bovine serum albumin (BSA).

$$Protein\ concentration\ (\mu g/\mu l) = \frac{mean\ OD595\ nM\ \times\ dilution\ factor\ \times\ C}{1000}$$

3.7 Western Blot

Western blot (WB) is a widely used technique for protein detection. First the proteins are denatured to give them a linearly form and mixed with a reducing agent, such as dithiothreitol (DTT), to give them a net negative charge. The proteins are separated by size, measured in kilodaltons (kDa), using sodium dodecyl sulfate–polyacrylamide gel electrophoresis (SDS-PAGE) where they will run towards the positively charged end when voltage is applied. Gels can have different concentrations of acrylamide, determining the pore-size of the gel. Low percentage represents a gel with large pores that allows smaller proteins to drift faster, and high percentage represents a gel with small pores that makes the small proteins drift slower. After gel electrophoresis, the proteins are transferred to a blotting membrane to make them accessible for detection with antibodies. The proteins are transferred by an electric current pulling the negatively charged proteins towards a positively charged end and onto the blotting membrane. Next, the membrane is blocked to prevent unspecific binding of antibodies to the blotting membrane during protein detection. Finally, specific primary and secondary antibodies are sequentially put onto the membrane to detect proteins of interest.

3.7.1 Polyacrylamide gel electrophoresis

After measuring the protein concentration in each sample, the samples were diluted to equal concentrations in 10 mM Tris-HCl (pH 8,0). After diluting the samples, 9 µl sample buffer was added to denature and create a net negative charge of the proteins. Sample buffer was prepared by diluting 1 M DTT (AppliChem, #A3668) 1:5 in 4X lithium dodecyl sulfate (LDS) buffer (NuPAGE® Invitrogen, #NP007). The samples were then heated on an 80˚C warming block for 10 min to ensure protein denaturation. Furthermore, loading mix (4X LDS diluted 1:4 in 10 mM Tris-HCl) and an Odyssey one-color protein molecular weight marker (IR Dye 800CW, LI-COR Bioscience, #926-32211) (4 µl odyssey ladder IR dye in 23 µl loading mix) were prepared.

The proteins were separated using a 4-12% polyacrylamide gel (NuPAGE® Novex® BIS-Tris Invitrogen, #NP0321BOX, #NP0322BOX, #WG1402BOX) with a pore size gradient that was fitting for the proteins to be detected. The selected gel was put in a Xcell Surelock Mini-Cell chamber (Nupage, Life Technology), and filled up with 1X 3-(N-morpholino) propanesulfonic acid (MOPS) running buffer (20X MOPS (NuPAGE Invitrogen, #NP0001-02) diluted 1:20 in distilled water). The gel electrophoresis was run at 200 V for 45 min.

3.7.2 Blotting

Blotting was performed using the iBlot™ 2 Dry Blotting System (ThermoFisher, Invitrogen, IB21001). After gel electrophoresis, the gel was placed on top of a nitrocellulose blotting membrane and placed inside the iBlot™ 2 Dry Blotting chamber. The blotting was run at 20V (1 min), 23V (4 min) and 25V (2 min).

3.7.3 Membrane blocking and immunostaining

Blocking the membrane was necessary to prevent unspecific binding of antibodies to the membrane during immunostaining. After blotting, the membrane was put in a fitting tube with the protein side facing the centre and added blocking buffer (ca 10 ml) for incubation on a roller (room temperature, 1 h in the dark). Blocking buffer was made by diluting Odyssey Blocking buffer (LI-COR Biosciences, #927-50000) 1:1 with 1X Tris-buffered saline (TBS) added 0,1% Tween20, TBST.

Blocking buffer was also used to dilute the primary and secondary antibodies used for fluorescent immunostaining of specific proteins. The primary and secondary antibodies used in this thesis is listed in Table 1 and Table 2, respectably. Immunostaining was performed by first adding the primary antibody to the membrane and incubating it on a roller overnight/1 h at 4˚C. Next, the membrane was washed 3x10 min with TBST before adding the secondary antibody and incubating it on a roller (1 h, dark) followed by another wash 3x10 min with TBS. After the last washing step, the membrane was dried before detecting the results on Odyssey Cl-x scanner (LI-COR).

***Table 1**: Primary antibodies used for immunostaining*

Antibody	**Species**	**Manufacturer**	**Dilution**	**Molecular weight**
IgK	Rabbit Monoclonal IgG	Abcam #ab134930	1:20 000	25 kDa
IRE1α	Rabbit Monoclonal IgG	Cell Signaling #3294S	1:1000	130 kDa
p-IRE1α	Rabbit Monoclonal IgG	Abcam #ab124945	1:5000	110 kDa
p-elf2α	Rabbit Monoclonal IgG	Cell Signaling #3597	1:1000	38 kDa
ATF6	Mouse Monoclonal IgG	Abcam #ab122897	1:1000	90 kDa (full length) 50 kDa (cleaved)
SQSTM1/p62	Guinea pig Polyclonal	Progen #GP62C	1:1000	52 kDa
LC3B	Rabbit Monoclonal IgG	Cell Signaling #3868	1:1000	14 kDa (LC3-II) 16 kDa (LC3-I)
TRIB3	Rabbit Polyclonal	Sigma Aldrich #HPA015272	1:200	45 kDa
GAPDH	Mouse Monoclonal IgG	Abcam #ab8245	1:30 000	37 kDa

***Table 2**: Secondary antibodies used for immunostaining*

Antibody	**Manufacturer**	**Dilution**
Goat anti-Rabbit IgG IR-Dye 800 CW	LI-COR Bioscience, #926-32211	1:5000
Donkey anti-Guinea pig IR-Dye 680 RD	LI-COR, Bioscience, #926-68077	1:10 000
Goat anti-Mouse IgG IR-Dye 680 RD	LI-COR Bioscience, #926-68070	1:10 000

3.8 Protein-fraction protocol

A protein-fraction protocol was used to see how different drugs affected the distribution and handling of proteins and protein aggregates in the MM cells. The cell suspension from each sample was divided into three different protein fractions; medium fraction (extracellular components), detergent soluble fraction and detergent resistant fraction (dense structures, protein aggregates). Cells were seeded (300 000 cells/ml) in 75 cm^2 flasks (30 ml) per condition and stimulated with the desired drugs and concentrations. After a 4 h incubation (5% CO_2-atmosphere, 37˚C), the cells were spun down (4˚C, 1000xg, 10 min). After this step, the supernatant and pellet were to be handled separately. The supernatant would represent the medium fraction and the pellet would represent the intracellular protein distribution, divided into detergent soluble and detergent resistant fraction.

3.8.1 Medium fraction

The supernatant was transferred to a new tube and spun down again (4˚C, 1000xg, 10 min). After the second centrifugation of the medium, 27 ml of the supernatant was transferred to a high-speed centrifugation tube (Thermo Scientific Nalgene®, #3139-0050, 50 ml) and spun down (4˚C, 45 000xg, 30 min) on a sorvall centrifuge (Thermo Scientific). The supernatant was discharged, and the pellet resuspended and washed 1x in 1 ml cold PBS before transferring the resuspended pellet to eppendorf (EP)-tubes and spun down (4˚C, 21 000xg, 30 min). The pellets were lysed in 20 µl 8 M Urea lysis buffer, vortexed (3x15 seconds) and stored at -80˚C until ready for WB analysis.

3.8.2 Detergent soluble and detergent resistant fraction

After pelleting the cells in the first centrifugation step, the cell pellet was washed 1x in cold PBS, transferred to EP-tubes and spun again (4˚C, 430xg, 10 min). The pellet was lysed in 500 µl TX100 lysis buffer and the samples were spun (4˚C, 1000xg, 10 min). The supernatant was transferred to new tubes and the protein concentration was measured using BioRad Protein Assay and adjusted to an equal concentration using the TX100 lysis buffer. This was performed to avoid that differences in protein level on WB was not due to a difference in the protein concentration between the samples. After adjusting the protein concentration, the samples were spun (4˚C, 10 000xg, 10 min) and the supernatant was determined the detergent soluble fraction while the pellet was further resuspended in 8 M Urea lysis buffer (20 µl) and determined the detergent resistant fraction. The samples were stored at -80˚C until ready for

WB analysis. Figure 10 illustrates the different steps in order to divide the samples after stimulation and incubation.

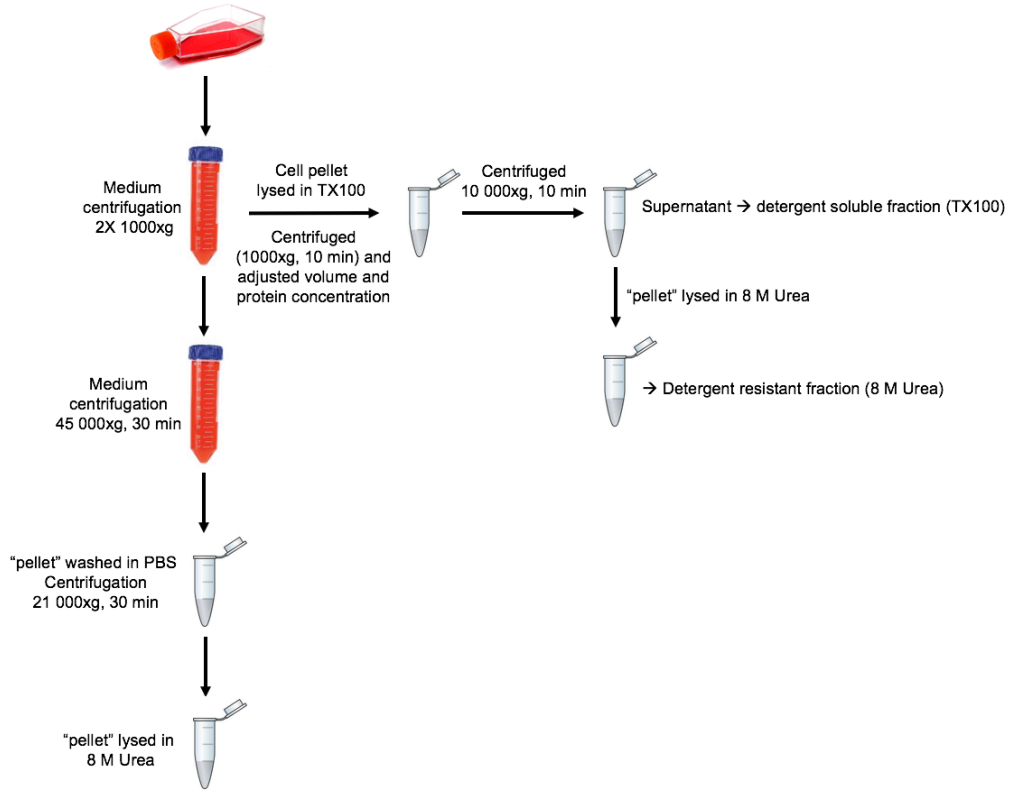

***Figure 10**: **Illustration of the different steps in the protein-fraction protocol**, where the proteins are separated into medium fraction (8 M Urea lysate), a detergent soluble fraction (TX100 lysate) and detergent resistant fraction (8 M Urea lysate) after stimulation and incubation.*

3.8.3 Protein-fraction detection

The protocol continued with performing a WB assay, as described in section 3.7, where 20 µl from each fraction sample was mixed with 7,5 µl sample buffer before heating and loading onto gel. After protein detection, the localization of the proteins can be assessed. If most of the protein can be observed in either the detergent soluble or detergent resistant fraction, the protein is mostly kept intracellular. An increase of protein in the detergent resistant fraction indicate that it is located in dense structures such as protein aggregates. If there is an increase of protein in medium fraction, the protein is located in the extracellular matrix, here medium.

To exclude that proteins detected in the medium fraction/extracellularly were due to cell death a CellTiter® Glo assay was performed simultaneously as the protein-fraction protocol. After incubation, aliquots (100 µl) from each condition were seeded in a 96-well opaque-walled multi plate (Corning Costar® plate, #3610) with triplicates for each condition and

equilibrated to room temperature before the rest of the CellTiter® Glo protocol was carried out as described in section 3.4.1.

3.9 Agarose gel electrophoresis

Agarose gel electrophoresis is a standard laboratory technique for separating DNA fragments by size (number of base pairs (bp)) and was used in this project for both visualization and purification of DNA fragments in assays such as Zero Blunt® Polymerase Chain Reaction (PCR) Cloning and lentiviral transduction, as described later. The principle for separating the DNA fragments are similar for the separation of proteins by polyacrylamide gel electrophoresis. DNA is negatively charged, and when voltage is applied, the DNA fragments will run towards the positively charged end. Further, the concentration of agarose in the gel determines the pore-size and thus the migration of the DNA fragments, where a low percentage of agarose (i.e. 0,7%) represents a large pore size and a high percentage of agarose (i.e. 3%) represents a small pore size.

Protocol

A 2% agarose solution was made by mixing 0,8 g SeaKem® LE Agarose (Lonza, #50004) with premade 0,5X tris acetate ethylenediaminetetraacetic acid (EDTA) (TAE) Buffer (40 ml) and melting the agarose in a microwave oven. The solution was equilibrated to 60˚C before use. When preparing the gel, 0,1 µl GelRed® Nucleic Acid Gel Stain (Biotin, #41003) was added per 10 ml agarose solution and mixed before pouring the solution into a gel tray with a well-comb. The gel was settled for about 20-30 min before the gel tray was placed in the electrophoresis unit where it was covered with 0,5X TAE Buffer before removing the well-comb. 2-log DNA Ladder (Biolabs, #N3200L) was prepared by diluting it in MQ-water to a concentration of 10 ng/µl before the ladder and samples were prepared for gel loading by adding 6X Gel Loading Dye, Purple (Biolabs, #BI0245). The gel was run at 90V for 60 min before detecting the result in Gel Logic 212 PRO (Carestream).

3.10 DNA and RNA isolation

Isolation of DNA and RNA from MM cell lines was performed in order to carry out assays such as Zero Blunt® PCR Cloning and quantitative real-time PCR (qRT-PCR), as described later. The Allprep DNA/RNA Mini Kit (QIAGEN®, #80204) was used for isolating DNA and RNA in this project. From the Allprep DNA/RNA Mini Handbook, the protocol

‘Simultaneous Purification of Genomic DNA and Total RNA from Animal Cells’ was used [75]. In short, one million cells per sample were pelleted and lysed in Buffer RLT Plus (350 µl). Next, the lysates were homogenized by vortexing (2 min) before transferring each sample to an Allprep DNA spin column placed in a collection tube and spinning them (8000xg, 30 seconds). The Allprep DNA spin column was placed in a new collection tube and stored at room temperature awaiting DNA isolation, and the flow-through was used for RNA isolation.

70% ethanol (350 µl) was mixed into the flow-through before transferring 700 µl of the sample to a RNeasy spin column. The column was spun (8000xg, 15 seconds) and the flow-through was discarded. Next, Buffer RW1 (700 µl) was added and the column was spun (8000xg, 15 seconds) before two wash-steps using Buffer RPE (500 µl). The RNeasy spin column was placed in a new collection tube and spun at full speed for 1 min to eliminate any carryover from Buffer RPE. Finally, RNase-Free water (30 µl) was added to the RNeasy spin column, now placed in an EP-tube, and incubated (2 min at room temperature) before eluting RNA (8000xg, 1 min).

For the DNA isolation, Buffer AW1 and AW2 (500 µl) was sequentially added to the Allprep DNA spin column and spun down (8000xg, 15 seconds and full speed, 2 min, respectively). Lastly, the Allprep DNA spin column, placed in an EP-tube, was added Buffer EB (50 µl) and incubated (2-3 min at room temperature) before eluting DNA (8000xg, 1 min). The concentration and purity of the isolated RNA and DNA was determined using Nanodrop™ (Thermo Fisher Scientific, ND-1000).

3.11 RNA to cDNA

Complementary DNA (cDNA) was made in order to carry out the Zero Blunt® PCR Cloning and qRT-PCR of the INA-6 IgK KO cell clones and IgK control cell clones, as described later. The High Capacity RNA-to-cDNA Kit (Applied Biosystems, #4387406) was used to perform reverse transcription of total RNA to single-stranded cDNA [76]. In short, 1 µg purified RNA (up to 9 µl) was mixed with 2X RT Buffer (5 µl), 20X RT Enzyme Mix (0,5 µl) and Nuclease-Free water to a total volume of 10 µl reaction mix. The reaction mix was placed on ice before starting the reverse transcription using a thermal cycler and the steps shown in Table 3.

***Table 3**: Overview of the thermal cycler steps used to perform reverse transcription of total RNA to cDNA*

	Step 1	**Step 2**	**Step 3**
Temperature	37˚C	95˚C	4˚C
Time	60 min	5 min	∞

3.12 Zero Blunt® PCR Cloning

The Zero Blunt® PCR Cloning was performed in the INA-6 IgK KO cell clones and IgK control cell clones in order to prepare them for sequencing of the *IgK* gene to find out exactly how the DNA sequence had been altered in the five IgK KO cell clones or, for the IgK control cell clones, to test that they contained a normal *IgK* DNA sequence.

In Zero Blunt® PCR Cloning, blunt-ended DNA fragments are ligated into a pCR-Blunt® vector. First, a PCR is performed generating blunt-ended PCR products. This is done by using a DNA polymerase other than Taq DNA polymerase which produce PCR products with an overhang of unpaired nucleotides and not a blunt end. Following is a ligation reaction inserting the blunt PCR fragments into the pCR-Blunt® vector. This vector contains a lethal E. coli gene, *ccdB (control of cell death B)*, that is fused with the C-terminal end of *LacZα*. When expressed, the *ccdB* gene is toxic for the bacterial cell thus inhibiting its growth but when a blunt-ended PCR product is ligated into the vector, the expression of LacZα-ccdB fusion gene is disrupted because the ligation takes place in part of the *LacZα* gene. This inhibits the expression of the *ccdB* gene and result in a positive selection of bacteria containing the blunt PCR ligate.

After ligation, the plasmid is transformed into competent E. coli which are spread on selective lysogeny broth (LB) agar plates. The pCR-Blunt® vector encodes a Kanamycin resistance which is transmitted to the bacterial cells containing the plasmid, thus allowing it to grow on LB agar plates which contain Kanamycin and inhibiting growth of other bacterial colonies. In this way, the bacterial colonies growing on the agar plates should only be colonies transformed with the blunt PCR ligated plasmid, ready for isolation and sequencing.

3.12.1 Generating blunt PCR product

The Zero Blunt® PCR Cloning Kit (Invitrogen, #44-0302) and user guide were used to perform this assay, but some deviations from the original guide was performed as further explained [77]. The kit used to generate the blunt PCR product from cDNA, was the KAPA HiFi HotStart ReadyMix (Roche Life Science, KK2601, #07958927001) using 100 ng cDNA template, 0,6 µM of each primer, *IgK* specific primers and the PCR run setup shown in Table 4.

Forward primer: IgKV3-11_F (Sigma Aldrich)
5'-AGGACCCAGAGGGAACCATG-3'

Reverse primer: IgKC-Full-Length-R (Sigma Aldrich)
5'-CTAACACTCTCCCCTGTTGAAG-3'

***Table 4**: PCR cycling setup for generating blunt PCR products*

Step	Temperature	Duration	Cycles
Initial denaturation	95˚C	3 min	1
Denaturation	98˚C	20 sec	28
Annealing	62˚C	15 sec	
Extension	72˚C	30 sec/kb	
Final Extension	72˚C	1 min/kb	1

3.12.2 Purification of blunt PCR product

After the PCR, an agarose gel electrophoresis was run in order to verify that the right PCR product had been made, with an expected length ~700 bp (Appendix 8.3). Following this step was the PCR purification where the QIAquick® PCR purification Kit (QIAGEN®, #28106) was used instead of the purification protocol described in the Zero Blunt® PCR Cloning user guide. In short, 5 volumes of Buffer PB was added to 1 volume of the PCR mix before transferring the sample to a QIAquick spin column. The column was spun (16100xg, 1 min) and the flow-through was discarded. Next, the column was washed by adding Buffer PE (750 µl) and spinning the column (16100xg, 1 min). The flow-through was discarded and the column was spun (16100xg, 1 min) to remove residual buffer. The column was placed in an EP-tube and incubated for 2 min after adding Buffer EB (30 µl). The PCR product was eluted

by spinning the column (16100xg, 1 min). The concentration and purity of the PCR product was measured by NanoDrop™.

3.12.3 Ligation into pCR-Blunt® vector and transformation into competent E. coli

Next, the purified blunt PCR product was to be ligated into the pCR-Blunt® vector in order to clone the *IgK* gene from each sample, where a 10:1 insert:vector molar ratio was used. The formula provided to estimate the amount of PCR product needed for the 10:1 insert:vector molar ratio is shown below. In the formula, y is the number of bp in the *IgK* gene, making y = 694 bp. The amount of insert was therefore estimated to be 49,57 ng.

$$x\ ng\ insert = \frac{(10)(y\ bp\ PCR\ product)(25\ ng\ linearized\ pCR - Blunt®)}{(3500\ bp\ pCR - Blunt®)}$$

A 10 µl ligation reaction mix was made by mixing 25 ng of pCR-Blunt® vector (1 µl), 49,57 ng blunt-ended PCR product (1-5 µl), 5X ExpressLink™ T4 DNA Ligase Buffer (2 µl), ExpressLink™ T4 DNA Ligase (5 U/µl) (1 µl) and sterile water to a total volume of 10 µl. The ligation reaction was run for 1 h to increase the cloning efficiency. Following, the ligated pCR-Blunt® vector was transformed into competent E. coli. One Shot® TOP10 cells (Invitrogen, #C404003) (50 µl) thawed on ice before adding 2 µl of the ligation reaction mix for a 30 min incubation on ice. After incubation on ice, the sample was heat-shocked at 42˚C for 45 s before putting the sample on ice again for 2 min. Room temperatured super optimal broth with catabolite repression (SOC) medium (250 µl) was added to the sample before incubation on a shaker for 1 h (37˚C, 250 rpm). After incubation, the sample was spread onto a selective LB agar plate (50 µg/ml Kanamycin) for overnight incubation (37˚C).

3.12.4 Detecting positive transformants and sample sequencing

Before isolating DNA and sending samples in for sequencing, the positive transformants (bacterial cell colonies with ligated insert present) had to be verified. Therefore, a PCR and an agarose gel electrophoresis were performed. For PCR, the Platinum™ PCR SuperMix High Fidelity Kit (Invitrogen, #12532-016), a segment of a bacterial colony, 200 nM of each primer (IgKV3-11_F and IgKC-Full-Length-R) and the PCR run setup in Table 5 were used. The PCR product was detected using gel electrophoresis, where a DNA fragment at ~700 bp verified a correct insert.

***Table 5**: PCR run setup for detection of positive transformants*

Step	Temperature	Duration	Cycles
Initial denaturation	94˚C	10 min	1
Denaturation	94˚C	20 sec	28
Annealing	62˚C	15 sec	
Extension	68˚C	1 min/kb	
Final Extension	72˚C	10 min/kb	1

Five verified positive transformants from each of the INA-6 IgK KO cell clones and IgK control cell clones were next prepared for sequencing by growing the chosen colonies overnight (37˚C, 250 rpm) in Falcon tubes containing 2 ml LB medium (50 µg/ml Kanamycin) before isolating the plasmids using QIAprep® Spin Miniprep Kit (QIAGEN®, #27106) [78]. In short, the overnight bacterial culture was pelleted by centrifugation (2800xg, 6 min), resuspended in Buffer P1 (250 µl) and transferred to EP-tubes. The sample was mixed with Buffer N3 (350 µl) before spinning (16100xg, 10 min). The supernatant (800 µl) was transferred to a QIAprep 2.0 spin column and spun (16100xg, 1 min). Next, the column was washed twice. First with Buffer PB (500 µl) and second with Buffer PE (750 µl) with centrifugation (16100xg, 1 min) in between and after. The column was centrifuged for another 1 min to remove residual buffer. The column was placed in an EP-tube and incubated for 2 min after adding Buffer EB (50 µl). The PCR product was eluted by spinning the column (16100xg, 1 min). The concentration and purity of the sample was measured by NanoDrop™. Lastly, the samples were shipped to Eurofins Genomics for sequencing together with either one of the forward or reverse primer listed below.

Forward primer: M13-F (Sigma Aldrich)
5’-GTAAAACGACGGCCAG-3’

Reverse primer: M13-R (Sigma Aldrich)
5’-CAGGAAACAGCTATGAC-3’

3.13 Protein mass spectrometry of an INA-6 IgK KO cell clone and IgK control

Due to certain findings after sequencing of the *IgK* gene in the INA-6 IgK KO cell clones and IgK control cell clones, it was of interest to investigate whether these finding would be reflected in an assay looking at IgK on a protein level. Mass spectrometry is a laboratory technique used for, among other things, accurate mass determination and characterization of proteins and was in this project used to quantify the level of IgK protein between an IgK KO clone and an IgK control clone. One of the IgK KO clones and one IgK control (Ctr) clone was chosen for this assay as a representative for the remaining IgK KO cell clones and IgK control cell clones. The representatives, IgK KO 2 and IgK Ctr 1, were randomly chosen. Total protein extracts were made from 1 million cells from each cell line by lysing them in 8 M Urea Lysis Buffer before being analysed by the core facility Proteomics and Modomics Experimental Core Facility (PROMEC) at NTNU.

3.14 qRT-PCR of INA-6 IgK KO cell clones and IgK control clones

It was of interest to see if there was any difference in the level of *IgK* RNA expression between the INA-6 IgK KO cell clones and IgK control clones. In order to find out how much of the *IgK* gene that got transcribed, a qRT-PCR assay was performed.

In conventional PCR, the amplified product is detected by an end-point analysis, meaning that the PCR product is detected when the PCR reaction is in its non-exponential plateau phase. The product is here usually used for visualization by gel electrophoresis, sequencing or cloned into plasmid for further experiments. In quantitative real-time PCR, on the other hand, the amplified product is measured after each reaction cycle, giving a real time quantification measurement of the product. There are two common methods for detecting the PCR product after each cycle. The first one uses sequence-specific fluorogenic probes of DNA, called TaqMan probes, while the other method involves a non-specific fluorescent dye that will bind to any double stranded DNA, called SYBR Green, which is used in this assay [79, 80]. During denaturation, the SYBR Green dye will be released and the fluorescent light will rapidly decrease. During polymerization of the template strand, the SYBR Green dye will bind as the double stranded PCR product is made and the amount of fluorescent light will increase. When the polymerization step is completed, SYBR Green will be bound to all the double stranded PCR product resulting in a net increase of fluorescent light. As the PCR cycle reactions will

continue to create more double stranded PCR products, more SYBR Green will be bound in a proportional manner [80].

The results of a qRT-PCR will be an exponential amplification curve (Figure 11). This curve is divided into two phases: the exponential phase and the non-exponential plateau phase. Initially in the exponential phase, the fluorescence levels are below the threshold line and are not detectable even though the PCR product accumulates exponentially. After a number of cycles, the fluorescence reaches a detectable level and the exponential growth can be observed on the plot. The number of cycles run when this occurs is called the quantification cycle (C_q or C_T). A low C_q means that there is a lot of template present in the sample initially, and a high C_q means that there is a lower level of template initially [79].

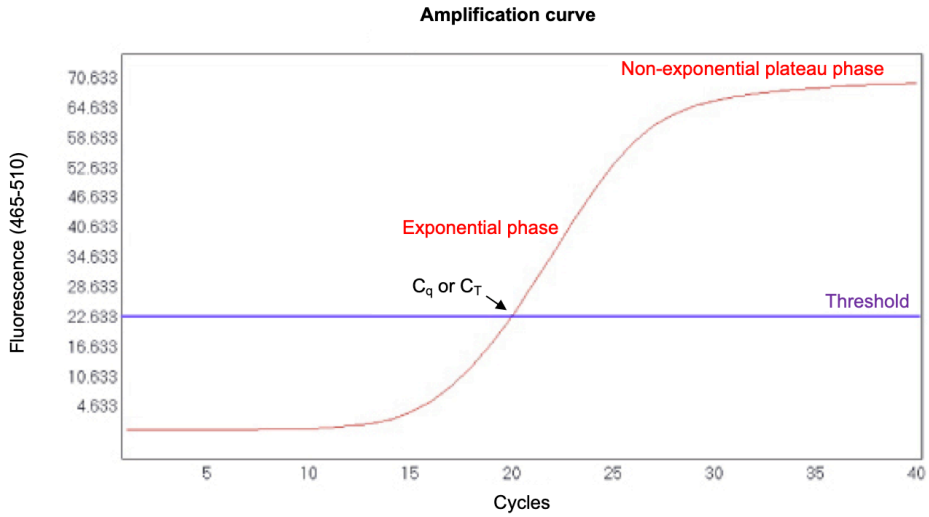

Figure 11: Illustration of an amplification curve after performing qRT-PCR. *The figure shows an exponential amplification curve divided into two phases; the exponential phase and the non-exponential plateau phase. In the exponential phase, the PCR product is amplified exponentially, and the non-exponential plateau phase is where the amplification slows down due to consummation of reaction components. C_q is where the amount of PCR product reaches a detectable level over the threshold line. The figure is adopted and edited from [81].*

Protocol

qRT-PCR was in this assay used to quantify the amount of *IgK* RNA produced in the IgK KO and IgK control cells. The qRT-PCR was performed by using the PerfeCTa® SYBR® Green FastMix®, ROX™ (Quantabio, #84071) [82] that contain all components needed for the PCR reaction except primers and template. In order to quantify the levels of *IgK* in the different cell lines, Glyceraldehyde 3-phosphate dehydrogenase (*GAPDH)*, was used as a housekeeping gene. The primers used for *IgK* and *GAPDH* is presented below.

Forward primer: IgKV3-11_R: (Sigma Aldrich)
5'-GCCTGGTACCAACAGAAACC-3'

Revers primer: IgK_constant-1: (Sigma Aldrich)
5'-GGCGGGAAGATGAAGACAGA-3'

Forward primer: GAPDH-F (Sigma Aldrich)
5'- CGAGATCCCTCCAAAATCAA -3'

Revers primer: GAPDH-R (Sigma Aldrich)
5'- TTCACACCCATGACGAACAT -3'

Reaction mixes (20 µl) were made with triplicates for each sample condition containing 2X PerfeCTa® SYBR® Green FastMix®, ROX™, forward primer (300 nM), reverse primer (300 nM), cDNA template (10 ng) and nuclease-free water (up to 20 µl). After sealing and mixing the samples, the PCR cycling was performed as shown in Table 6.

***Table 6**: qRT-PCR setup for detection of IgK and GAPDH in INA-6 IgK KO cell clones and IgK controls*

Step	Temperature	Time	
Initial denaturation	95°C	2 min	
PCR cycling	95°C	3 sec	40 cycles
	60°C	20 sec	
Dissociation stage	95°C	15 sec	Melting curve
	60°C	1 min	
	95°C	15 sec	

The C_q from each sample was used to calculate the relative quantification of RNA expression using IgK Ctr 1 as the control and the $\Delta\Delta C_q$ method for calculation of fold change expression level [83].

3.15 Attempting to overexpress SQSTM1 in an INA-6 SQSTM1 KO #3-2 cell line using lentiviral transduction

Lentiviral transduction was performed in an INA-6 SQSTM1 KO #3-2 cell line in an attempt to reintroduce the *SQSTM1* gene into the SQSTM1 KO cells. It was of interest to examine whether observed changes due to SQSTM1 KO would be reversed back to its normal manner of conduct.

3.15.1 Isolation of SQSTM1 KO #3-2 cells by dilution technique

To ensure that all the cells would be identical before the lentiviral transduction, an isolation of a single SQSTM1 KO clone was carried out. The cells were diluted to a concentration of 0,5 cell/well and seeded (100 µl/well) in two 96-well plates to increase the chances of only a single cell to end up in the well. The plates were incubated at 37ºC, 5% CO_2 atmosphere and monitored for a couple weeks to see if a single cell clone was established. As the clones expanded, they were sub-cultivated to a 6-well plate in order to allow the clone to expand. After a couple of weeks, they were moved into separate flasks. One of the clones, referred to as SQSTM1 KO #3-2 clone 3, was randomly chosen for further cultivation and experiments since all the clones had similar density and seemed capable.

3.15.2 Principles of lentiviral transduction

Lentiviral vectors are one of the most used viral vectors when transducing cells with different genes. After inserting a gene specific sequence into a lentiviral vector, the cells are infected with the virus. In this way, the specific gene sequence is integrated into the target cells genome and expressed. The lentivirus can integrate their genome into both dividing and non-dividing cells due to its complex structure containing all the essential genes needed.

Gateway cloning technology was used to generate a *SQSTM1* expression vector. Gateway cloning technology uses site-specific recombination of so-called “Gateway att” sites to first, create an entry clone with the gene of interest which is then used to create an expression vector carrying the gene (Figure 12). The first step is carried out by a BP reaction where an attB flanked PCR product with the gene is recombined with a special plasmid called a donor vector resulting in an entry clone. The entry clone, containing the gene now flanked with attL, is further used in an LR reaction where it is recombined with a destination vector resulting in an expression vector containing the gene of interest.

A previous made entry clone (pENTRY-SQSTM1, made by post.doc researcher Sagar R. Darvekar) containing the *SQSTM1* gene was used, so performing the BP reaction was not necessary. Thus the protocol for lentiviral transduction could start directly with the LR reaction. The destination vector used to make the *SQSTM1* expression vector and a control expression vector, contain a green fluorescent protein (GFP). The GFP would mark the transfected cells with a green fluorescent tag.

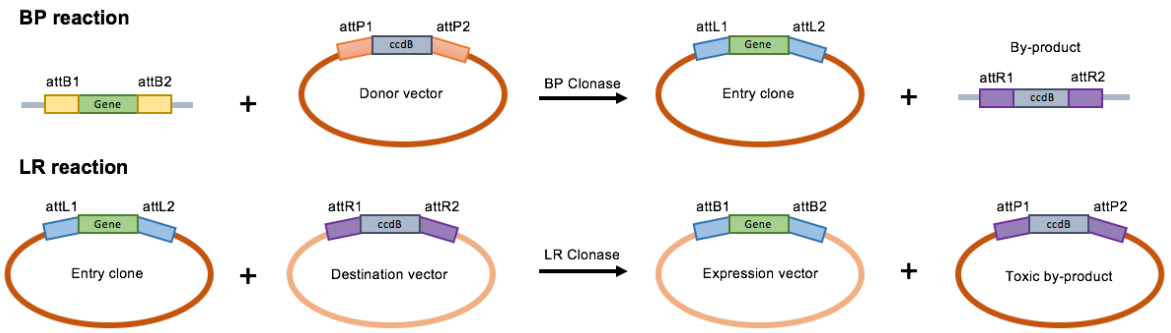

***Figure 12**: **An illustration of the Gateway reactions** showing the different types of plasmids and enzymes involved in both the BP (attB + attP recombination sites) and LR (attL + attR recombination sites) reaction. The LR reaction result in a lentiviral expression vector that is able to infect and integrate its genome into target cells.*

3.15.3 Mutating the pENTRY-SQSTM1 plasmid

Before making the *SQSTM1-GFP* fusion gene expression vector, the *SQSTM1* stop codon had to be removed in order for the GFP tag to be expressed in the transduced cells. Sequencing of a SQSTM1-GFP expression plasmid showed that a deletion of one stop-codon nucleotide would be sufficient to obtain a *SQSTM1-GFP* fusion gene (Figure 13). Since the entry clone (ca 3,6 kb) is of much smaller size than the expression vector (ca 10 kb), it was assumed that the *SQSTM1* stop-codon would be more easily mutated in the entry clone.

The QuikChange Site-Directed Mutagenesis Kit (Agilent Technologies, #200519-5) was used to mutate the pENTRY-SQSTM1 clone [84]. The primers designed for this assay, containing the desired mutation, are listed below.

Forward primer: Q5-Mut-SQSTM1_stop-F (Sigma Aldrich)
5′-GCATCCCCCGCCGTTGTACCACTTTTGC-3′

Reverse primer: Q5_Mut_SQSTM1_stop_R (Sigma Aldrich)
5′-GCAAAAGTGGTACAACGGCGGGGGATGC-3′

A 50 µl reaction mix containing 10X reaction buffer (5 µl), pENTRY-SQSTM1 plasmid (26 ng), forward (125 ng) and reverse (125 ng) primer, dNTP mix (1 µl), MQ-water up to a total volume of 50 µl and PfuTurbo DNA polymerase (2.5 U/µl) (1 µl) was made and the cycling parameters for the PCR was set up as shown in Table 7.

***Table 7**: PCR run setup as part of the QuikChange Site-Directed Mutagenesis of the pENTRY-SQSTM1 plasmid*

Cycles	Temperature	Time
1	95°C	30 seconds
16	95°C	30 seconds
	55°C	1 min
	68°C	3 min 36 seconds

After a Dpn I restriction enzyme (10 U/µl) (1 µl) was added to the PCR product to digest the non-mutated parental DNA templates (37°C, 1 h), transformation of the mutated pENTRY-SQSTM1 plasmid into XL1-Blue supercompetent cells (Agilent Technologies, #200519-4) was performed as described previously using SOC media and selective LB agar plates containing Kanamycin (50 µg/ml). Colonies from the LB agar plate were prepared for plasmid isolation by growing the colonies overnight (37˚C, 250 rpm) in Falcon tubes containing 3 ml LB medium with Kanamycin (50 µg/ml). The plasmids were isolated using QIAprep® Spin Miniprep Kit (QIAGEN®, #27106). In order to verify that the correct plasmid had been obtained, the plasmids were sequenced by Eurofins Genomics using the primer listed below.

Forward primer: SQSTM1-End-F (Sigma Aldrich)
5'-ACCCACAGGGCTGAAGGAAG-3'

3.15.4 Making the SQSTM1-GFP expression vector

As the *SQSTM1* stop-codon now had been removed from the *SQSTM1* gene located in the entry clone, it was time to run the LR reaction, generating a SQSTM1-GFP expression vector ready for transduction into the INA-6 SQSTM1 KO #3-2 clone 3 cells (Figure 13C). The Gateway® LR Clonase™ II Enzyme Mix Kit (Invitrogen, #11791-020) was used to perform the LR reaction together with the entry clone and a destination vector, pLVU/GFP (Appendix 8.4). pLVU/GFP was a kind gift from Lars Ittner (Addgene plasmid #24177) [85].

The LR reaction was carried out as described in the product information sheet [86]. In short, the mutated pENTRY-SQSTM1 plasmid (142,8 ng/µl) was mixed with pLVU/GFP (141,8 ng/µl) and Tris EDTA (TE) Buffer (to a total volume of 8 µl) before adding the LR clonase™ II enzyme mix (2 µl). The reaction mix was incubated at room temperature for 1 h. To terminate the LR reaction, Proteinase K (1 µl) was added to the reaction mix before a 10 min incubation at 37˚C.

The SQSTM1-GFP expression vector was next transformed into competent DH5-α E. coli (3.12.3 Ligation into pCR-Blunt® vector and transformation into competent E. coli) and spread onto selective LB agar plates for overnight incubation (37˚C). The expression vector contained an antibiotic resistance against Ampicillin, meaning that the transformed competent DH5-α E. coli had to be grown on selective LB agar plates and medium containing Ampicillin (100 µg/ml). Clones from the selective LB agar plate were, after incubation, prepared for plasmid isolation by growing the colonies overnight (37˚C, 250 rpm) in Falcon tubes containing 3 ml LB medium with Ampicillin (100 µg/ml).

Before starting the plasmid isolation protocol, glycerol-stocks were made out of the transformed competent DH5-α E. coli for later use when preparing the plasmid for lentiviral transduction. The stocks were made by mixing 60% Glycerol (250 µl) with transformed competent DH5-α E. coli from overnight LB culture (750 µl) before storing the stock at -80˚C. QIAprep® Spin Miniprep Kit (QIAGEN®, #27106) was used for plasmid isolation, as described before, and the plasmids were shipped to Eurofins Genomics for sequencing verification with the SQSTM1-End-F primer.

A. Part of SQSTM1-GFP expression vector sequencing

CAAAGCATCCCCCGCCGTTGTGA C CAC TTT TGC CCA CCT CTT CTG CGT GAA TCG AAT
TCT AGA CTA GAC CCA GCT TTC TTG TAC AAA GTG GTT GAT ATC CAG CAC AGT GGC GGC
CGC TCG AGT CTA GAG GGC CCG CGG TTC GAA ATGGTGAGCAAGGGCGAGGAGC

B. Q5® Site-Directed Mutagenesis

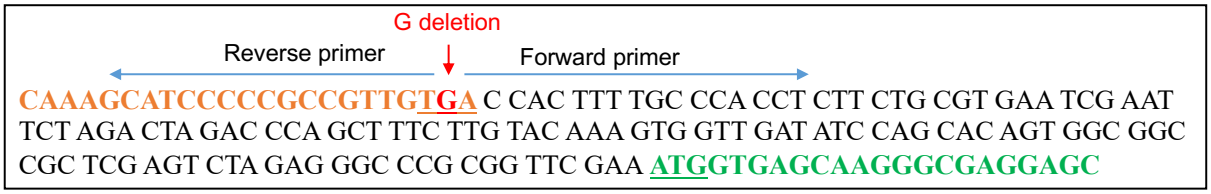

CAAAGCATCCCCCGCCGTTGTGA C CAC TTT TGC CCA CCT CTT CTG CGT GAA TCG AAT
TCT AGA CTA GAC CCA GCT TTC TTG TAC AAA GTG GTT GAT ATC CAG CAC AGT GGC GGC
CGC TCG AGT CTA GAG GGC CCG CGG TTC GAA ATGGTGAGCAAGGGCGAGGAGC

C. *SQSTM1-GFP* fusion gene after ligation

CAAAGCATCCCCCGCCGTTG TAC CAC TTT TGC CCA CCT CTT CTG CGT GAA TCG AAT
TCT AGA CTA GAC CCA GCT TTC TTG TAC AAA GTG GTT GAT ATC CAG CAC AGT GGC GGC
CGC TCG AGT CTA GAG GGC CCG CGG TTC GAA ATGGTGAGCAAGGGCGAGGAGC

***Figure 13**: **The sequence shown is a draft of the sequencing result of a SQSTM1-GFP expression vector**. Orange is the end of the SQSTM1 gene and green is the beginning of the GFP gene. The nucleotides in the middle are part of the plasmid. **A.** Illustrates the SQSTM1 stop-codon and the faulty reading-frame inhibiting a SQSTM1-GFP fusion gene. This illustrate what needed to be done with the SQSTM1 stop-codon in order to obtain the right reading-frame for SQSTM1-GFP fusion gene expression. **B.** Illustrates the deletion-method used for the Site-Directed Mutagenesis. Two primers designed in the QuikChange Primer Design program was used, excluding the G in the SQSTM1 stop-codon when running a PCR. Here, only one of the primers are shown as the other primer binds to the antisense strand of the plasmid. **C.** After the LR-reaction and ligation of the two generated strands, the new reading-frame resulted in a SQSTM1-GFP fusion gene.*

3.15.5 Making the GFP control-vector

When transducing the INA-6 SQSTM1 KO #3-2 clone 3 cells with a GFP-tagged lentiviral vector to reintroduce *SQSTM1*, it was also of interest to generate a GFP-tagged control vector without the gene. This vector would also be transfected into the SQSTM1 KO #3-2 clone 3 cells resulting in two clone populations, where both would be GFP-tagged but only one overexpressing the *SQSTM1* gene. This was to be carried out to ensure that the control cells had gone through the same process as the *SQSTM1* overexpressed cells.

The vector used to make the control-vector is the same destination vector used when making the SQSTM1-GFP expression vector. This vector, pLVU/GFP, had to be modified in order to be used as a control-vector by removing the lethal *ccdB* region. This was carried out by first cutting the vector using the enzyme, EcoRV (Biolabs, #R0195L), which cuts outside of the attR1 and attR2 sites surrounding the *ccdB* and *CmR* (Chloramphenicol resistance) region. The restriction enzyme reaction was carried out by mixing pLVU/GFP (2 µg), 10X NEBuffer™ 3.1 (Biolabs, #B7203S) (4 µl), prediluted 100X BSA (Biolabs, #B9001S) (4 µl),

EcoRV enzyme (2 µl) and MQ-water up to a total volume of 40 µl. The reaction mix was incubated at 37˚C for 4 h and stopped by heating at 80˚C for 20 minutes.

To check that the right product had been obtained, the linearized plasmid was run on an agarose gel after incubation with the restriction enzyme. The linearized product that was of right size was then extracted from the gel and purified using the QIAquick Gel Extraction Kit (QIAGEN®, #28704). In short, the DNA fragment was harvested from the gel and mixed with 3 volumes of Buffer QG per 1 volume of gel (100 mg ≈ 100 µl) for dissolving (50˚C, 10 min) the gel. Next, the sample was added 1 volume of isopropanol, transferred to a QIAquick spin column and spun (16100xg, 1 min). Buffer QG (500 µl) was added to the spin column and spun down again (16100xg, 1 min). The column was washed by adding Buffer PE (750 µl) and after centrifugation (16100xg, 1 min), the column was spun again to remove residual buffer. Lastly, the column was placed in an EP-tube and incubated for 4 min after adding Buffer EB (30 µl). The DNA was eluted by spinning the column (16100xg, 1 min) and the concentration and purity of the sample was measured by NanoDrop™.

Following, was the ligation reaction ligating together the pLVU/GFP vector without the *ccdB* region. A 20 µl ligation reaction mix was made by mixing 10X T4 DNA Ligase Buffer (Biolabs, #B0202S) (2 µl), 68 ng pLVU/GFP vector, MQ-water up to a total volume of 20 µl and T4 DNA Ligase (Biolabs, #M0202) (1 µl). The reaction mix was incubated overnight (16˚C, 16 h) and heat inactivated at 65°C for 10 minutes. The pLVU/GFP vector was now ready for amplification by transformation into DH5-α competent E. coli. After seeding onto a selective LB agar plate for overnight incubation, clones were prepared for plasmid isolation by incubation overnight (37˚C, 250 rpm) in Falcon tubes containing 3 ml LB medium with Ampicillin (100 µg/ml). Glycerol-stocks were made (3.15.4 Making the SQSTM1-GFP expression vector) out of the transformed competent DH5-α E. coli for later use when preparing the plasmid for lentiviral transduction. Lastly the plasmid was isolated using QIAprep® Spin Miniprep Kit (QIAGEN®, #27106) and the concentration and purity of the sample was measured by NanoDrop™.

3.15.6 Preparing GFP control-vector and SQSTM1-GFP expression vector for lentiviral transduction

Both the GFP control-vector and the SQSTM1-GFP expression vector were prepared for transduction into INA-6 SQSTM1 KO #3-2 clone 3 cells by using the EndoFree® Plasmid Maxi Kit (QIAGEN, #12362) [87]. In short, the GFP control-vector and the SQSTM1-GFP expression vector were seeded onto selective LB agar plates, using their glycerol-stocks made from previous transformations (3.15.4 Making the SQSTM1-GFP expression vector and 3.15.5 Making the GFP control-vector) and incubated overnight (37˚C). From these agar plates, a single clone was picked and grown in 3 ml selective LB medium (37˚C, 250 rpm) for 8 h before diluted 1:500 in 200 ml selective LB medium and incubated overnight (37˚C, 250 rpm). After harvesting, lysing and filtering the lysate, the GFP control- and SQSTM1-GFP expression vector were eluted, precipitated and distributed in two Falcon tubes before centrifugation (4˚C, 9000xg, 45 min). After centrifugation, the pellets were transferred to EP-tubes, spun down (4˚C, 15 000xg, 30 min) and washed 2x with 1,5 ml endotoxin-free 70% ethanol. Lastly, the pellet was airdried and redissolved in Tris-EDTA (TE) buffer (200 µl) before measuring the concentration and purity of the plasmids on NanoDrop™.

3.15.7 Lentiviral transduction of INA-6 SQSTM1 KO #3-2 clone 3 cells

Lentiviral transduction was performed using a 2nd generation system using the packaging and envelope plasmids, psPAX2 and pMD2.G, necessary for virus generation and the transfer plasmids, SQSTM1-GFP plasmid and GFP control plasmid. As shown in Figure 14, the three different types of plasmids are first transfected into adherent Human Embryonic Kidney (HEK) 293T cells. The HEK293T cell line is a derivative of HEK293 cells that contain a Simian Virus 40 (SV40) Tumour (T) antigen, making it highly transfectable [88, 89]. The transfected HEK293T cells will produce virus containing the transfer plasmid gene and transport it out of the cells, into the medium/supernatant (Figure 14). The medium is transferred to the target cells where it will transduce the cells, making them integrate the transfer plasmid gene into its own genome.

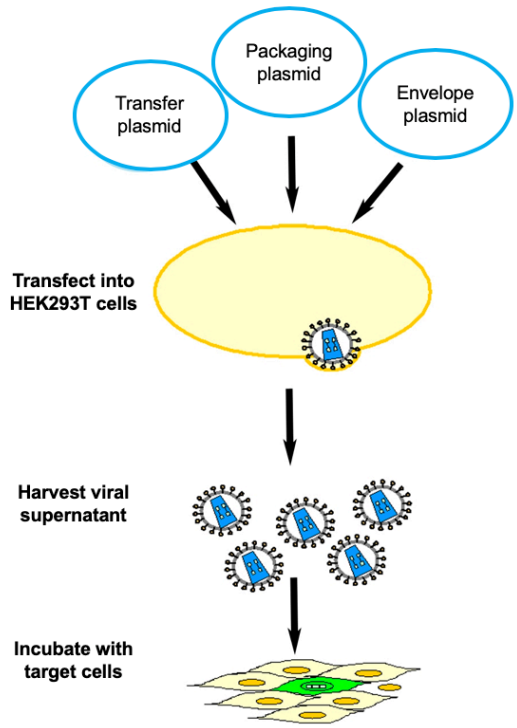

Figure 14: The basic steps in lentiviral transduction using the 2nd generation system. *The three plasmids will be transfected into HEK293T cells, where the plasmids will be integrated into the HEK293T cells genome and virus will be produced. The virus will be transferred to the target cells and the target plasmid gene will be integrated into the target cells. Figure is adopted and edited from [90].*

The protocol for lentiviral transduction was divided into 5 days. The first day, HEK293T cells (600 000 cells) were seeded in 60 mm culture plate dishes per condition with 3 ml of medium (Dulbecco's Modified Eagle's Medium (DMEM) (Sigma Aldrich, #D6429) containing L-glutamine (2 mmol/l) and 10% FCS). The cells were incubated overnight (37˚C, 8% CO_2 atmosphere). The next day, SQSTM1-GFP plasmid and GFP control plasmid (5 µg) were each mixed with the packaging and envelope plasmids, psPAX2 (2,25 µg) and pMD2.G (0,75 µg). In addition, Gene Juice (Novagen, #70967) (15 µl) was mixed with serum-free DMEM (300 µl) for each condition and incubated at room temperature (5 min). Next, the plasmid mixture was mixed together with the Gene Juice mixture before incubation at room temperature (5-15 min). The two plasmid solutions were added dropwise to separate HEK293T cells, prepared the day before, and placed back in incubation (37˚C, 8% CO_2 atmosphere). On the third day, the medium of HEK293T cells was changed into the medium of INA-6 SQSTM1 KO #3-2 clone 3 cells (INA-6 medium) and incubated at a 5% CO_2 atmosphere (37˚C). Both plasmids were transfected into HEK293T cells, detected by fluorescent light from the GFP tag. The following day, SQSTM1 KO #3-2 clone 3 cells (500 000 cells/200 µl) were seeded onto a 6 well plate (1 well/condition) and added 16 µg Polybrene (100 µg/µl stock prediluted 1:100). HEK293T cell medium were filtered onto the

SQSTM1 KO #3-2 clone 3 cells, and new INA-6 medium was added to the HEK293T cells. This was repeated once again the same day and the next morning before adding fresh INA-6 medium to the SQSTM1 KO #3-2 clone 3 cells and leaving them for 3 days.

When checking the cells to see if the transduction was successful, only the GFP control plasmid had been successfully transduced into SQSTM1 KO #3-2 clone 3 cells. This was detected with fluorescent light emitted from the positively transfected cells. Unfortunately, for an unknown reason, the SQSTM1-GFP plasmid had not been transduced into the SQSTM1 KO #3-2 clone 3 cells meaning we were not able to overexpress SQSTM1 in the SQSTM1 KO cells.

4.0 Results

4.1 Determining the method for representation of cell viability

Since MM patients often develop resistance towards treatment, it is of great value to test new drugs, preferably in combination with previously established drugs to try and reverse the resistance as well as increase the success of treatment. Measurement of cell viability was used in this thesis to evaluate the drug sensitivity, towards both clinically approved drugs, such as CFZ, BZ and HCQ, and drug candidates, such as BafA1, in MM cell lines. The cell sensitivity toward a given drug or combination of drugs, such as combining proteasome inhibitors with autophagy inhibitors, would help assess the effectiveness and cytotoxicity of the drug(s). Annexin V/Propidium iodide -staining is a viability assay that separates between living and non-living cells but is a time-consuming assay. Therefore, we wanted to test whether CellTiter® Glo, a quick performable assay that measure ATP-production from living cells, could be used as a representation of cell viability. Thus, results from CellTiter® Glo and Annexin V/Propidium iodide -staining was compared by setting up two identical assays at the same time.

First, INA-6 cells were stimulated with the PIs, CFZ and BZ, with and without the autophagy inhibitor, BafA1, because these are all drugs and concentrations that was used in assays presented later in this thesis. BafA1 is a potent autophagy inhibitor often used for *in vitro* studies of cancer, however it is not clinically approved. As illustrated in Figure 15, there was a clear similarity between the CellTiter Glo® assay (measured as relative luciferase units (RLU, (%)) and the Annexin V/Propidium iodide -staining assay (measured as % of viable cells) after a 4-hour incubation.

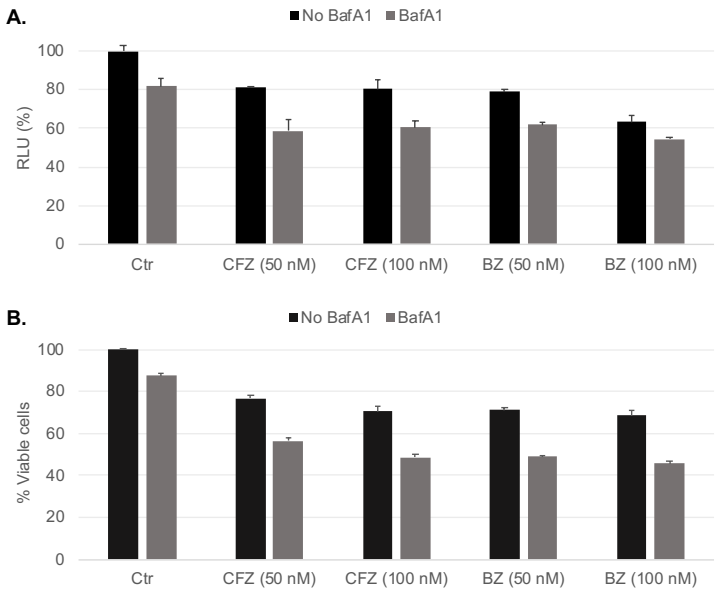

***Figure 15**: **CellTiter® Glo and Annexin V/Propidium iodide -staining assay of INA-6 cells. A.** INA-6 cells were seeded (30 000 cells/well) in a 96-well opaque-walled multi plate with triplicates per condition and stimulated with carfilzomib (CFZ) (50 nM, 100 nM) and bortezomib (BZ) (50 nM, 100 nM) with and without bafilomycin A1 (BafA1) (90 nM) for 4 h and analysed using CellTiter Glo® assay. The results were calculated relative to the control sample (ctr) and are given as Relative Luciferase Units (RLU) (%). **B.** INA-6 cells were seeded (60 000 cells/well) in a 96-well plate with duplicates per condition and stimulated with CFZ (50 nM, 100 nM) and BZ (50 nM, 100 nM) with and without BafA1 (90 nM) for 4 h. The cells were stained with Annexin V/propidium iodide and analysed using Flow cytometry. The result is given as % viable cells relative to the control sample. This assay was performed once, and the standard deviations are calculated between the triplicates/duplicates per condition.*

Another 4-hour assay assessing the similarity between the CellTiter® Glo and Annexin V/Propidium iodide -staining method was performed after stimulation with BafA1 and different concentrations of HCQ, comparing the effect of the two autophagy inhibitors used in this thesis. As illustrated in Figure 16, both the CellTiter® Glo and Annexin V/Propidium iodide -staining method showed very similar results based on the level of, respectably, ATP levels in living cells measured and percentage of viable cells detected after both BafA1 and HCQ stimulation.

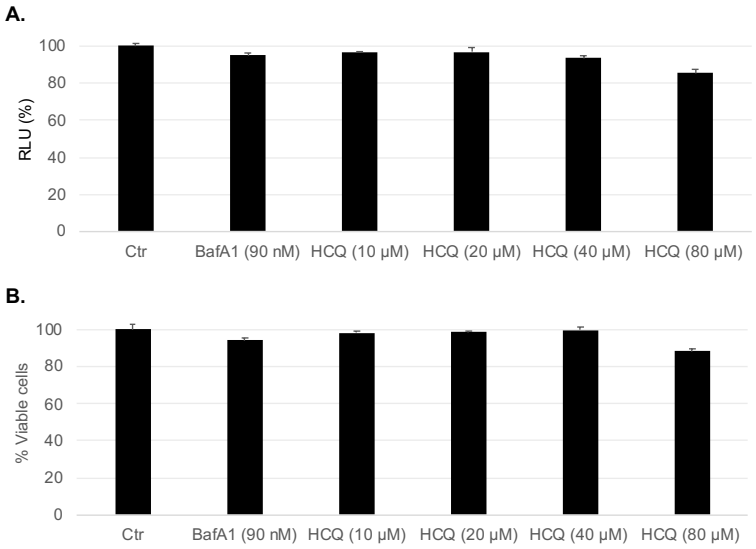

***Figure 16**: **CellTiter® Glo and Annexin V/Propidium iodide -staining assay in INA-6 cells. A.** INA-6 cells were seeded (30 000 cells/well) in a 96-well opaque-walled multi plate with triplicates per condition and stimulated with bafilomycin A1 (BafA1) (90 nM) and increasing concentrations of hydroxychloroquine (HCQ) (10-80 µM) for 4 h and analysed using CellTiter Glo® assay. The results were calculated relative to the control sample (ctr) and are given as relative luciferase units (RLU) (%). **B.** INA-6 cells were seeded (60 000 cells/well) in a 96-well plate with duplicates per condition and stimulated with BafA1 (90 nM) and increasing concentrations of HCQ (10-80 µM) for 4 h. The cells were stained with Annexin V/propidium iodide and analysed using Flow cytometry. The results are given as % viable cells as determined by flow scatter analysis. This assay was performed once, and the standard deviations are calculated between the triplicates/duplicates per condition.*

To ensure that CellTiter Glo® also could be used as a reliable cell viability representation after a longer time of incubation, INA-6 cells were stimulated with CFZ and BZ with and without HCQ for 24 hours. As the INA-6 cells are very sensitive against PIs, the concentrations chosen for a 24-hour stimulation was lower. Again, as shown in Figure 17, the ATP-levels measured and percentage of viable cells detected in the INA-6 cells after drug stimulation were fairly similar. Dissimilarities between the two assays observed for the highest concentrations of both CFZ (4 nM and 8 nM) and BZ (6 nM and 12 nM) are believed to be caused by difficulties in gating during the flow scatter analysis of these samples (Scatter not shown).

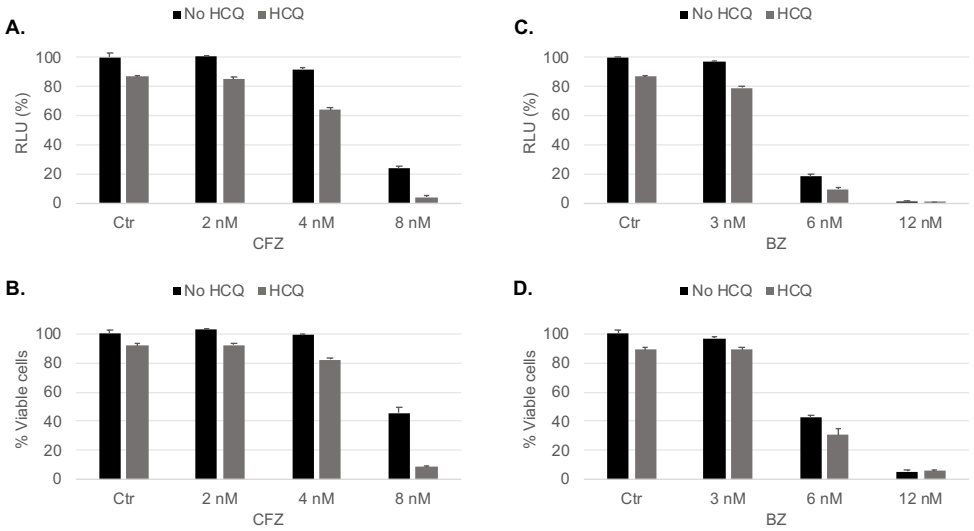

Figure 17: CellTiter® Glo and Annexin V/Propidium iodide -staining assay in INA-6 cells. ***A.*** *and* ***C.*** *INA-6 cells were seeded (30 000 cells/well) in a 96-well opaque-walled multi plate with triplicates per condition and stimulated with* ***A.*** *carfilzomib (CFZ) (2-8 nM) and* ***C.*** *bortezomib (BZ) (3-12 nM) with and without hydroxychloroquine (HCQ) (10 µM) for 24 h and analysed using CellTiter Glo® assay. The results were calculated relative to the control sample (ctr) and are given as relative luciferase units (RLU) (%).* ***B.*** *and* ***D.*** *INA-6 cells were seeded (60 000 cells/well) in a 96-well plate with duplicates per condition and stimulated with* ***B.*** *CFZ (2-8 nM) and* ***D.*** *BZ (3-12 nM) with and without HCQ (10 µM) for 24 h. The cells were stained with Annexin V/propidium iodide and analysed using Flow cytometry. The results are given as % viable cells as determined by flow scatter analysis. This assay was performed once, and the standard deviations are calculated between the triplicates/duplicates per condition.*

Based on the similarities observed between the cell viability assay using Annexin V/Propidium iodide -staining and CellTiter® Glo, it was decided that CellTiter® Glo assay could be used as a method measuring cell viability throughout this thesis.

4.2 Drug sensitivity testing of PI adapted Multiple Myeloma cell lines

Adapting MM cell lines to PIs are a valuable tool when studying the mechanisms of drug resistance. Two types of PI adapted cell lines, INA-6 and AMO-1, were available in our lab. INA-6 cells only produce free Ig kappa light chains (IgK) and AMO-1 cells produce IgA isotype with kappa light chains, thus representing two different model systems that is of interest to study when investigating drug resistance. However, before using them in this thesis it was important to verify their lowered drug sensitivity against CFZ and BZ.

4.2.1 Drug sensitivity of PI adapted INA-6 cell lines

To verify the increased tolerance of the PI adapted INA-6 cells against PIs, INA-6-WT, INA-6-CFZR and INA-6-BZR cells were treated with increasing concentrations of CFZ and BZ for 24 h before detecting the ATP-levels from living cells using CellTiter® Glo assay. As illustrated in Figure 18, the INA-6-CFZR and INA-6-BZR cells were less sensitive to both

CFZ and BZ compared to the INA-6-WT cells. When stimulating with CFZ (Figure 18A), the INA-6-CFZR cells clearly tolerated higher concentrations of CFZ compared to INA-6-WT, with almost 50% viable cells after stimulation with 16 nM CFZ whereas INA-6-WT had around 50% viable cells between 2-4 nM CFZ. Notably, INA-6-BZR were greatly cross-resistant and had an even lower sensitivity towards CFZ than the INA-6-CFZR cells, with more than 50% viable cells after treatment with 16 nM CFZ. When stimulating with BZ (Figure 18B), INA-6-BZR had a clear lower sensitivity than INA-6-WT and INA-6-CFZR with approximately 40% viable cells after 12 nM of BZ treatment, whereas the INA-6-CFZR cells had almost no viable cells after treatment with 12 nM of BZ.

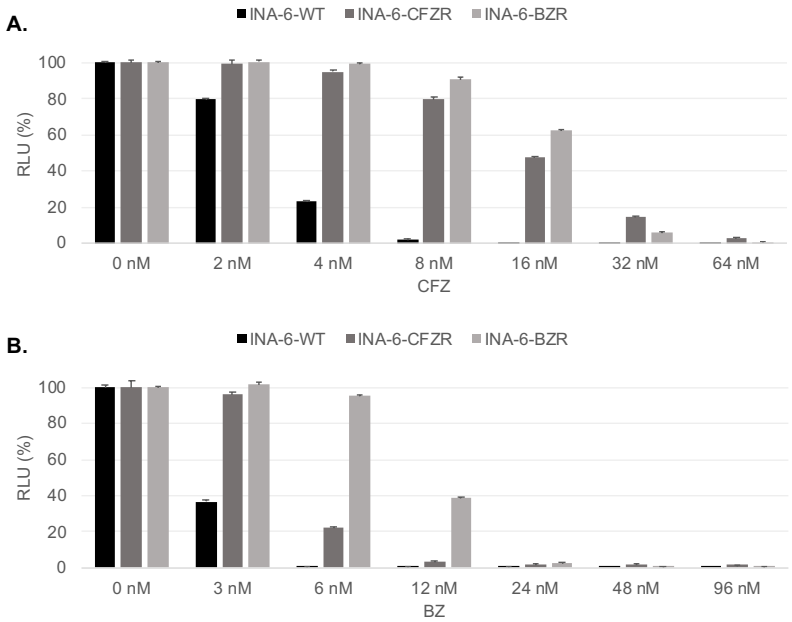

***Figure 18**: **Proteasome inhibitor (PI) sensitivity of PI adapted INA-6 cell lines**. INA-6 wild type (INA-6-WT), INA-6 carfilzomib resistant (INA-6-CFZR) and INA-6 bortezomib resistant (INA-6-BZR) cells were seeded (30 000 cells/well) and stimulated with increasing concentrations of **A.** CFZ (2-64 nM) and **B.** BZ (3-96 nM) with triplicates per condition for 24 h and analysed using CellTiter Glo®. The measured amount of bioluminescence was calculated relative to the control sample (0 nM) and are given as relative luciferase units (RLU) (%). This assay was performed once, and the standard deviations are calculated between the triplicates per condition.*

4.2.2 Drug sensitivity of PI adapted AMO-1 cell lines

The level of drug sensitivity towards CFZ and BZ was also verified in the PI adapted AMO-1 cell lines. AMO-1-WT, AMO-1-CFZR and AMO-1-BZR cells were treated with increasing concentrations of CFZ and BZ for 24 h before detecting the results using CellTiter® Glo assay. As illustrated in Figure 19, AMO-1-CFZR and AMO-1-BZR cells had a remarkable lowered drug sensitivity towards both CFZ and BZ compared to AMO-1-WT and the PI adapted INA-6 cells. Also, the PI adapted AMO-1 cells showed to be less cross-resistant than

the PI adapted INA-6 cell lines. After CFZ treatment with 1000 nM (Figure 19A), AMO-1-CFZR still had approximately 50% viable cells. AMO-1-BZR, on the other hand, had around 10% viable cells after 62,5 nM of CFZ. When treating the cells with BZ (Figure 19B), the AMO-1-BZR cell line had over 60% viable cells after treatment with 500 nM BZ, while AMO-1-CFZR had 60% viable cells after treatment with 31,25 nM BZ.

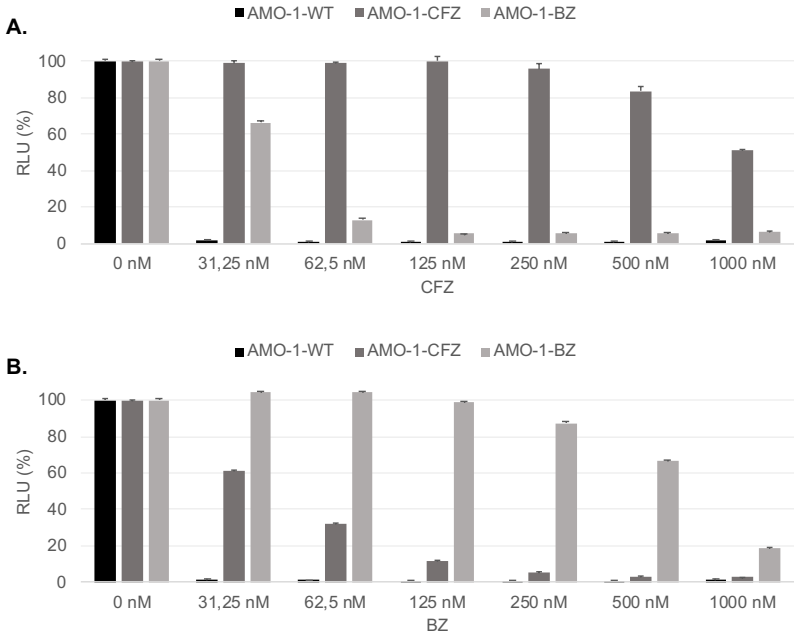

***Figure 19**: **Proteasome inhibitor (PI) sensitivity of PI adapted AMO-1 cell lines.** AMO-1 wild type (AMO-1-WT), AMO-1 carfilzomib resistant (AMO-1-CFZR) and AMO-1 bortezomib resistant (AMO-1-BZR) cells were seeded (30 000 cells/well) and stimulated with increasing concentrations of **A.** CFZ (31,25-1000 nM) and **B.** BZ (31,25-1000 nM) with triplicates per condition for 24 h and analysed using CellTiter Glo® assay. The measured amount of bioluminescence was calculated relative to the control sample (0 nM) and are given as relative luciferase units (RLU) (%). This assay was performed once, and the standard deviations are calculated between the triplicates per condition.*

To conclude, the PI adapted cell lines, both INA-6 and AMO-1, were verified to have a greatly lowered sensitivity against CFZ and BZ compared to the WT cell lines and were thus used throughout this project when exploring mechanisms of PI resistance development.

4.3 Exploring effects of autophagic inhibition in combination with PIs in PI adapted AMO-1 cell lines

As a therapeutic target, inhibition of the proteasomes has shown good clinical effects in MM patients [46]. However, some MM patients display intrinsic resistance and most develop acquired resistance against PIs over time [54]. Previous work in the myeloma group has shown good synergistic effect of inhibiting both the cells protein degradation pathways, the

proteasome by CFZ and autophagy by HCQ, in MM cell lines and primary cells, while this synergy has not been observed with BZ and HCQ [61]. They also found that HCQ partly reversed the resistance against CFZ in CFZ adapted INA-6 cells.

As we were in possession of another PI adapted MM cell line, AMO-1, producing a different Ig composition than INA-6, it was of interest to test whether the PI adapted AMO-1 cell lines also had a good synergistic effect of HCQ and if HCQ could reverse PI resistance in these cells. Thus, the PI adapted AMO-1 cell lines were stimulated with increasing concentrations of its respective PI with and without the autophagy inhibitor HCQ before detecting cell viability using CellTiter® Glo assay.

As shown in Figure 20A, HCQ potentiated CFZ induced apoptosis in AMO-1-WT significantly after 4 nM CFZ in combination with 10 µM HCQ. On the other hand, HCQ seemed to have little or no effect on BZ-induced apoptosis in AMO-1-WT. Alone, HCQ induced some cytotoxic effect on the AMO-1-WT cells. These results were similar to what the myeloma group had previously seen in INA-6 cells [61].

As for the AMO-1-CFZR and AMO-1-BZR cells, Figure 20B show that HCQ alone seemed to induce a cytotoxic effect on the AMO-1-CFZR cells which did not seem to increase with increasing concentrations of CFZ. However, the two highest concentrations of CFZ (500 nM and 1000 nM) had a significant cytotoxic response in combination with 10 µM HCQ. Since almost 80% of the AMO-1-CFZR cells were still viable after 1000 nM CFZ, an assay including 2000 nM CFZ was performed (Appendix 8.5) and AMO-1-CFZR still had about 50% viable cells with a clear cytotoxic effect of an HCQ-combination. As for the AMO-1-BZR cells, Figure 20C indicate that HCQ seem to have no cytotoxic effect when alone and in combination with BZ.

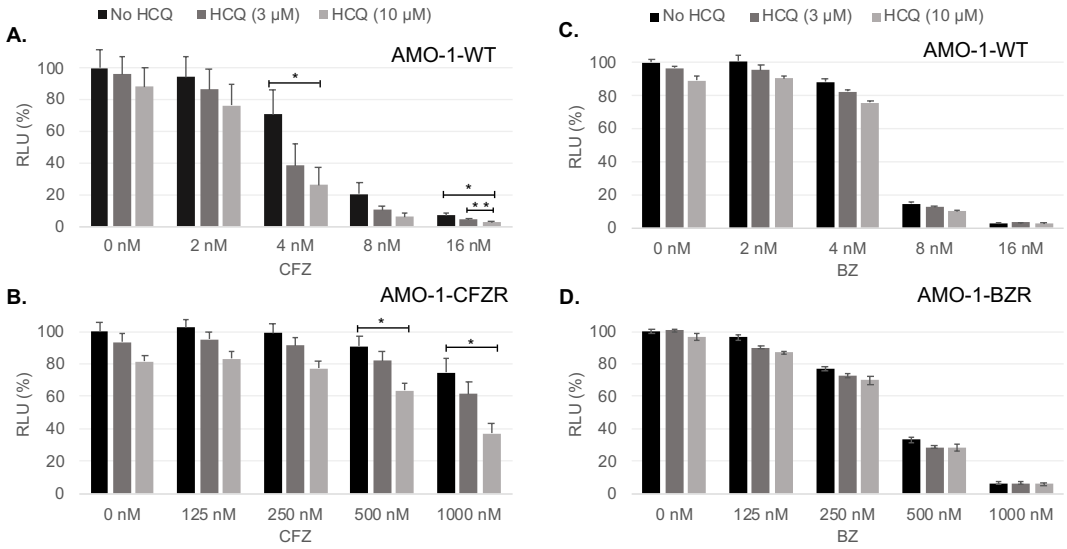

***Figure 20**: **Effects of autophagic inhibition in combination with proteasome inhibitors (PIs) in wild type (WT) and PI adapted AMO-1 cell lines**. **A.** AMO-1-WT cells were seeded (30 000 cells/well) and stimulated with increasing concentrations of CFZ (125-1000 nM) with or without hydroxychloroquine (HCQ) (3 µM, 10 µM) with triplicates per condition. **B.** AMO-1 carfilzomib resistant (AMO-1-CFZR) cells were seeded (30 000 cells/well) and stimulated with increasing concentrations of CFZ (125-1000 nM) with or without HCQ (3 µM, 10 µM) with triplicates per condition. **C.** AMO-1-WT cells were seeded (30 000 cells/well) and stimulated with increasing concentrations of BZ (125-1000 nM) with or without HCQ (3 µM, 10 µM) with triplicates per condition. **D.** AMO-1 bortezomib resistant (AMO-1-BZR) cells were seeded (30 000 cells/well) and stimulated with increasing concentrations of BZ (125-1000 nM) with or without HCQ (3 µM, 10 µM) with triplicates per condition. The cells were incubated for 24 h and analysed using CellTiter Glo® assay. In figure A. and B., the relative luciferase units (RLU) (%) are shown as the mean +SEM (Standard Error of the Mean) of three independent experiments. The RLU (%) from figure C. and D. are representative for 2 independent experiments. The results were calculated relative to the control sample (0 nM, no HCQ) and are given as RLU (%). The PI adapted AMO-1 cell lines had prior to the experiments been cultivated in 90 nM of its respective PI. The asterisks indicate statistically significant difference (an unpaired two-tailed Student's T-test; *, $p < 0.05$; **, $p < 0.01$) after adjusting for the HCQ effect with no PI.*

To conclude, HCQ seem to cause a small synergistic effect in cell cytotoxicity in combination with CFZ in AMO-1-CFZR and AMO-1-WT cells. In contrast, no effect on the cytotoxicity was observed when HCQ was combined with BZ.

4.4 Detecting IgK protein expression levels in PI adapted INA-6 and AMO-1 cell lines

Cells have the ability to adapt to stressful conditions such as drug treatment by modifying the expression and/or activity of different proteins. It has previously been proven in the myeloma group that PI adapted INA-6 cells, predominantly producing free IgK, modifies their protein expression level of IgK [71]. Surprisingly, for the two PI adapted INA-6 cell lines the expression of IgK was totally different. While INA-6-CFZR cells had turned down its IgK expression, INA-6-BZR cells had upregulated its IgK expression compared to INA-6-WT. Why these two PIs induce different responses towards IgK expression in the INA-6 cells is still unknown. The significantly downregulated IgK expression level in INA-6-CFZR and

upregulation of IgK expression in INA-6-BZR was also verified in this project as observed in Figure 21A and B. Based on these finding, it was of interest to investigate if similar modifications of IgK expression levels were present in PI adapted AMO-1 cells as well. The difference in Ig composition expressed between INA-6 and AMO-1 cells was also a factor that made it interesting to investigate if PI adapted AMO-1 cells had altered its IgK expression level.

As shown in Figure 21C, D and E, both AMO-1-CFZR and AMO-1-BZR cells had downregulated its IgK expression compared to AMO-1-WT. However, while the BZ adapted AMO-1 cell had about halved the expression of IgK, AMO-1-CFZR cells had completely downregulated IgK protein expression, similar to INA-6-CFZR. Although, AMO-1 cells predominantly produce IgK connected to IgA, we were able to detect IgK by the IgK primary antibody used. Noteworthy, IgK is normally detected at 25 kDa, however in the AMO-1 cell lines two protein bands for IgK were detected, with a weak band at 25 kDa and a strong band at approximately 30 kDa. Although the reason for this is unknown, we speculated that the 30 kDa IgK has gone through some type of modification. Also, despite that the modified IgK was most prominent, IgK expression seemed to be regulated similarly in the normal IgK and modified IgK.

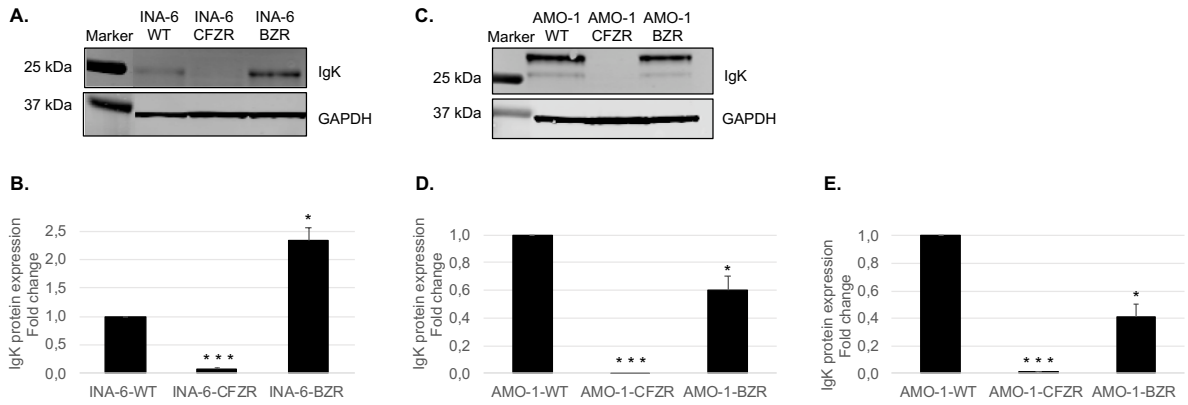

***Figure 21**: **Levels of immunoglobulin kappa light chain (IgK) in proteasome inhibitor (PI) adapted INA-6 and AMO-1 cell lines. A.** Basal protein expression levels of IgK in PI adapted INA-6 cell lines compared to wild type (WT) with **B.** Protein quantification and fold change calculation. **C.** Basal protein expression level of IgK in PI adapted AMO-1 cell lines compared to WT with, **D.** and **E.,** protein quantification and fold change calculation. 2 million cells per cell line were lysed in 8 M Urea lysis buffer before loading 60 µg protein onto the gel. After protein separation by gel electrophoresis, IgK- and GAPDH-levels were determined by immunoblotting. The fold change was calculated, in D. the modified IgK and in E. the normal IgK, by normalizing the signal quantifications against a housekeeping protein (GAPDH) and made relative to the respective WT cell line. The protein fold change results are shown as the mean +SEM (Standard error of the mean) of three independent experiments and the blots shown are a representative of the three experiments. The asterisks indicate statistically significant difference (an unpaired two-tailed Student's T-test; *****, $p < 0.05$; *******, $p < 0.001$).*

4.5 PI drug sensitivity in INA-6 IgK KO cell clones

Due to the fact that adaptation to CFZ and BZ caused different alterations in IgK expression levels of both INA-6 and AMO-1 cell lines, it was hypothesized that altered IgK expression might alter the MM cell lines drug sensitivity to PIs. If so, one would expect less drug sensitivity toward CFZ in cell lines where IgK was no longer expressed. The hypothesis was tested by looking at cell viability of five INA-6 IgK knockout (KO) cell clones and two different IgK control clones, made by CRISPR/Cas9 technology and single cell cloning [71], after stimulation with increasing concentrations of CFZ and BZ. Also, regular INA-6 cells were included as a reference to the IgK control clones.

As shown in Figure 22, there was a clear clonal difference in PI drug sensitivity between the INA-6 IgK KO cell clones. IgK KO 5 had a significant lower drug sensitivity to 4 nM CFZ than the IgK Ctr 1 clone (Figure 22A). IgK KO 5 also had lower drug sensitivity to BZ treatment (6 nM) compared to the IgK control clones (Figure 22B), although not significant ($p = 0{,}166$). On the other hand, IgK KO clone 2, 3 and 4 did not show any change in drug sensitivity to either CFZ or BZ. The IgK control cell lines were behaving fairly similar to the normal INA-6 cells, but a small clonal difference between the IgK control clones was observed.

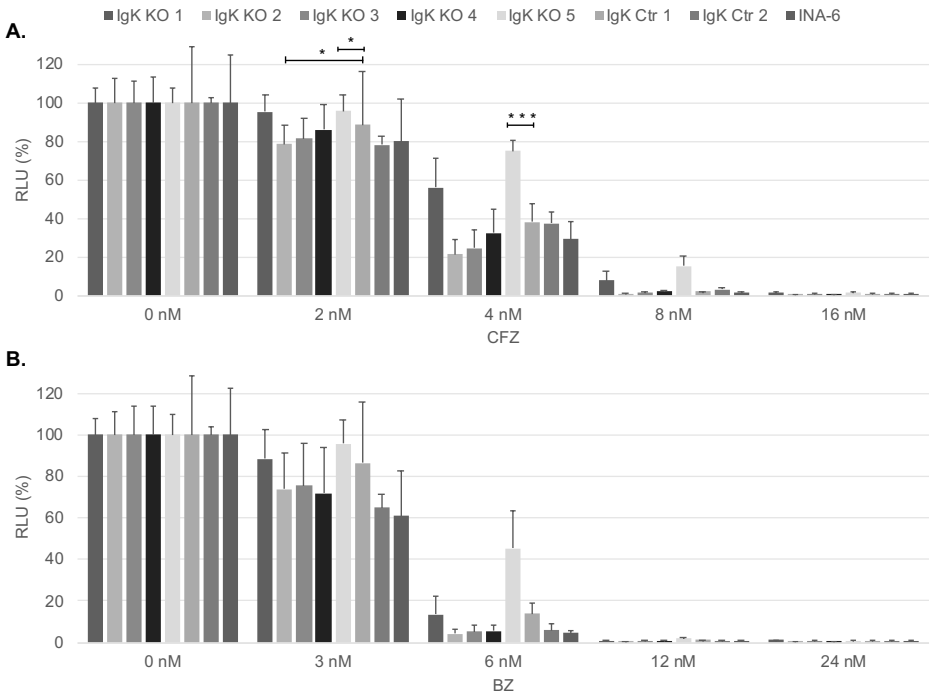

Figure 22: Proteasome inhibitor (PI) sensitivity assay of INA-6 immunoglobulin kappa light chain (IgK) knockout (KO) cell clones, control cell lines and normal INA-6*. INA-6 cells were seeded (30 000 cells/well) and stimulated with increasing concentrations of* ***A.*** *carfilzomib (CFZ) (2-16 nM) and* ***B.*** *bortezomib (BZ) (3-24 nM), with triplicates per condition for 24 h and analysed using CellTiter Glo® assay. The measured amount of bioluminescence was calculated relative to the control samples (0 nM) and are given as relative luciferase units (RLU) (%). Three independent experiments were performed, and the sensitivity results are shown as the mean +SEM (Standard error of the mean). The asterisks indicate a statistically significant difference compared to IgK Ctr 1 (an unpaired two-tailed Student's T-test; *, $p < 0.05$; ***, $p < 0.001$).*

Thus, due to large clonal differences observed regarding PI drug sensitivity between the INA-6 IgK KO clones, it was difficult to make any conclusions of the effect of knocking out IgK when assessing PI drug sensitivity.

4.6 Characterization of INA-6 IgK KO cell clones and IgK control clones

Due to the discovery of clonal differences when evaluating PI drug sensitivity of the INA-6 IgK KO clones, it was sought to further characterize these clones to disclose any reasons for the clonal differences. First, it was of interest to investigate the level of IgK protein in the INA-6 IgK KO and IgK control clones by WB and, as shown in Figure 23, no basal levels of IgK was detected in any of the IgK KO clones.

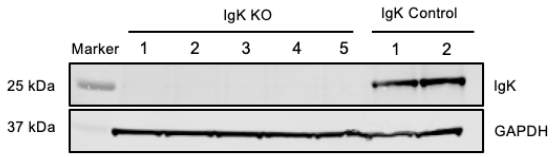

***Figure 23**: **Immunoglobulin kappa light chain (IgK) protein detection in INA-6 IgK knockout (KO) cell clones and control clones**. 1 million cells per IgK KO clone and control clone were lysed in 8 M Urea lysis buffer before loading 60 µg protein onto gel. After protein separation by gel electrophoresis, IgK- and GAPDH-levels were detected by immunoblotting.*

4.6.2 Identifying *IgK* gene alteration in the INA-6 IgK KO cell clones

When generating the INA-6 IgK KO cell clones, using CRISPR/Cas9 technology, the *IgK* gene was cut in its constant Ig light chain region with the help of guide RNA (gRNA) oligo and the Cas9 protein (Figure 24A). In order to investigate if the INA-6 IgK KO clones had any differences in their *IgK* gene that could explain the clonal difference, and to characterize precisely how the *IgK* gene had been altered during the CRISPR/Cas9 modification, the IgK KO and IgK control clones were sequenced. Sequencing-results of the *IgK* gene from IgK KO clones and IgK control cell clones revealed that all the five IgK KO clones had obtained the exact same alteration. Cas9 had cut the *IgK* gene in a serine leading to a single nucleotide insertion of a guanine (G) causing a frameshift and an early stop codon, as shown in Figure 24B and Appendix 8.6, leaving a truncated IgK gene and protein. The sequencing results from the IgK control clones were identical to the normal *IgK* gene.

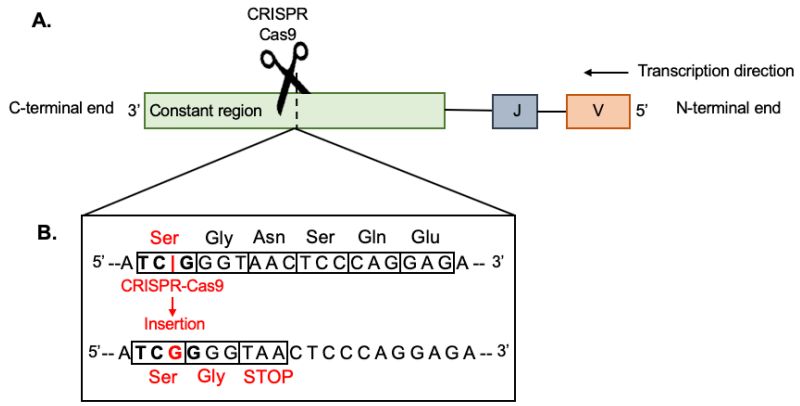

***Figure 24**: **Illustration of the immunoglobulin kappa light chain (IgK) protein and alterations made during the production of IgK knockout (KO) cell clones using CRISPR/Cas9 technology. A.** IgK protein construct illustrating where the DNA had been cut by Cas9. **B.** The amino acid and nucleotide sequence where gRNA bound and Cas9 cut the DNA. The red colour represents the affected amino acids and the inserted nucleotide.*

This result shows that 2/3 of the transcript still will be produced, with the C-terminal end missing. We thus decided to investigate the datasheet for the IgK primary antibody in order to see why no IgK was detected in the WB assay and found that the primary antibody used for IgK detection was a monoclonal antibody that binds only to the C-terminal end of the protein.

Thus, the WB assay is not a reliable method to verifying the INA-6 IgK KO clones (see 4.6 Characterization of INA-6 IgK KO cell clones and IgK control). Based on this, it was speculated whether the IgK protein was produced or not in the IgK knockout cell lines.

4.6.3 IgK protein characterization of INA-6 IgK KO 2 and IgK Control 1 by mass spectrometry

In order to characterize the truncated IgK protein in the INA-6 IgK KO cell clones, cell lysates from the IgK KO 2 and IgK Ctr 1 cells were analyzed by mass spectrometry. This was done in order to figure out if, and in case how much of, the truncated IgK protein was being produced in the IgK KO clones. The results revealed that, compared to the IgK control clone, 25% of IgK protein was still present in the IgK KO 2 clone. In addition, the IgK protein was 3/4 the size of the normal IgK in the IgK control clone, as expected. Thus, the INA-6 IgK KO clones seem to rather be a knock down with 75% less IgK expressed, compared to the IgK control cell line, probably due to a faster degradation. To sum up, IgK is still produced in the IgK KO clones but in a truncated version. However, the clones would still be referred to as IgK KO throughout this thesis.

4.6.4 *IgK* RNA expression levels of INA-6 IgK KO cell clones and IgK control clones

Since IgK in only one of the INA-6 IgK KO clones and one of the IgK control clones had been characterized by mass spectrometry, we further wanted to investigate the level of *IgK* RNA expression in all the INA-6 IgK KO clones and IgK controls. Since IgK KO clone 5 was the only IgK KO clone found to be significantly less sensitive towards CFZ, and to some degree also towards BZ, we speculated that IgK KO 5 expressed less *IgK* RNA than the other IgK KO clones. However, as shown in Figure 25, only a minimal clonal difference was observed between the five different IgK KO clones. Surprisingly, a notable difference in *IgK* RNA expression between the two IgK control cell lines was observed. IgK Ctr 1 expressed over double the amount of *IgK* RNA than IgK Ctr 2.

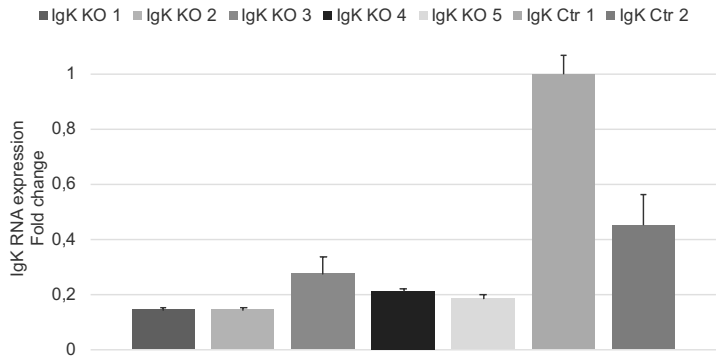

***Figure 25**: **qRT-PCR analysis of immunoglobulin kappa light chain (IgK) RNA expression levels in INA-6 IgK knockout (KO) clones and IgK control clones.** RNA was isolated and converted to cDNA before quantifying the level of IgK RNA expression using qRT-PCR and SYBR Green detection method (3.14 qRT-PCR of INA-6 IgK KO cell). The IgK RNA expression was normalized to GAPDH. The quantification cycle (C_q) from each sample was used to calculate the relative quantification of IgK RNA expression using IgK Ctr 1 as the control and the $\Delta\Delta C_q$ method for calculation of expression level fold change [83]. This assay was performed once, and the standard deviations are calculated between the triplicates per condition.*

Taken together, no clonal differences in the RNA levels of *IgK* were observed between the five INA-6 IgK KO cell clones. Thus, even though some interesting results during this characterization was obtained, such as discovering that all five IgK KO clones had the exact same single nucleotide mutation and that the IgK KO clones were more of a knock down, we could not explain, based on our results, the difference in PI drug sensitivity observed between the clones. Therefore, we conclude that if there is a future wish to investigate IgK knockout in MM research, new IgK KO clones should be made with the attempt to cut the *IgK* gene earlier in the sequence, i.e. in the variable region. We therefore turned our focus to other molecular mechanisms that might be important for developing resistance to PIs and decided to focus more on the role of the autophagy receptor, SQSTM1, and its role in protein aggregation and secretion of IgK in MM cell lines.

4.7 Detecting SQSTM1 protein expression levels in PI adapted INA-6 and AMO-1 cell lines

Inhibition of proteasomes has been shown to cause an upregulation of SQSTM1 and SQSTM1-positive protein aggregates in MM cell lines [59, 61], thus thought to increase the autophagic flux. When the proteasomes are inhibited, ubiquitinated cargo marked for degradation will accumulate in the cells, thus increasing the cells proteotoxic stress. SQSTM1 is thought to reduce this proteotoxic stress by the ability to bind ubiquitinated cargo and link these structures to the autophagic degradation machinery. Together, we hypothesized that SQSTM1 might be involved in the development of PI drug resistance in MM. Therefore, it

was of interest to investigate if the PI adapted MM cell lines had changed their basal expression level of SQSTM1. Previously obtained results from the myeloma group showed an increase of, both protein and mRNA, SQSTM1 in CFZ adapted INA-6 cells [61]. Here the protein levels of SQSTM1 in both PI adapted INA-6 and AMO-1 cell lines were analysed.

The PI adapted INA-6 cell lines had significantly upregulated its basal protein expression level of SQSTM1, with a 6-fold change in the INA-6-BZR cells and an almost 4-fold in the INA-6-CFZR (Figure 26A and B), which was in line with earlier findings [61, 70]. In the PI adapted AMO-1 cell lines (Figure 26C and D), on the other hand, the protein expression level of SQSTM1 was more or less not found changed in the AMO-1-CFZR cells compared to AMO-1-WT, while the AMO-1-BZR cells seemed to have an upregulated basal protein expression level of SQSTM1, although not significantly (p-value = 0.06).

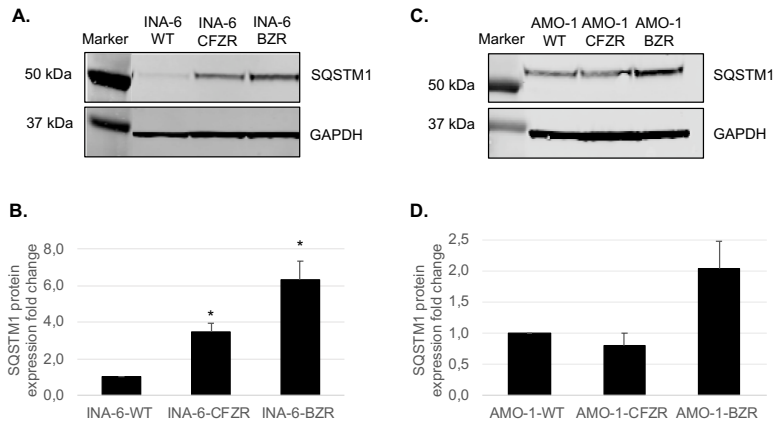

***Figure 26**: **Levels of sequestosome 1 (SQSTM1) in proteasome inhibitor (PI) adapted INA-6 and AMO-1 cell lines. A.** Western blot (WB) of SQSTM1 protein expression levels in PI adapted INA-6 cell lines compared to wild type (WT) and **B.** fold change calculations between the PI adapted INA-6 cell lines and WT. **C.** WB of SQSTM1 protein expression level in PI adapted AMO-1 cell lines compared to WT and **D.** fold change calculations of SQSTM1 expression between PI adapted AMO-1 cell lines and WT. 2 million cells per cell line were lysed in 8 M Urea lysis buffer before loading 60 µg protein onto gel. After protein separation by gel electrophoresis, SQSTM1-levels were detected using immunoblotting. The SQSTM1 expression fold change was calculated by normalizing the signal quantifications against GAPDH and made relative to the respective WT cell line. The results are shown as the mean +SEM (standard error of the mean) of three independent experiments and the blots are a representative of the three experiments. The asterisks indicate statistically significant difference (an unpaired two-tailed Student's T-test; *, $p < 0.05$).*

In conclusion, both BZ adapted INA-6 and AMO-1 cells had turned up their SQSTM1 protein expression levels, suggesting that SQSTM1 may play a role in BZ drug resistance. However, for the CFZ adapted cell lines, SQSTM1 protein expression level seem to be cell line dependent, where INA-6-CFZR cells significantly increased protein level of SQSTM1 while the level of SQSTM1 expression in AMO-1-CFZR cells remained more or less unchanged.

4.8 Investigating a possible SQSTM1-dependent secretion of IgK in Multiple Myeloma cells

Up to 50% of MM patients develop renal failure mostly due to insoluble casts made up of free Ig light chains, i.e. IgK, produced and secreted by MM cells. The condition is associated with poorer prognosis, however treating the renal failure seem to better the patient's condition [17, 18]. As such a significant part of MM patients are affected by this condition, it was of interest to investigate how these free light chain structures are being secreted by MM cells.

Unpublished results obtained in the myeloma group, indicate that SQSTM1 is secreted by MM cells together with free IgK when stimulating the cells with PIs in combination with the autophagy inhibitor, BafA1 (Appendix 8.7A). We therefore considered the possibility that SQSTM1 may reduce the proteotoxic stress induced by PI drug treatment, by the ability to bind ubiquitinated misfolded IgK and form protein aggregates by self-polymerization. Although such protein aggregates are normally degraded by autophagy, one can think that if the amount of protein aggregates exceed the lysosomal capacity (as illustrated by the stimulation of autophagy inhibitors), the cells are prone to die. So, in order for the MM cells to survive, we speculate that MM cells may secrete these protein aggregates as a survival process. Preliminary results obtained in the myeloma group, observed decreased levels of IgK in the cell media of SQSTM1 KO cell lines after autophagy inhibition by BafA1, indicating a possible role of SQSTM1 in the secretion of IgK (Appendix 8.7B). Therefore, it was of interest to further investigate whether SQSTM1 could be responsible for the secretion of aggregated misfolded IgK, as seen in MM patients with renal failure, after PI drug treatment and if this could be a possible novel drug resistance mechanism in MM.

4.8.1 The effects of autophagy inhibition on protein secretion

In order to verify that IgK was released to the cell media in response to autophagic inhibition also using the clinically approved autophagy inhibitor HCQ, INA-6 cells were treated with both BafA1 and HCQ. In order to investigate what was released from the cells in response to autophagy inhibitors, a special protein-fraction assay was used to differentiate proteins based on their density and location (see 3.8 Protein-fraction protocol). The detergent resistant fraction (8 M Urea fraction) represent intracellularly dense structures, such as protein aggregates, the detergent soluble fraction (TX100 fraction) represent soluble proteins inside

the cells and the medium fraction (lysed in 8 M Urea lysis buffer) are the extracellular components released out of the cells.

As Figure 27A shows, the SQSTM1 levels identified in the detergent resistant fraction in response to both BafA1 and HCQ stimulation had an evident increase compared to the control sample. Interestingly, there was also a clear increase of SQSTM1 in the medium fraction in response to autophagy inhibition by both BafA1 and HCQ. IgK was mainly located in the detergent soluble fraction. Surprisingly, despite that no change was observed in the detergent resistant fraction after BafA1 treatment, IgK was clearly increased in response to HCQ. Further, the level of IgK in the medium fraction was also clearly increased after autophagy inhibition by both BafA1 and HCQ. Also, the lipidated form of LC3B was enriched in the medium fraction after inhibition of autophagy.

In order to verify that the differences observed between the samples in the protein-fraction blot was not due a different level of autophagy inhibition, a total protein assay was performed in parallel with the protein-fraction assay (Figure 27B). The increase in the lipidated form of LC3B, which is enriched on the autophagosomal membrane, was equal after BafA1 and HCQ treatment indicating that both BafA1 and HCQ clearly inhibited autophagy in these cells to the same degree. As shown in Figure 27C, the autophagy inhibitors did not cause much cell death thus excluding that the proteins located in the medium fraction was due to cell death. Since HCQ is a clinically approved autophagy inhibitor and no great differences was observed between the different concentrations tested, HCQ (40 μM) was chosen as the autophagy inhibitor in further experiments.

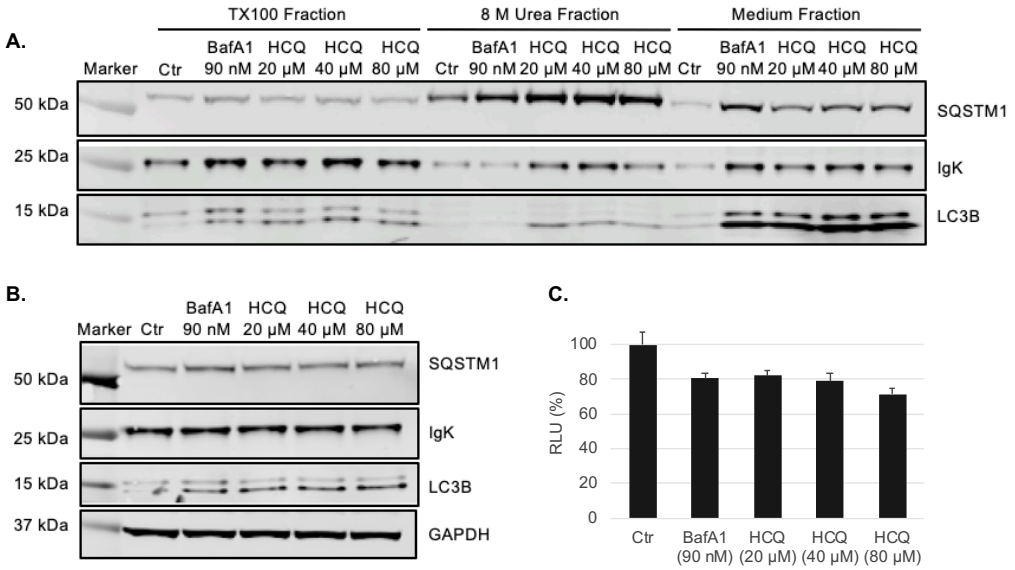

***Figure 27**: **Autophagy inhibition and protein secretion in INA-6 cells.** INA-6 cells were treated with bafilomycin A1 (BafA1) (90 nM) and hydroxychloroquine (HCQ) (20-80 µM) for 4 h. **A.** 9 million cells per condition were harvested and separated into detergent soluble (TX100) fraction, detergent resistant (8 M Urea) fraction and medium fraction 3.8 Protein-fraction protocol. After protein separation by gel electrophoresis, sequestosome 1 (SQSTM1)-, immunoglobulin kappa light chain (IgK)- and LC3B-levels were detected by immunoblotting. Since total sample volume were analyzed, for detergent resistant and medium fraction, no loading control was used. **B.** Total protein lysates (2 million cells/condition) were made using 8 M Urea lysis buffer before loading 60 µg protein onto gel. After protein separation by gel electrophoresis, SQSTM1-, IgK- and LC3B-levels were detected by immunoblotting. GAPDH was also detected as a loading control. **C.** After the 4 h incubation, aliquots of the INA-6 cells to be used for protein fractioning were seeded (30 000 cells/well) with triplicates per condition and analyzed using CellTiter Glo® assay. The measured bioluminescence was calculated relative to the control samples (Ctr) and are given as relative luciferase units (RLU) (%). This assay was performed once, and the standard deviations are calculated between the triplicates per condition.*

To sum up, dense structures, most probably aggregated protein structures containing both SQSTM1 and IgK, increased upon autophagy inhibition and some of these structures were released from the cells and identified extracellularly in the cell media.

4.8.2 Exploring combinatory effects of PIs and HCQ on protein secretion

Earlier findings in the myeloma group has shown that BafA1 stimulation induced a greater release of proteins in combination with PIs than alone (Appendix 8.7A). It was therefore of interest to study the combinatory effects of HCQ and PIs and if the combination would induce a greater release of proteins than HCQ alone, as previously observed with BafA1. For this assay we used a high PI drug concentration (100 nM) in order to be somewhat certain that the proteasomes had been affected in the short time of stimulation (4 h).

When INA-6 cells were stimulated with the PIs or HCQ alone, there was a clear accumulation of both SQSTM1 and IgK in the detergent resistant fraction. However, the combination of PIs

and HCQ seemed to cause a further accumulation of SQSTM1 and IgK in this fraction (Figure 28A). Also, SQSTM1 was identified in the medium when stimulated with HCQ, although no further increase was seen when in combination with PIs. Interestingly, IgK seemed to be additionally increased in the medium fraction when combining PIs and HCQ indicating more IgK to be released when inhibiting both the cells proteasomal and lysosomal degradation systems. This additional release of IgK-positive structures was observed despite any large difference in cell death between cells treated with HCQ alone or HCQ in combination with PIs (Figure 28B). The lipidated form of LC3B increased in HCQ stimulated cells in all fractions but did not seem to further increase when in combination with PIs.

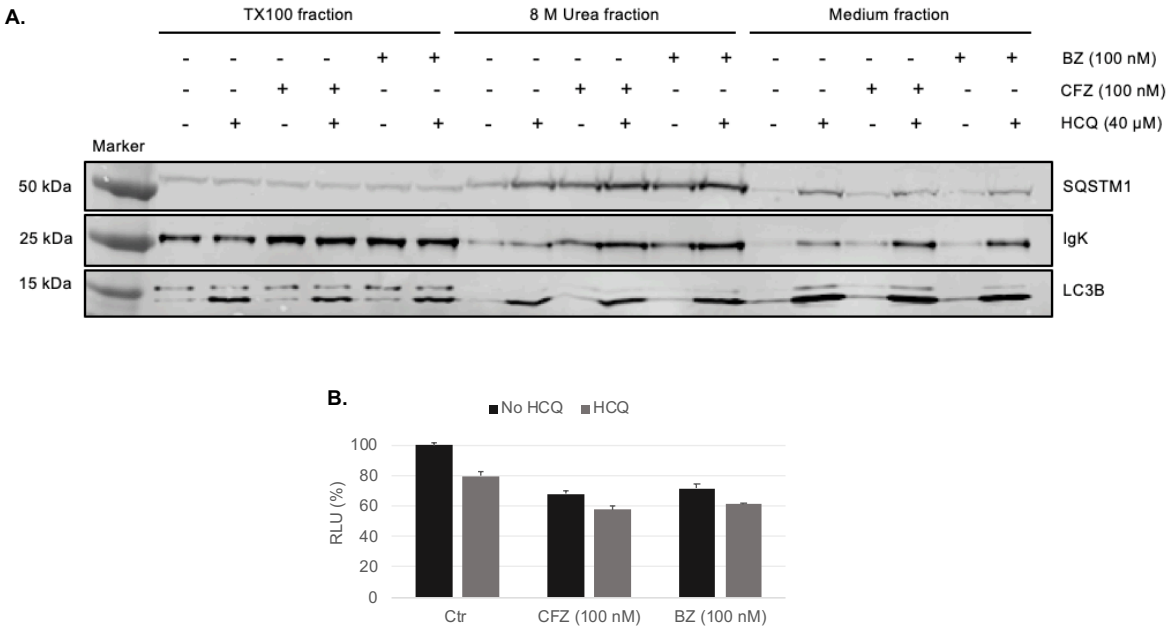

Figure 28: Protein aggregation and secretion of sequestosome 1 (SQSTM1), immunoglobulin kappa light chain (IgK) and LC3B upon concomitant proteasome inhibitor (PI) and autophagy inhibition in INA-6. *INA-6 cells were treated with carfilzomib (CFZ) (100 nM) and bortezomib (BZ) (100 nM) with and without hydroxychloroquine (HCQ) (40 µM) for 4 h.* ***A.*** *9 million cells per condition were harvested and the proteins separated into detergent soluble (TX100) fraction, detergent resistant (8 M Urea) fraction and medium fraction (3.8 Protein-fraction protocol). After protein separation by gel electrophoresis, SQSTM1-, IgK- and LC3B-levels were detected by immunoblotting. Since total sample volume were analyzed, for detergent resistant and medium fraction, no loading control was used.* ***B.*** *CellTiter® Glo assay of aliquots (30 000 cells/well) from when the samples for protein-fraction protocol was harvested. Seeded out triplicates per condition. The measured bioluminescence was calculated relative to the control samples (Ctr) and are given as relative luciferase units (RLU) (%). These results are representative of two individual experiments.*

In summary, inhibiting both the cells proteasomal and lysosomal degradation system seemed to cause further accumulation of both SQSTM1 and IgK in dense, detergent resistant, structures compared to inhibiting only one of the protein degradation pathways. Interestingly, more IgK-positive structures was identified in the cell media of cells stimulated with PIs in combination with HCQ than alone. However, no further increase in secretion of SQSTM1

was observed after combinatory treatment. Based on this result we cannot state a role of SQSTM1 in the secretion of IgK.

4.8.3 Effect of autophagy inhibition on protein secretion in INA-6 IgK KO clones

As our results were conflicting regarding whether SQSTM1 plays a role in IgK secretion, we wanted to study this using another approach. It was therefore investigated if the levels of SQSTM1 detected in the medium fraction would be less prominent in cells expressing lower levels of IgK upon autophagy inhibition, this time by HCQ. In other words, it was speculated whether a lower expression level of IgK, would cause less secretion of aggregated structures containing SQSTM1. We therefore used the INA-6 IgK KO cells, which we previously have shown to produce a truncated IgK and only 25% of the normal IgK amount. Due to the large quantity of samples that would be obtained if all the IgK KO cell clones were to be assessed, only two of the IgK KO cell clones were chosen for this assay (IgK KO 3 and IgK KO 5) along with the two IgK control clones and regular INA-6 cells. The two IgK KO clones were chosen based on the difference between them observed in the PI drug sensitivity assay, with one being less sensitive (IgK KO 5) and the other similar to the IgK controls (IgK KO 3) (Figure 22).

Figure 29 shows that there were not any lower levels of SQSTM1 in the medium fraction of the IgK KO cell clones, thus not in conformity with our theory of a SQSTM1 dependent IgK release. This was not due to HCQ not affecting the cells as the level of lipidated LC3B clearly accumulated upon HCQ stimulation, proving that autophagy was inhibited. IgK KO 3 and IgK KO 5 seemed to respond fairly similar, as expected, same as for the controls. As shown in Figure 29C, the autophagy inhibition did not cause much cell death thus excluding that the proteins located in the medium fraction was due to cell death.

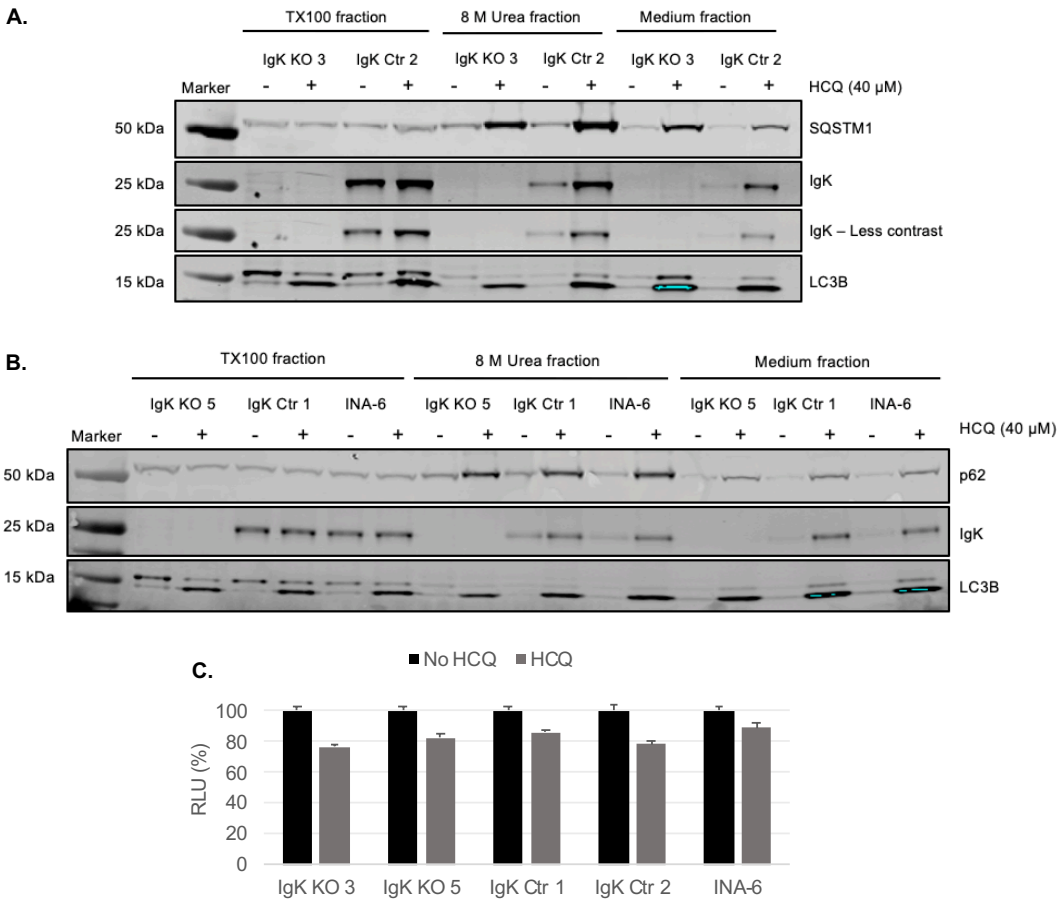

Figure 29: Protein secretion of sequestosome 1 (SQSTM1) upon autophagy inhibition in INA-6 immunoglobulin kappa light chain (IgK) knockout (KO) cell clones and controls. *INA-6 and INA-6 IgK KO cell clones and controls were stimulated with hydroxychloroquine (HCQ) (40 µM) for 4 h.* ***A.*** *and* ***B.*** *9 million cells per condition were harvested and the proteins separated into detergent soluble (TX100) fraction, detergent resistant (8 M Urea) fraction and medium fraction 3.8 Protein-fraction protocol. After protein separation by gel electrophoresis, SQSTM1-, IgK- and LC3B-levels were detected by immunoblotting. Since total sample volume were analyzed, for detergent resistant and medium fraction, no loading control was used.* ***C.*** *CellTiter® Glo assay of aliquots (30 000 cells/well) from when the samples for protein-fraction protocol were harvested. Seeded out triplicates per condition. The measured bioluminescence was calculated relative to the control samples (Ctr) and are given as relative luciferase units (RLU) (%). This assay was performed once, and the standard deviations are calculated between the triplicates per condition.*

In summary, although autophagy inhibition using HCQ showed a clear increase in the autophagy markers, SQSTM1 and LC3B, the results show no or little difference in protein secretion of SQSTM1 between the INA-6 IgK KO clones and IgK controls when inhibiting autophagy. These results, somewhat contradicting the preliminary result, showing reduced IgK secretion of SQSTM1 KO cell lines (Appendix 8.7B), makes the investigation of SQSTM1s role in protein secretion more difficult to evaluate.

4.9 Protein secretion after autophagy inhibition of PI adapted AMO-1 cells

Even though we observed contradicting results on SQSTM1s role in protein secretion in INA-6 cells, we still wanted to investigate if autophagy inhibition would cause release of SQSTM1 and misfolded protein structures, such as Igs, from PI adapted MM cell lines. The PI adapted AMO-1 cell lines were chosen for this, since it had been investigated previously in the myeloma group in the PI adapted INA-6 cell lines (Appendix 8.8). First, an assay testing PI drug sensitivity was performed on the PI adapted AMO-1 cell lines after stimulation with autophagy inhibitors, BafA1 and HCQ, in order to decide which drug and concentration to be used in the protein-fraction assay. It was aimed for a concentration where the cells seemed to respond to these drugs but without causing a lot of cell death.

As shown in Figure 30, only AMO-1-WT and AMO-1-BZR seemed to be affected by the higher concentrations of HCQ (20 µM and 40 µM) with AMO-1-CFZR seemingly unaffected by all of the concentrations tested. Noteworthy, the only drug and concentration to cause a reaction for all three AMO-1 cell lines was 180 nM of BafA1. However, because BafA1 is not clinically approved, it was of more interest to investigate the effect of the clinically approved autophagy inhibitor, HCQ. Thus, it was decided that 40 µM of HCQ would continue to be used.

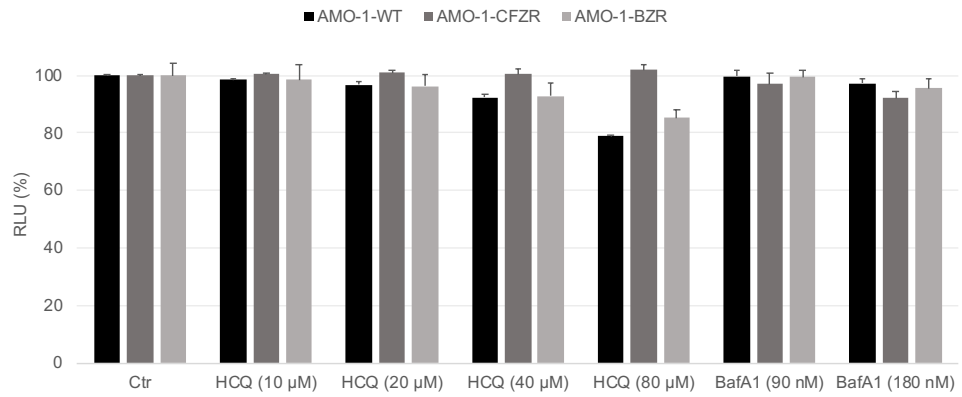

Figure 30: CellTiter® Glo assay of proteasome inhibitor (PI) adapted AMO-1 cell lines*. AMO-1 wild type (WT), AMO-1 carfilzomib resistant (AMO-1-CFZR) and AMO-1 bortezomib resistant (AMO-1-BZR) cells were seeded (30 000 cells/well) and stimulated with increasing concentrations of hydroxychloroquine (HCQ) and bafilomycin A1 (BafA1), with triplicates per condition, for 4 h and analysed using CellTiter Glo® assay. The measured bioluminescence was calculated relative to the control samples (0 nM) and are given as relative luciferase units (RLU) (%). This assay was performed once, and the standard deviations are calculated between the triplicates per condition.*

As expected, SQSTM1 accumulates in both detergent soluble and detergent resistant fractions after HCQ treatment in both AMO-1-WT and the two PI adapted AMO-1 cell lines, most likely representing heavy protein structures like protein aggregates. No accumulation was observed after HCQ in the detergent soluble fraction. However, there was a clear increase of aggregated SQSTM1 in the detergent resistant fraction of AMO-1-WT and AMO-1-BZR cells, most probably representing protein aggregates. Surprisingly, less SQSTM1 was accumulated after HCQ stimulation in AMO-1-CFZR cells compared to both AMO-1-WT and AMO-1-BZR cells. However, in the medium fraction, SQSTM1 was enriched after HCQ stimulation in AMO-1-WT and AMO-1-CFZR cells while no SQSTM1 was detectable from the AMO-1-BZR cells (Figure 31A). Also, LC3B was clearly enriched in the medium fraction in response to HCQ treatment for AMO-1-WT and AMO-1-CFZR cells, while surprisingly no LC3B seemed to be released from AMO-1-BZR cells (Figure 31A).

The IgK protein expression levels were similar to previous results (Figure 21C, D and E). While in the detergent soluble fraction there were not detected any accumulation of IgK in response to HCQ, IgK accumulated in the detergent resistant fraction in AMO-1-WT, suggesting aggregation of the protein into more dense structures that was dissolved after centrifugation. Surprisingly, no IgK were detected in the medium fraction, neither after HCQ treatment, of the cell lines tested.

From the results of total protein extracts, shown in Figure 31B, the lipidated form of LC3B increased more or less to the same extent in the different cell lines after HCQ stimulation, suggesting that autophagy was inhibited equally in these cells. Hence, difference in the level of autophagy inhibition may not explain the differences observed regarding release of IgK and SQSTM1 in these cells. HCQ stimulation did seem to cause a small increase of SQSTM1 expression in AMO-1-WT and AMO-1-BZR, although not in AMO-1-CFZR. However, it was noted that the total expression level of SQSTM1 in this assay seemed to contradict what was seen previously for the basal SQSTM1 protein expression level in these cell lines (Figure 26). The total expression of IgK did not seem to be affected by HCQ in any of the cell lines. HCQ treatment did not cause much cell death thus excluding that amount of proteins located in the medium fraction was due to cell death, as shown in Figure 31C. Regarding IgK detection in this assay (Figure 31A and B), a double band was also here observed as previously seen (Figure 21C).

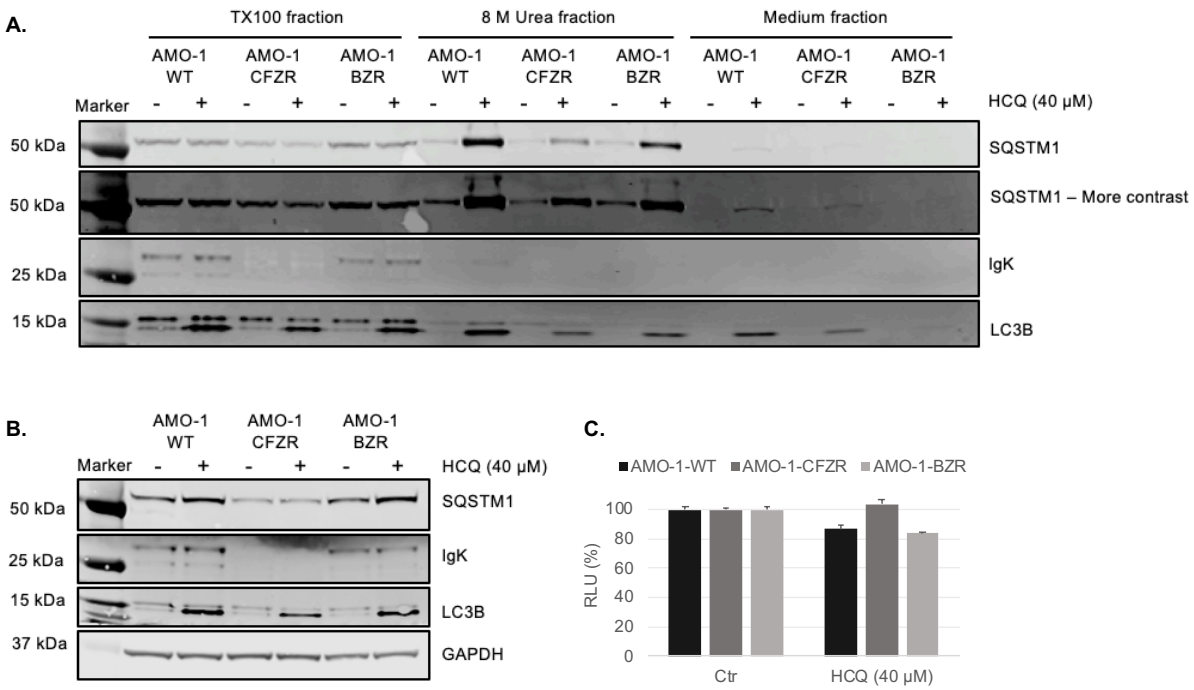

Figure 31: Protein secretion of sequestosome 1 (SQSTM1) and immunoglobulin kappa light chain (IgK) upon autophagy inhibition in proteasome inhibitor (PI) adapted AMO-1 cell lines. *AMO-1 wild type (WT), AMO-1 carfilzomib resistant (AMO-1-CFZR) and AMO-1 bortezomib resistant (AMO-1-BZR) cells were treated with hydroxychloroquine (HCQ) (40 µM) for 4 h.* ***A.*** *9 million cells per condition were harvested and the proteins separated into detergent soluble (TX100) fraction, detergent resistant (8 M Urea) fraction and medium fraction 3.8 Protein-fraction protocol. After protein separation by gel electrophoresis, SQSTM1-, IgK- and LC3B-levels were detected by immunoblotting. Since total sample volume were analyzed, for detergent resistant and medium fraction, no loading control was used.* ***B.*** *Total protein lysates (2 million cells/condition) were made using 8 M Urea lysis buffer before loading 60 µg protein onto gel from each sample. After protein separation by gel electrophoresis, SQSTM1-, IgK- and LC3B-levels were detected by immunoblotting. GAPDH was used as a loading control.* ***C.*** *CellTiter® Glo assay of aliquots (30 000 cells/well) from when the samples for protein-fraction protocol was harvested. Seeded out triplicates per condition. The measured bioluminescence was calculated relative to the control samples (Ctr) and are given as relative luciferase units (RLU) (%). This assay was performed once, and the standard deviations are calculated between the triplicates per condition.*

In conclusion, the increase in expression level of the lipidated form of LC3B indicate that autophagy had been inhibited, however the low IgK levels detected in this experiment and the contradictory results compared to previous results (Figure 26) regarding the levels of expressed SQSTM1 in the cell lines, makes the result difficult to evaluate. Very little protein was found in the medium fraction of PI adapted AMO-1 cell lines, which differs from the results observed in the INA-6 cells (Appendix 8.8).

4.10 Detecting expression levels of MDR1 in PI adapted AMO-1 and INA-6 cells

Further we wanted to investigate other possible PI drug resistance mechanisms. As mentioned in the introduction, overexpression of MDR1 was found to be the most significantly changed

protein by being upregulated in the CFZ adapted MM cells, AMO-1 (1.6.2 MDR1 overexpression) [57]. The PI adapted AMO-1 cell lines used to discover this, are the same AMO-1 cell lines used in this thesis. MDR1 is located in the cell membrane where it pumps foreign substances, such as drugs, out of the cells [56]. Hence, MDR1 might be important in drug resistance mechanisms by reducing CFZ inhibition through drug efflux. Based on this fact, we wanted to test the expression levels of MDR1 in both INA-6 and AMO-1 PI adapted cell lines and their respective control cell lines, using the AMO-1 cell line as a positive control. As expected, MDR1 was clearly upregulated in AMO-1-CFZR cells, as described by Prof. Dr. med. Christoph Driessen and co-workers [57]. However, in the CFZ adapted INA-6 cells only a very weak MDR1 protein band was observed (Figure 32).

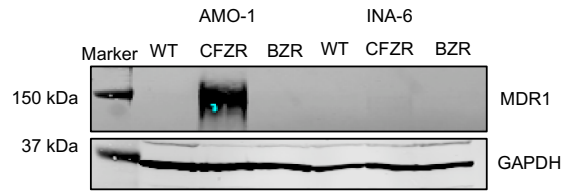

Figure 32: Levels of multidrug resistance protein 1(MDR1) in proteasome inhibitor (PI) adapted INA-6 and AMO-1 cell lines. *2 million cells were lysed in 8 M Urea lysis buffer and 60 µg protein was loaded onto gel. After protein separation using gel electrophoresis, MDR1-levels were detected by immunoblotting and GAPDH was used as a loading control.*

Thus, the results suggest that upregulation of the drug pump, MDR1, is not the main mechanism of resistance in the CFZ adapted INA-6 cell line, and further, that PI adapted MM cell lines acquire different drug resistance mechanisms both between cell lines, but also depending on the PI used.

4.11 Investigation of ER-stress in INA-6 and AMO-1 cells

MM cells are assumed to have a high amount of misfolded proteins, due to the abundant production of Igs. This will in turn induce ER-stress and activate the UPR. When investigating PI resistance mechanisms, it was of interest to include the whether there were changes in ER-stress involved. Assays trying to induce and investigate the role of ER-stress in the INA-6 IgK knockout cells and the PI adapted MM cell lines was performed. However, with the concentrations and timepoints used, no signs of increased ER-stress in response to PIs was observed or there was obtained contradictory results thus making it hard to interpret whether changes in ER-stress is a mechanism involved in PI resistance (Appendix 8.9).

5.0 Discussion

Multiple myeloma (MM) is a rare cancer formed by malignant plasma cells producing abundant amounts of immunoglobulins (Igs). Drugs specifically targeting the proteasome have shown good clinical effects in managing the disease. However, MM patients either display an intrinsic resistance or develop an acquired resistance against the proteasome inhibitors (PIs) over time [18, 46, 54]. Due to the occurrence of relapsed and refractory MM patients, MM is considered an incurable cancer. The mechanisms through which MM cells develop drug resistance towards PIs remain unclear. Identification of specific processes that mediate resistance to PIs will facilitate the development of novel therapies and may improve the survival of MM patients.

5.1 Combining proteasome and autophagy inhibition in Multiple Myeloma therapy

Eukaryotic cells use two different protein degradation systems; the ubiquitin-proteasome system (UPS), that can be targeted by the proteasome inhibitors (PIs), carfilzomib (CFZ) and bortezomib (BZ), and autophagy that can be inhibited by hydroxychloroquine (HCQ). In MM, the overproduction of monoclonal Igs is thought to cause a lot of protein misfolding and formation of protein aggregates. Thus, the good clinical effects observed in MM patients treated with PIs [46], indicate that the MM cells are dependent on a functional protein degradation machinery to avoid stress and cell death.

As treatment with PIs lead to the formation of protein aggregates in MM cells [59, 61], the myeloma group hypothesized that since these protein aggregates normally would have been eliminated through autophagy, a combinatory inhibition of both the proteasomal and autophagic degradation pathway could potentiate the cytotoxic effect of PIs. As they speculated, it was found that HCQ potentiated CFZ-induced cell death, *in vitro*, in several MM cell lines such as ANBL6, JJN3 and INA-6, and primary MM cells [61, 91]. These findings have also been observed *in vivo* when looking at MM grown in mice after proteasome and autophagy inhibition [91]. We thus wanted to investigate this finding in another MM cell line, AMO-1, and as expected the results showed a significant synergistic cytotoxic effect of combining HCQ and CFZ (Figure 20A).

The myeloma group also observed that stimulation with HCQ had a reversible effect on CFZ resistance in CFZ adapted INA-6 cells [61]. Interestingly, this was also observed in the CFZ adapted AMO-1 cells (Figure 20C). Despite that the reversible effects in the CFZ adapted INA-6 cells, after HCQ stimulation, were much stronger than observed here, in the CFZ adapted AMO-1 cells, it was very interesting that the previously observed synergistic cytotoxic effect of combining CFZ with HCQ also was observed in AMO-1 cells. Taken together, these results support that this could be the case for several other MM cell lines and that it also might be important in MM patient therapy.

There was not observed any synergistic effects on cytotoxicity of combining HCQ with BZ in the assays performed in this thesis (Figure 20C and D). This is in line with other *in vitro* studies performed where HCQ seemed to have no effect on the cytotoxicity of BZ and even an antagonistic effect in some MM cell lines [60, 61]. On the other hand, a phase I trial tested the combinatory effect of HCQ and BZ for relapsed or refractory MM patients where it was implied a feasibility for this approach in MM therapy [92]. However, there was some uncertainties whether the minor cytotoxic effects observed was due to BZ alone or the combination of HCQ and BZ. The results obtained, both in this thesis and previously, steers towards the suggestion of an HCQ-CFZ-combination as a possible treatment strategy in MM, and not HCQ-BZ.

Because HCQ is a widely used drug for both malaria and autoimmune diseases, an extensive toxicity-profile has been established, as opposed to an autophagy inhibitor that has not been clinically approved. However, the combination of HCQ with CFZ may cause new toxic effects that should be investigated. In fact, the myeloma group, in cooperation with a medical clinic at St. Olavs hospital, has initiated a phase I clinical trial starting up later this year testing the combination of HCQ and CFZ in MM patients.

5.2 SQSTM1-dependent protein secretion as a novel drug resistance mechanism

Up to 50% of MM patients develop renal failure due to the secretion of Ig light chains from MM cells that can form insoluble casts in the tubular system of the kidneys [15, 16, 18]. This condition is associated with poorer prognosis, thus identifying the process of which Ig light chains are secreted is of great value. MM cells are thought to generate a lot of misfolded Igs that is subsequently tagged by ubiquitin for protein degradation [58-60]. The autophagy

receptor SQSTM1 have the ability to bind such structures and form protein aggregates by self-polymerizing. Inhibition of the proteasome degradation pathway by PI stimulation in MM cell lines, has been shown to cause a compensatory increase in autophagic flux [60]. Over time, this increased need for lysosomal degradation may exceed the lysosomal capacity and thus the cells are in need of another way to dispose these protein aggregates, or the cancer cells are prone to die due to the accumulation of misfolded proteins. Based on this, research in the myeloma group and in this thesis have investigated the possibility of SQSTM1 playing a role in the secretion of the FLCs that can form insoluble casts and cause renal failure in MM patients. Also, a SQSTM1-dependent secretion of FLCs, such as IgK, may represent a novel drug resistance mechanism in MM as a way to dispose these non-functional FLCs and preserve homeostasis in the cancer cells. Both an inhibition of autophagosome-lysosome fusion by BafA1 and HCQ, and an exceed of the lysosomal capacity, will lead to autophagosomes that are not degraded. Thus SQSTM1-dependent protein secretion as a possible drug resistance mechanism could be relevant for both a possible future combinatory treatment, with PIs and HCQ, and long-time treatment with PIs.

As previously observed in the myeloma group (Appendix 8.7A), we found that IgK- and SQSTM1-positive dense protein structures were released from INA-6 cells in response to autophagic inhibition (Figure 27 and Figure 28). Further supporting a role for SQSTM1 in the release of IgK were the previously obtained results observing decreased levels of IgK released from INA-6 SQSTM1 KO cell lines (Appendix 8.7B). However, not supporting the hypothesis are the results obtained here (Figure 28) and previously (Appendix 8.8) in INA-6 cells. Despite observing a further increase of released IgK in the cell media after autophagy inhibition in combination with PIs in these results, it was not observed the same synergistic accumulation for SQSTM1 in the cell media after combinatory stimulation. One explanation for this could be that the cells do not need more SQSTM1 in order to shuttle the accumulating amounts of IgK out of the cells when inhibiting both arms of degradation due to SQSTM1s ability to self-polymerize.

Also contradicting the hypothesis of a SQSTM1-dependent IgK secretion was the observation that INA-6 IgK KO cells did not display any less SQSTM1 released compared to the INA-6 IgK control cell lines and regular INA-6 cells (Figure 29). Since INA-6 SQSTM1 KO cells had decreased levels of IgK in the cell media we hypothesized that the opposite would be seen in the IgK KO cells. However, the level of IgK did not seem to affect the level of SQSTM1 in

the cell media. At the same time, the INA-6 IgK KO cell clones was found to still produce a significant amount of IgK, thus perhaps the IgK levels was not low enough in these cells to cause the presumed decrease of released SQSTM1 in the absence of IgK.

With regard to the number of assays conducted, where most only have been performed once, one can neither confirm nor renounce the hypothesis of a SQSTM1-dependent secretion of IgK from MM cells. However, IgK seem to be released from INA-6 cells after the same time and stimuli as, although not proven to be dependent on, SQSTM1 in all assays even though the amount released between them varied. To further validate the role of SQSTM1 in the release of IgK, it would have been interesting to see whether an overexpression of SQSTM1 in the INA-6 SQSTM1 KO #3-2 clone 3 cell line would have reversed the decrease in IgK secretion observed, thus supporting the hypothesis of an SQSTM1-dependent IgK secretion. Establishment of such cells were unfortunately not successful in the course of this project.

Interestingly, the autophagy machinery, including SQSTM1, have been suggested to be involved in an unconventional secretion of intracellular cargo in other cells, a process known as secretory autophagy [93, 94]. Secretory autophagy was first connected to the unconventional secretion of the inflammatory cytokine IL-1β that lack the peptides needed for conventional secretion [93, 95]. Secretory autophagy has also been linked to the clearing of protein aggregates from cells in neurodegenerative diseases such as Alzheimer's disease and Parkinson disease [93, 96-98]. SQSTM1 and ubiquitin have been detected extracellularly in both α-synuclein inclusion bodies (found in Parkinson disease) and amyloid β peptide aggregates (found in Alzheimer's disease) [96-98]. However, the specific mechanism of which these protein aggregates are released from the cell and the specific role of SQSTM1 remain to be identified.

Future work investigating protein secretion as a possible resistance mechanism should be to obtain more replicas of the assays that have been performed in this thesis using the protein-fraction assay in order to verify the tendencies observed. Thus it would be easier to interpret if the results observed are true and how to proceed with further investigation of these protein-secreting processes. Especially for the MM patients with light chain myeloma, knowing how the FLCs are being transported out of the cells, causing renal failure and poorer prognosis, would be of great meaning.

5.3 Development of PI drug resistance in Multiple Myeloma

In MM, the two arms of protein degradation have shown to be in close interplay, indicated by increased cytotoxicity in INA-6 and AMO-1 cells when stimulating them with CFZ in combination with HCQ. Why inhibition of autophagy renders different effects in combination with CFZ and BZ is not well understood. The PIs used in this thesis both inhibit the proteolytic activity of proteasomes, but in a slightly different way. BZ is a reversible PI and CFZ an irreversible PI, both binding the proteolytic subunit, ß5, of the proteasome. In the investigation of PI adapted MM cell lines in this thesis, the two drugs seem to affect the MM cells differently, causing them to regulate their protein expression levels of mainly IgK and SQSTM1.

Both the INA-6 and AMO-1 cells resistant to BZ had clearly upregulated their level of SQSTM1 expression (Figure 26). However, regarding IgK expression, the BZ adapted INA-6 cells had significantly upregulated their protein level of IgK, while the BZ adapted AMO-1 cells had reduced its IgK expression level, for both modified and unmodified IgK, compared to their control cells (Figure 21). Both the CFZ adapted MM cells, on the other hand, had significantly turned down all of their protein expression level of IgK. Such as for BZ, adaptation to CFZ had caused an upregulation of SQSTM1 in INA-6 cells while the level of SQSTM1 remained unchanged in the CFZ adapted AMO-1 cells (Figure 26).

Why treatment with CFZ and BZ can lead to different expressional changes of proteins that are a central part of the MM cells, and why a single PI can cause a different response between MM cell lines, remains an enigma. As PIs are thought to work by increasing the protein folding burden to cause MM cell death, there is no logical reason as for why a further upregulation of IgK expression would support the drug resistance against BZ in INA-6 cells that already produce abundant amounts of IgK. The complete downregulation of IgK in the CFZ adapted MM cell lines and a reduction of IgK expression in the BZ adapted AMO-1 cells, is a more logic modification because it most likely will relieve the protein folding burden, although the reason why IgK is downregulated is unknown. Since SQSTM1 expression is induced by cellular stress and the presence of protein aggregates, this could explain the clear upregulation of SQSTM1 in PI adapted INA-6 cells and BZ adapted AMO-1 cells. On the other hand, the SQSTM1-level of CFZ adapted AMO-1 cells was so to speak not affected. Although these results may indicate that these MM cells adapt to PIs by changing

the protein level of IgK and SQSTM1, it should be of note that PI resistance may likely be caused by various other mechanisms as previously introduced [53-57, 59, 60, 63].

Others have reported a possible resistance mechanism in the AMO-1 cells resistant to CFZ, by the upregulation of the cell membrane protein, MDR1, that have the ability to pump drugs and other toxins out of the cell [57]. High expression of MDR1 have been identified to have a negative impact in several other pathologies, such as autoimmune diseases and acute myeloid leukaemia, where MDR1 inhibition have shown some promising results in patients [99]. An upregulated MDR1 expression in the CFZ adapted AMO-1 cells was also verified in this thesis, however drug resistance by drug efflux does not seem to account for the BZ resistance in AMO-1 cells and no change in MDR1 levels was observed in PI adapted INA-6 cells (Figure 32).

Taken together, these regulations of protein expression in the PI adapted MM cell lines seem to be different depending on the PI used but also on which PI adapted MM cell line one is investigating, thus providing a possible insight as to how complex the resistance development in MM is. Regarding further investigations, it would have been interesting to investigate if these changes also can be observed in MM primary cells that are resistant towards PIs.

In this thesis, only a few of the suggested possible resistance mechanisms against PIs have been presented [54], as well as the investigation of a novel resistance mechanism regarding protein secretion, but there is still a far way to go in solving the PI resistance puzzle and further research of the field should be of great priority. Proteomics data of both the PI adapted MM cell lines, AMO-1 [100] and INA-6 (obtained in the myeloma group), have been generated, where significant changes in protein expression have been identified in the PI adapted cell lines compared to level of protein expression in the respective WT cell line. Thus, future research could focus on investigating if there are any proteins or signal pathways that are regulated similarly between the two PI adapted MM cell lines that may help find potential processes involved in PI drug resistance.

5.4 Methodology

When studying the results obtained from cytotoxicity and protein expression assays of the PI adapted INA-6 and AMO-1 cell lines, it is important to take into consideration how they were generated. The PI adapted INA-6 cell lines were generated by cultivating the cells in an increasing amount of drug concentration for 6 months to a final dose of 10 nM PI, while the PI adapted AMO-1 cell lines were made by continuous drug exposure for >12 months [100], thus most probably explaining the large difference in PI sensitivity. Also, before conducting the assays the PI adapted INA-6 cell lines had been cultivated without its respective drug (also in previously obtained results in the myeloma group), thus still being resistant, while the PI adapted AMO-1 cell lines had been cultivated with 90 nM of its respective PI. This difference could have affected the results obtained from these cell lines.

The cultivational differences between the two PI adapted MM cell lines, could have had an effect on the results obtained from the investigation of the combinatory effect of HCQ with CFZ. HCQ seemed to reverse most of the CFZ resistance in CFZ adapted INA-6 cells [61] but did not exert the same level of reversing CFZ resistance in the CFZ adapted AMO-1 cells (Figure 20B). Perhaps if the AMO-1-CFZR cells had been cultivated without CFZ, the combinatory effect would have been more similar to the results obtained in CFZ adapted INA-6 cells.

Also to be taken in consideration, the way the two PI adapted MM cell lines modified their protein expression of IgK, SQSTM1 and MDR1 could also have been affected by how they were cultivated beforehand of the assays. MDR1 was clearly upregulated in the CFZ adapted AMO-1 cells but not in the CFZ adapted INA-6 cells. However, AMO-1-CFZR had been cultivated in CFZ before the assay (representing long term CFZ treatment) and INA-6-CFZR had not (representing a more CFZ resistant state), thus MDR1 might have been upregulated in CFZ adapted INA-6 cells also if they have had been cultivated in CFZ beforehand. In light of this, it would have been interesting to cultivate the PI adapted AMO-1 cell lines without their respective PI, for a couple of months or so, to inspect whether it would affect the level of basal expression of IgK, SQSTM1 and MDR1 but also if it would have changed the PI sensitivity and combinatory effect with HCQ.

When detecting IgK in the PI adapted AMO-1 cell lines, it was noticed that IgK was detected in two separate protein bands. IgK is normally detected at 25 kDa, however a larger version of

IgK was observed at approximately 30 kDa (Figure 21 and Figure 31). It seemed like the IgK protein had been modified in some way, perhaps by ubiquitination. Peculiarly, this was also observed in the PI adapted INA-6 cell lines (Appendix 8.8). It was first wondered if this IgK modification could be a response to PI adaptation or drug stimulation, however the modification was also detected in the WT cell lines and also without any drug stimulation. In addition, the cells seemed to either possess more of the modified form of IgK (Figure 21 and Figure 31) or the modified protein was the one most affected by drug stimulation (Appendix 8.8), although the regulation of IgK between them was very similar at a basal level (Figure 21C, D and E). Investigating exactly what type of IgK modification have been made could be performed in future research by attempting to extract both normal and modified IgK proteins band after gel electrophoresis and characterize them by mass spectrometry. Thus, a possible reason as to why these modifications were only detected in the PI adapted and WT MM cell lines may be identified.

When characterizing the five INA-6 IgK KO clones it was detected by sequencing that, despite being picked by single cell cloning, all the five IgK KO clones had gotten the exact same single nucleotide insertion after the *IgK* DNA cutting by Cas9 (Figure 24). Thus, we speculated that, before picking the five single clones, maybe one of the IgK knockouts had gotten some sort of growth advantage which led to a vast majority of cells originating from one single IgK KO clone that was later chosen during single cell cloning. On the other hand, this does not add up with the clear clonal differences detected when investigating PI sensitivity (Figure 22), where IgK KO 5 had a greatly lowered sensitivity towards CFZ and BZ, unlike the other IgK KO clones. The assay investigating *IgK* RNA expression level could not either contribute to an explanation of the clonal differences between the INA-6 IgK KO clones. A possible reason for the clonal difference could be gRNA off-target effects which could have led to the cutting of DNA outside the *IgK* gene, thus causing IgK KO mutant clones and different characteristics between them. However, in order to detect this the whole genome of the INA-6 IgK KO clones would have to be sequenced and it would be as searching for a needle in a haystack. Thus, it would probably be better to try to make new INA-6 IgK KO clones that are cut earlier in the sequence leading to no IgK expression.

All of the assays in this thesis have been performed *in vitro*, allowing us to study MM cell lines and potential therapies as well as a possible novel drug resistance mechanism in a safe and effective manner. However, the findings obtained from such investigations are not

necessarily directly translatable to MM patients. An absence of biokinetics and other influencing factors makes it difficult to deduce *in vitro* results to what one could expect *in vivo*, which is the case for the assays performed in this thesis.

6.0 Conclusions

Although the drug resistance mechanisms against proteasome inhibitors (PIs) in MM have been studied widely for many years, much is still unknown. In this thesis there has been shown that HCQ increased the cytotoxicity of CFZ in AMO-1 cells. In addition, HCQ seemed to somewhat reverse CFZ resistance in CFZ adapted AMO-1 cells. Since this also have been observed in PI adapted INA-6 cells, these results may suggest a possible novel therapy for several MM patients.

Interestingly, CFZ adapted MM cells and BZ adapted AMO-1 cells had considerably turned down their IgK expression level, while INA-6 BZ adapted cells had significantly upregulated its IgK expression. Also, SQSTM1 expression had been clearly upregulated in BZ adapted MM cells and CFZ adapted INA-6 cells. These changes in protein expression suggests that PI adapted MM cell lines could acquire different drug resistance mechanisms both between cell lines, but also depending on the PI used.

Another possible resistance mechanism is the release of misfolded proteins in response to PIs or autophagic inhibition. By analysing the cell media of INA-6 cells, it was observed that both SQSTM1 and IgK was released from the cells in dense protein structures in response to autophagic inhibition. Interestingly, when both UPS and autophagy was inhibited a synergic accumulation of these proteins were observed. Taken together, this suggests that SQSTM1 may be involved in protein secretion, and hence be involved in development of drug resistance. As we could not confirm that the release of IgK was SQSTM1-dependent, further research is needed in investigating protein secretion as a novel resistance mechanism.

In order to investigate the role of IgK in development of drug resistance, a characterization of the five INA-6 IgK KO clones and two IgK control clones was attempted due to clonal differences detected during an PI sensitivity assay. However, no results that could explain the differences in PI sensitivity between the clones was obtained.

As upregulation of drug efflux pump MDR1 had been previously detected in CFZ adapted AMO-1 cells as a possible CFZ resistance mechanism, we speculated if this was the case for the CFZ adapted INA-6 cells, however close to no MDR1 expression was observed, neither in the BZ adapted INA-6 cells.

7.0 References

1. Rollig C, Knop S, Bornhauser M. Multiple myeloma. Lancet (London, England). 2015;385(9983):2197-208. Epub 2014/12/30. doi: 10.1016/s0140-6736(14)60493-1. PubMed PMID: 25540889.
2. Christian Gerecke D, Stephan Fuhrmann D, Strifler S, Martin Schmidt-Hieber PD, Hermann Einsele P, Stefan Knop P. The Diagnosis and Treatment of Multiple Myeloma Dtsch Arztebl Int. 2016;113(27-28):470-6. doi: 10.3238/arztebl.2016.0470. PubMed Central PMCID: PMCPMC4973001.
3. Mateos M-V, Landgren O. MGUS and Smoldering Multiple Myeloma: Diagnosis and Epidemiology In: Roccaro A, Ghobrial I, editors. Plasma cell Dyscrasias. Cancer Treatment and Research 169: Springer, Cham; 2016. p. 3-12.
4. SEER Cancer Stat Facts: Myeloma Bethesda, MD, https://seer.cancer.gov/statfacts/html/mulmy.html National Cancer Institute; 2018.
5. Cancer in Norway 2016 - Cancer incidence, mortality, survival and prevalence in Norway. Oslo: Cancer Registry of Norway: 2017.
6. Manier S, Salem KZ, Park J, Landau DA, Getz G, Ghobrial IM. Genomic complexity of multiple myeloma and its clinical implications. Nature Reviews Clinical Oncology. 2016;14:100. doi: 10.1038/nrclinonc.2016.122.
7. Corre J, Munshi N, Avet-Loiseau H. Genetics of multiple myeloma: another heterogeneity level? Blood. 2015;125(12):1870. doi: 10.1182/blood-2014-10-567370.
8. Magrangeas F, Cormier M-L, Descamps G, Gouy N, Lodé L, Mellerin M-P, et al. Light-chain only multiple myeloma is due to the absence of functional (productive) rearrangement of the IgH gene at the DNA level. Blood. 2004;103(10):3869. doi: 10.1182/blood-2003-07-2501.
9. Rajkumar SV, Kumar S. Multiple Myeloma: Diagnosis and Treatment. Mayo Clinic proceedings. 2016;91(1):101-19. doi: 10.1016/j.mayocp.2015.11.007. PubMed PMID: 26763514.
10. Drug therapies for multiple myeloma https://themmrf.org/multiple-myeloma/treatment-options/standard-treatments/: Multiple Myeloma Research Foundation; [cited 2019 05/09].
11. Stem Cell Transplants https://themmrf.org/multiple-myeloma/treatment-options/stem-cell-transplants/: Multiple Myeloma Research Foundation; [cited 2019 05/09].
12. Quach H, Ritchie D, Stewart AK, Neeson P, Harrison S, Smyth MJ, et al. Mechanism of action of immunomodulatory drugs (IMiDS) in multiple myeloma. Leukemia. 2009;24:22. doi: 10.1038/leu.2009.236.
13. Papadas A, Asimakopoulos F. Mechanisms of Resistance in Multiple Myeloma. In: Mandalà M, Romano E, editors. Mechanisms of Drug Resistance in Cancer Therapy. Cham: Springer International Publishing; 2018. p. 251-88.
14. Abbas AK, Litchman AHH, Pillai S. Antibodies and Antigens Cellular and Molecular Immunology. 9th ed. Philadelphia, PA 19103-2899: Elsevier; 2017. p. 97-115.
15. Caillon H, Attal M, Moreau P, Dejoie T. Multiple Myeloma (MM): Impact of Immunoglobulin Isotype on the Speed of Response. Blood. 2015;126(23):4191.
16. Yadav P, Merz M, Mai EK, Försti A, Jauch A, Goldschmidt H, et al. Cytogenetic aberrations in multiple myeloma are associated with shifts in serum immunoglobulin isotypes distribution and levels. Haematologica. 2018;103(4):e162-e4. doi: 10.3324/haematol.2017.184226. PubMed PMID: 29419430.

17. Rosner MH, Perazella MA. Acute Kidney Injury in Patients with Cancer. New England Journal of Medicine. 2017;376(18):1770-81. doi: 10.1056/NEJMra1613984.
18. Rafae A, Malik MN, Abu Zar M, Durer S, Durer C. An Overview of Light Chain Multiple Myeloma: Clinical Characteristics and Rarities, Management Strategies, and Disease Monitoring. Cureus. 2018;10(8):e3148-e. doi: 10.7759/cureus.3148. PubMed PMID: 30345204.
19. Abbas AK, Litchman AH, Pillai S. Lymphocyte Development and Antigen Rceptor Gene Rearrangement. Cellular and molecular immunology 9th ed. Philadelphia, PA: Elsevier; 2018. p. 179-208
20. Paul WE, Hardy RR. The Immune system, B-Lymphocyte Development. In: Paul WE, editor. Fundamental Immunology 7th ed. Philadelphia, PA 19103 USA: Lippincott Williams & Wilkins 2013. p. 1-22, 215-45.
21. Janeway CA, Travers P, Walport M, Shlomchik M. The Development and Survival of Lymphocytes Immunobiology 5th ed. New York, USA: Garland Publishing; 2001.
22. Delves PJ, Martin SJ, Burton DR, Roitt IM. Development and evolution of the immune response Roitt´s Essential Immunology 13th ed. Chichester, West Sussex: John Wiley & Sons, Ltd; 2017. p. 291-318.
23. Delves PJ, Martin SJ, Burton DR, Roitt IM. Antibodies. Roitt´s Essential Immunology 13th ed. Chichester, West Sussex: John Wiley & Sons, Ltd; 2017. p. 69-96.
24. Paul WE, Max EE, Fugmann S. Immunoglobulins: Molecular Genetics In: Paul WE, editor. Fundamental immunology 7th ed. Philadelphia, PA 19103 USA: Lippincott Williams & Wilkins 2013. p. 150-82.
25. Owen JA, Punt J, Stranford SA. B-cell Development Kuby Immunology. 7th ed: W.H Freeman and Company 2013. p. 329-56.
26. Abbas AK, Litchman AHH, Pillai S. Immunologic Tolerance and Autoimmunity Cellular and Molecular Immunology. 9th ed. Philadelphia, PA 19103-2899: Elsevier 2017. p. 325-50.
27. Abbas AK, Litchman AHH, Pillai S. B Cell Activation and Antibody Production Cellular and Molecular Immunology. 9th ed. Philadelphia, PA 19103-2899: Elsevier; 2017. p. 251-74.
28. Klein U, Dalla-Favera R. Germinal centres: role in B-cell physiology and malignancy. Nature Reviews Immunology. 2008;8:22. doi: 10.1038/nri2217.
29. Tanaka K. The proteasome: overview of structure and functions. Proceedings of the Japan Academy Series B, Physical and biological sciences. 2009;85(1):12-36. Epub 01/14. doi: 10.2183/pjab.85.12. PubMed PMID: 19145068.
30. Lilienbaum A. Relationship between the proteasomal system and autophagy. International journal of biochemistry and molecular biology. 2013;4(1):1-26. PubMed PMID: 23638318.
31. Tooze SA, Yoshimori T. The origin of the autophagosomal membrane. Nature cell biology. 2010;12(9):831-5. Epub 2010/09/03. doi: 10.1038/ncb0910-831. PubMed PMID: 20811355.
32. Glick D, Barth S, Macleod KF. Autophagy: cellular and molecular mechanisms. The Journal of pathology. 2010;221(1):3-12. Epub 2010/03/13. doi: 10.1002/path.2697. PubMed PMID: 20225336; PubMed Central PMCID: PMCPMC2990190.
33. Cotzomi-Ortega I, Aguilar-Alonso P, Reyes-Leyva J, Maycotte P. Autophagy and Its Role in Protein Secretion: Implications for Cancer Therapy. Mediators of Inflammation. 2018;2018:4231591. doi: 10.1155/2018/4231591. PubMed PMID: PMC6304875.
34. Tooze SA, Dikic I. Autophagy Captures the Nobel Prize. Cell. 2016;167(6):1433-5. Epub 2016/12/03. doi: 10.1016/j.cell.2016.11.023. PubMed PMID: 27912049.

35. Ohsumi Y. Molecular dissection of autophagy: two ubiquitin-like systems. Nature Reviews Molecular Cell Biology. 2001;2:211. doi: 10.1038/35056522.
36. Johansen T, Lamark T. Selective autophagy mediated by autophagic adapter proteins. Autophagy. 2011;7(3):279-96. Epub 2010/12/30. PubMed PMID: 21189453; PubMed Central PMCID: PMCPMC3060413.
37. Kabeya Y, Mizushima N, Ueno T, Yamamoto A, Kirisako T, Noda T, et al. LC3, a mammalian homologue of yeast Apg8p, is localized in autophagosome membranes after processing. The EMBO journal. 2000;19(21):5720-8. Epub 2000/11/04. doi: 10.1093/emboj/19.21.5720. PubMed PMID: 11060023; PubMed Central PMCID: PMCPMC305793.
38. Pankiv S, Clausen TH, Lamark T, Brech A, Bruun JA, Outzen H, et al. p62/SQSTM1 binds directly to Atg8/LC3 to facilitate degradation of ubiquitinated protein aggregates by autophagy. The Journal of biological chemistry. 2007;282(33):24131-45. Epub 2007/06/21. doi: 10.1074/jbc.M702824200. PubMed PMID: 17580304.
39. Kim B-W, Kwon DH, Song HK. Structure biology of selective autophagy receptors. BMB reports. 2016;49(2):73-80. doi: 10.5483/BMBRep.2016.49.2.265. PubMed PMID: 26698872.
40. Sanchez-Martin P, Komatsu M. p62/SQSTM1 - steering the cell through health and disease. Journal of cell science. 2018;131(21). Epub 2018/11/07. doi: 10.1242/jcs.222836. PubMed PMID: 30397181.
41. Galluzzi L, Pietrocola F, Bravo-San Pedro JM, Amaravadi RK, Baehrecke EH, Cecconi F, et al. Autophagy in malignant transformation and cancer progression. The EMBO journal. 2015;34(7):856-80. Epub 2015/02/26. doi: 10.15252/embj.201490784. PubMed PMID: 25712477; PubMed Central PMCID: PMCPMC4388596.
42. Yan Y, Jiang K, Liu P, Zhang X, Dong X, Gao J, et al. Bafilomycin A1 induces caspase-independent cell death in hepatocellular carcinoma cells via targeting of autophagy and MAPK pathways. Scientific Reports. 2016;6:37052. doi: 10.1038/srep37052 https://www.nature.com/articles/srep37052#supplementary-information.
43. Mauvezin C, Nagy P, Juhász G, Neufeld TP. Autophagosome–lysosome fusion is independent of V-ATPase-mediated acidification. Nature Communications. 2015;6:7007. doi: 10.1038/ncomms8007 https://www.nature.com/articles/ncomms8007#supplementary-information.
44. Chude CI, Amaravadi RK. Targeting Autophagy in Cancer: Update on Clinical Trials and Novel Inhibitors. International journal of molecular sciences. 2017;18(6):1279. doi: 10.3390/ijms18061279. PubMed PMID: 28621712.
45. Al-Bari MA. Chloroquine analogues in drug discovery: new directions of uses, mechanisms of actions and toxic manifestations from malaria to multifarious diseases. The Journal of antimicrobial chemotherapy. 2015;70(6):1608-21. Epub 2015/02/20. doi: 10.1093/jac/dkv018. PubMed PMID: 25693996.
46. Gandolfi S, Laubach JP, Hideshima T, Chauhan D, Anderson KC, Richardson PG. The proteasome and proteasome inhibitors in multiple myeloma. Cancer and Metastasis Reviews. 2017;36(4):561-84. doi: 10.1007/s10555-017-9707-8.
47. Kane RC, Farrell AT, Sridhara R, Pazdur R. United States Food and Drug Administration approval summary: bortezomib for the treatment of progressive multiple myeloma after one prior therapy. Clinical cancer research : an official journal of the American Association for Cancer Research. 2006;12(10):2955-60. Epub 2006/05/19. doi: 10.1158/1078-0432.ccr-06-0170. PubMed PMID: 16707588.

48. Mohan M, Matin A, Davies FE. Update on the optimal use of bortezomib in the treatment of multiple myeloma. Cancer management and research. 2017;9:51-63. Epub 2017/03/11. doi: 10.2147/cmar.s105163. PubMed PMID: 28280389; PubMed Central PMCID: PMCPMC5338851.
49. Chen D, Frezza M, Schmitt S, Kanwar J, Dou QP. Bortezomib as the first proteasome inhibitor anticancer drug: current status and future perspectives. Current cancer drug targets. 2011;11(3):239-53. PubMed PMID: 21247388.
50. Hungria VTdM, Crusoé EdQ, Bittencourt RI, Maiolino A, Magalhães RJP, Sobrinho JdN, et al. New proteasome inhibitors in the treatment of multiple myeloma. Hematology, Transfusion and Cell Therapy. 2018. doi: https://doi.org/10.1016/j.htct.2018.07.003.
51. Steiner RE, Manasanch EE. Carfilzomib boosted combination therapy for relapsed multiple myeloma. OncoTargets and therapy. 2017;10:895-907. Epub 2017/03/01. doi: 10.2147/ott.s102756. PubMed PMID: 28243125; PubMed Central PMCID: PMCPMC5317297.
52. Chhabra S. Novel Proteasome Inhibitors and Histone Deacetylase Inhibitors: Progress in Myeloma Therapeutics. Pharmaceuticals (Basel, Switzerland). 2017;10(2). Epub 2017/04/12. doi: 10.3390/ph10020040. PubMed PMID: 28398261; PubMed Central PMCID: PMCPMC5490397.
53. Ri M, Iida S, Nakashima T, Miyazaki H, Mori F, Ito A, et al. Bortezomib-resistant myeloma cell lines: a role for mutated PSMB5 in preventing the accumulation of unfolded proteins and fatal ER stress. Leukemia. 2010;24:1506. doi: 10.1038/leu.2010.137 https://www.nature.com/articles/leu2010137#supplementary-information.
54. Robak P, Drozdz I, Szemraj J, Robak T. Drug resistance in multiple myeloma. Cancer Treat Reviews. 2018:199-208. doi: https://doi.org/10.1016/j.ctrv.2019.09.001.
55. Franke NE, Niewerth D, Assaraf YG, van Meerloo J, Vojtekova K, van Zantwijk CH, et al. Impaired bortezomib binding to mutant beta5 subunit of the proteasome is the underlying basis for bortezomib resistance in leukemia cells. Leukemia. 2012;26(4):757-68. Epub 2011/09/24. doi: 10.1038/leu.2011.256. PubMed PMID: 21941364.
56. Yasuhisa K, Shin-ya M, Michinori M, Kazumitsu U. Mechanism of multidrug recognition by MDR1/ABCB1. Cancer Science. 2007;98(9):1303-10. doi: 10.1111/j.1349-7006.2007.00538.x.
57. Besse A, Stolze SC, Rasche L, Weinhold N, Morgan GJ, Kraus M, et al. Carfilzomib resistance due to ABCB1/MDR1 overexpression is overcome by nelfinavir and lopinavir in multiple myeloma. Leukemia. 2018;32(2):391-401. Epub 2017/07/06. doi: 10.1038/leu.2017.212. PubMed PMID: 28676669; PubMed Central PMCID: PMCPMC5808083.
58. Carroll RG, Martin Seamus J. Autophagy in Multiple Myeloma: What Makes You Stronger Can Also Kill You. Cancer Cell. 2013;23(4):425-6. doi: 10.1016/j.ccr.2013.04.001.
59. Milan E, Perini T, Resnati M, Orfanelli U, Oliva L, Raimondi A, et al. A plastic SQSTM1/p62-dependent autophagic reserve maintains proteostasis and determines proteasome inhibitor susceptibility in multiple myeloma cells. Autophagy. 2015;11(7):1161-78. Epub 2015/06/05. doi: 10.1080/15548627.2015.1052928. PubMed PMID: 26043024; PubMed Central PMCID: PMCPMC4590585.
60. Hoang B, Benavides A, Shi Y, Frost P, Lichtenstein A. Effect of autophagy on multiple myeloma cell viability. Molecular Cancer Therapeutics. 2009;8(7):1974-84. doi: 10.1158/1535-7163.Mct-08-1177.
61. Baranowska K, Misund K, Starheim KK, Holien T, Johansson I, Darvekar S, et al. Hydroxychloroquine potentiates carfilzomib toxicity towards myeloma cells. Oncotarget.

2016;7(43):70845-56. doi: 10.18632/oncotarget.12226. PubMed PMID: 27683126; PubMed Central PMCID: PMCPMC5342593.
62. Hoang B, Benavides A, Shi Y, Frost P, Lichtenstein A. Effect of autophagy on multiple myeloma cell viability. Molecular Cancer Therapeutics. 2009;8(7):1974. doi: 10.1158/1535-7163.MCT-08-1177.
63. Aronson LI, Davies FE. DangER: protein ovERload. Targeting protein degradation to treat myeloma. Haematologica. 2012;97(8):1119-30. Epub 2012/05/15. doi: 10.3324/haematol.2012.064923. PubMed PMID: 22580998; PubMed Central PMCID: PMCPMC3409807.
64. Sano R, Reed JC. ER stress-induced cell death mechanisms. Biochimica et biophysica acta. 2013;1833(12):3460-70. Epub 2013/07/16. doi: 10.1016/j.bbamcr.2013.06.028. PubMed PMID: 23850759; PubMed Central PMCID: PMCPMC3834229.
65. Wang M, Law M, Castellano R, Law B. The unfolded protein response as a target for anticancer therapeutics. Critical Reviews in Oncology / Hematology. 2018;127:66-79. doi: https://doi.org/10.1016/j.critrevonc.2018.05.003.
66. Schubert U, Antón LC, Gibbs J, Norbury CC, Yewdell JW, Bennink JR. Rapid degradation of a large fraction of newly synthesized proteins by proteasomes. Nature. 2000;404(6779):770-4. doi: 10.1038/35008096.
67. Flamment M, Hajduch E, Ferre P, Foufelle F. New insights into ER stress-induced insulin resistance. Trends in endocrinology and metabolism: TEM. 2012;23(8):381-90. Epub 2012/07/10. doi: 10.1016/j.tem.2012.06.003. PubMed PMID: 22770719.
68. Yorimitsu T, Nair U, Yang Z, Klionsky DJ. Endoplasmic reticulum stress triggers autophagy. The Journal of biological chemistry. 2006;281(40):30299-304. Epub 2006/08/12. doi: 10.1074/jbc.M607007200. PubMed PMID: 16901900; PubMed Central PMCID: PMCPMC1828866.
69. Bernales S, McDonald KL, Walter P. Autophagy counterbalances endoplasmic reticulum expansion during the unfolded protein response. PLoS biology. 2006;4(12):e423. Epub 2006/11/30. doi: 10.1371/journal.pbio.0040423. PubMed PMID: 17132049; PubMed Central PMCID: PMCPMC1661684.
70. Malach PM. Effects of combinational treatment of proteasome inhibitors and exportin-1 inhibitor on multiple myeloma cells - focusing on the role of SQSTM1: NTNU; 2018.
71. Abhijeet R. The role of immunoglobulin Kappa Ligh Chain on Proteasome Inhibitors cytotoxic effect in Multiple Myeloma cells: NTNU; 2018.
72. Cellosaurus INA-6 (CVCL_5209) ExPASy - the SIB bioinformatics Resource Portal [2018.08.30]. Available from: https://web.expasy.org/cellosaurus/CVCL_5209
73. Cellosaurus AMO1 (CVCL_1806) ExPASy - the SIB bioinformatics Resource Portal [2019.02.17]. Available from: https://web.expasy.org/cellosaurus/CVCL_1806
74. CellTiter-Glo® Luminescent, Cell Viability Assay. https://no.promega.com/-/media/files/resources/protocols/technical-bulletins/0/celltiter-glo-luminescent-cell-viability-assay-protocol.pdf?la=en Promega; 2015.
75. AllPrep DNA/RNA Mini Handbook. https://www.qiagen.com/fr/resources/resourcedetail?id=bbd50261-3b80-4657-ad58-6a5a97b88821&lang=en QIAGEN; 2005.
76. High Capacity RNA-to-cDNA Kit https://www.thermofisher.com/order/catalog/product/4387406: Thermo Fisher Scientific 2018.

77. Zero Blunt PCR Cloning Kit. https://www.thermofisher.com/order/catalog/product/K270020 Invitrogen, Life technologies Corporation; 2013.
78. QIAprep® Spin Miniprep Kit - Quick-Start Protocol. https://www.qiagen.com/no/resources/resourcedetail?id=56b0162c-23b0-473c-9229-12e8b5c8d590&lang=en: QIAGEN®; 2015.
79. What is Real-Time PCR (qPCR)? http://www.bio-rad.com/en-no/applications-technologies/what-real-time-pcr-qpcr?ID=LUSO4W8UU Bio-Rad Laboratories, Inc.; [cited 2019 01/14].
80. TaqMan vs. SYBR Chemistry for Real-Time PCR https://www.thermofisher.com/no/en/home/life-science/pcr/real-time-pcr/real-time-pcr-learning-center/real-time-pcr-basics/taqman-vs-sybr-chemistry-real-time-pcr.html: Thermo Fisher Scientific [cited 2019 01/14].
81. Rodriguez-Lazaro D, Hernandez M. Real-time PCR in Food Science: Introduction. Current issues in molecular biology. 2013;15:25-38. Epub 2013/03/21. PubMed PMID: 23513038.
82. PerfeCTa® SYBR® Green FastMix®, ROX™ https://www.quantabio.com/media/wysiwyg/pdfs/IFU/IFU-050.1%20REV%20A%2095073%20(PerfeCTa%20SYBR%20Green%20FastMix,%20ROX%20PPS)-2016-11%20EFF%2008DEC2016.pdf Quantabio BioSciences, Inc.; 2016.
83. Livak KJ, Schmittgen TD. Analysis of relative gene expression data using real-time quantitative PCR and the 2(-Delta Delta C(T)) Method. Methods (San Diego, Calif). 2001;25(4):402-8. Epub 2002/02/16. doi: 10.1006/meth.2001.1262. PubMed PMID: 11846609.
84. QuikChange Site-Directed Mutagenesis Kit - Instruction Manual https://www.agilent.com/cs/library/usermanuals/public/200518.pdf Agilent Technologies, Inc. ; 2015.
85. Krupka N, Strappe P, Gotz J, Ittner LM. Gateway-compatible lentiviral transfer vectors for ubiquitin promoter driven expression of fluorescent fusion proteins. Plasmid. 2010;63(3):155-60. Epub 2010/02/06. doi: 10.1016/j.plasmid.2010.01.002. PubMed PMID: 20132838.
86. Gateway™ LR Clonase™ II Enzyme Mix https://www.thermofisher.com/order/catalog/product/11791100 Thermo Fisher Scientific 2015.
87. EndoFree Plasmid Purification Handbook. https://www.qiagen.com/us/resources/resourcedetail?id=f8ed5bab-15c3-4211-bfa8-4fbe207aad74&lang=en QIAGEN; 2015.
88. UniProtKB - P03070 (LT_SV40) [Internet]. UniProt. 1986 [cited 04/24/2019].
89. Cellosaurus HEK293T (CVCL_0063) ExPASy - the SIB bioinformatics Resource Portal [cited 2019 04/24]. Available from: https://web.expasy.org/cellosaurus/CVCL_0063.
90. Pantropic Lentiviral Expression Systems https://www.cellbiolabs.com/pantropic-promoterless-lentiviral-expression-system: Cell Biolabs, Inc.; [cited 2019 04/24].
91. Jarauta V, Jaime P, Gonzalo O, de Miguel D, Ramírez-Labrada A, Martínez-Lostao L, et al. Inhibition of autophagy with chloroquine potentiates carfilzomib-induced apoptosis in myeloma cells in vitro and in vivo. Cancer Letters. 2016;382(1):1-10. doi: https://doi.org/10.1016/j.canlet.2016.08.019.

92. Vogl DT, Stadtmauer EA, Tan K-S, Heitjan DF, Davis LE, Pontiggia L, et al. Combined autophagy and proteasome inhibition: a phase 1 trial of hydroxychloroquine and bortezomib in patients with relapsed/refractory myeloma. Autophagy. 2014;10(8):1380-90. Epub 2014/05/20. doi: 10.4161/auto.29264. PubMed PMID: 24991834.
93. Ponpuak M, Mandell MA, Kimura T, Chauhan S, Cleyrat C, Deretic V. Secretory autophagy. Current opinion in cell biology. 2015;35:106-16. Epub 2015/05/17. doi: 10.1016/j.ceb.2015.04.016. PubMed PMID: 25988755.
94. Kimura T, Jia J, Claude-Taupin A, Kumar S, Choi SW, Gu Y, et al. Cellular and molecular mechanism for secretory autophagy. Autophagy. 2017;13(6):1084-5. doi: 10.1080/15548627.2017.1307486.
95. Dupont N, Jiang S, Pilli M, Ornatowski W, Bhattacharya D, Deretic V. Autophagy-based unconventional secretory pathway for extracellular delivery of IL-1β. The EMBO journal. 2011;30(23):4701-11. doi: 10.1038/emboj.2011.398. PubMed PMID: 22068051.
96. Nilsson P, Loganathan K, Sekiguchi M, Matsuba Y, Hui K, Tsubuki S, et al. Aβ Secretion and Plaque Formation Depend on Autophagy. Cell Reports. 2013;5(1):61-9. doi: https://doi.org/10.1016/j.celrep.2013.08.042.
97. Zatloukal K, Stumptner C, Fuchsbichler A, Heid H, Schnoelzer M, Kenner L, et al. p62 Is a common component of cytoplasmic inclusions in protein aggregation diseases. The American journal of pathology. 2002;160(1):255-63. doi: 10.1016/S0002-9440(10)64369-6. PubMed PMID: 11786419.
98. Ejlerskov P, Rasmussen I, Nielsen TT, Bergström A-L, Tohyama Y, Jensen PH, et al. Tubulin polymerization-promoting protein (TPPP/p25α) promotes unconventional secretion of α-synuclein through exophagy by impairing autophagosome-lysosome fusion. The Journal of biological chemistry. 2013;288(24):17313-35. Epub 2013/04/29. doi: 10.1074/jbc.M112.401174. PubMed PMID: 23629650.
99. Bossennec M, Di Roio A, Caux C, Ménétrier-Caux C. MDR1 in immunity: friend or foe? Oncoimmunology. 2018;7(12):e1499388-e. doi: 10.1080/2162402X.2018.1499388. PubMed PMID: 30524890.
100. Soriano GP, Besse L, Li N, Kraus M, Besse A, Meeuwenoord N, et al. Proteasome inhibitor-adapted myeloma cells are largely independent from proteasome activity and show complex proteomic changes, in particular in redox and energy metabolism. Leukemia. 2016;30(11):2198-207. Epub 2016/05/27. doi: 10.1038/leu.2016.102. PubMed PMID: 27118406.
101. Thapsigargin. https://www.sigmaaldrich.com/catalog/product/sigma/t9033?lang=en&region=NO: Sigma Aldrich; 2001.

8.0 Appendix

8.1 8 M Urea Lysis Buffer

8 M Urea LB	Concentration	In buffer	5 000 µl
Urea	60,06 g/mol	8 M	0,24 g
Triton-X	100%	0,50%	2,50 µl
DTT	1 M	0,1 M	50 µl
PI/Complete	25X	1X	20 µl
PIC2	100X	2X	10 µl
PIC3	100X	2X	10 µl
Benzonase	250 U/µl	0,25 U/µl	0,50 µl
MQ water			407,50 µl

Preparation of 8 M Urea Lysis Buffer. A premade mix of Urea (Merck Millipore, 1084890500), Triton-X (Sigma, T8787) and Milli-Q water was added Dithiothreitol (DTT), Complete® Protease Inhibitor (PI; Roche Diagnostics, #11873580001), Phosphatase Inhibitor Cocktail (PIC) 2 and 3 (P5726 and P0044, Sigma) and Benzonase (Sigma Aldrich, #E1014-5KU) dependent on the required total volume. DTT breaks disulfid-bridges between proteins and Benzonase denatures DNA.

8.2 TX100 Lysis Buffer

TX100 LB	Concentration	In buffer	5 000 µl
NP-40	100%	1%	50 µl
Triton-X	100%	0,25%	12,5 µl
Tris-HCl pH 8,0	1 M	0,05 M	250 µl
NaCl	1 M	0,15 M	750 µl
EDTA pH 8,0	0,5 M	0,001 M	10 µl
PI/Complete	25X	1X	200 µl
PIC2	100X	2X	100 µl
PIC3	100X	2X	100 µl
Benzonase	250 U/µl	0,25 U/µl	5 µl
MQ water			3 527,5 µl

Preparation of TX100 Lysis Buffer. A premade mix of Nonidet P40 (NP-40) (VWR, #9036-19-5), Triton-X (Sigma Aldrich, #9002-93-1), Tris-HCl pH 8,0 (VWR, #77-86-1), NaCl (EMSURE®, #7647-14-5), EDTA pH 8,0 (Sigma Aldrich, #E6758) and Milli-Q water was added PI/Complete, PIC2/PIC3 and Benzonase dependent on the required total volume.

8.3 Detection of Immunoglobulin kappa light chain PCR product

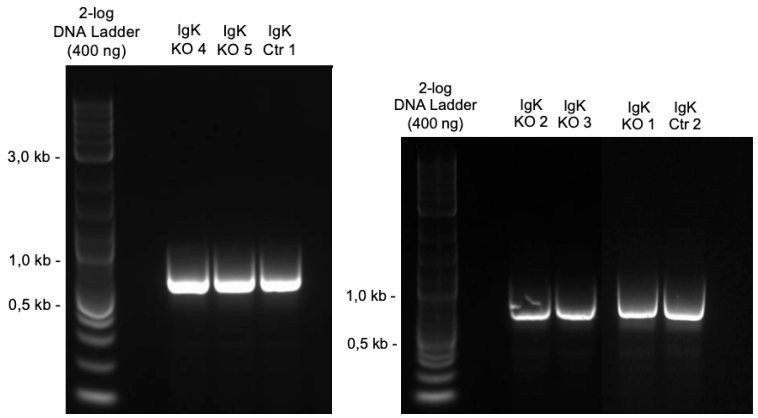

Detection of PCR product to ensure that the correct PCR product had been made. An agarose gel electrophoresis was carried out as described in 3.9 Agarose gel electrophoresis using a 2% agarose gel and a 2-log DNA Ladder. IgK had an expected length of ~700 bp.

8.4 Destination plasmid used in LR reaction to generate SQSTM1-GFP expression plasmid

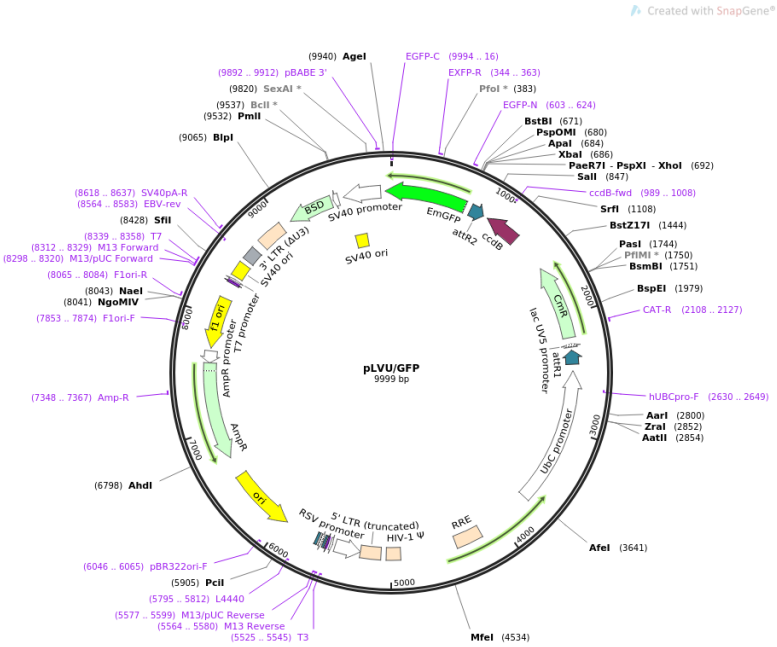

pLVU-GFP (Addgene, #24177) destination vector used together with mutated pENTRY-SQSTM1 in LR reaction to generate the SQSTM1-GFP expression plasmid used in the transduction of SQSTM1 KO #3-2 cells. It was also used to create the GFP control plasmid.

8.5 Additional results on the effects of autophagosomal inhibition in combination with PIs in PI adapted AMO-1 cell lines

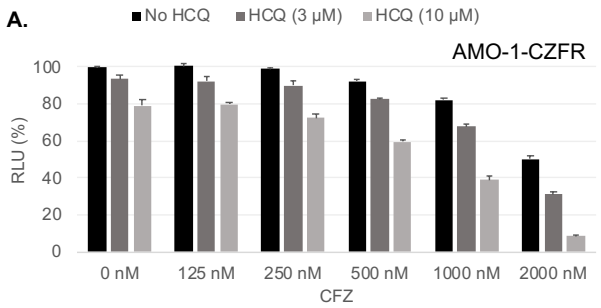

CellTiter® Glo assay of PI adapted AMO-1 cell lines. Cells were seeded (30 000 cells/well) and stimulated with increasing concentrations of CFZ with and without HCQ, with triplicates per condition, before an 24 h incubation. The results are calculated relative to the control sample (0 nM, no HCQ) and are given as RLU (%). **A.** AMO-1-CFZR cell stimulated with 125-2000 nM CFZ with and without HCQ (3 µM and 10 µM).

8.6 Kappa light chain sequence in INA-6 IgK KO clones and IgK controls

A.

ATGGAAGCCCCAGCTCAGCTTCTCTTCCTCCTGCTACTCTGGCTCCCAGATACCACCGGAG
AAATTGTGTTGACACAGTCTCCAGCCACCCTGTCTTTGTCTCCAGGGGAAAGAGCCACCCT
CTCCTGCAGGGCCAGTCAGAGTGTTAGCAGCTTCTTAGCCTGGTACCAACAGAAACCTGGC
CAGGCTCCCAGGCTCCTCATCTATGATGCATCCAACAGGGCCACTGGCATCCCAGGCAGG
TTCAGTGGCAGTGGGTCTGGGACAGACTTCACTCTCACCATCAGCAGCCTAGAGCCTGAAG
ATTTTGCAGTTTATTACTGTCAGCAGCGTAACAACTGGCCTCCGTTCACTTTCGGCCCTGGG
ACCAAAGTGGATATCAAACGAACTGTGGCTGCACCATCTGTCTTCATCTTCCCGCCATCTGA
TGAGCAGTTGAAATCTGGAACTGCCTCTGTTGTGTGCCTGCTGAATAACTTCTATCCCAGAG
AGGCCAAAGTACAGTGGAAGGTGGATAACGCCCTCCAATCGGGTAACTCCCAGGAGAGTG
TCACAGAGCAGGACAGCAAGGACAGCACCTACAGCCTCAGCAGCACCCTGACGCTGAGCA
AAGCAGACTACGAGAAACACAAAGTCTACGCCTGCGAAGTCACCCATCAGGGCCTGAGCT
CGCCCGTCACAAAGAGCTTCAACAGGGGAGAGTGTT**TAG**

B.

ATGGAAGCCCCAGCTCAGCTTCTCTTCCTCCTGCTACTCTGGCTCCCAGATACCACCGGAG
AAATTGTGTTGACACAGTCTCCAGCCACCCTGTCTTTGTCTCCAGGGGAAAGAGCCACCCT
CTCCTGCAGGGCCAGTCAGAGTGTTAGCAGCTTCTTAGCCTGGTACCAACAGAAACCTGGC
CAGGCTCCCAGGCTCCTCATCTATGATGCATCCAACAGGGCCACTGGCATCCCAGGCAGG
TTCAGTGGCAGTGGGTCTGGGACAGACTTCACTCTCACCATCAGCAGCCTAGAGCCTGAAG
ATTTTGCAGTTTATTACTGTCAGCAGCGTAACAACTGGCCTCCGTTCACTTTCGGCCCTGGG
ACCAAAGTGGATATCAAACGAACTGTGGCTGCACCATCTGTCTTCATCTTCCCGCCATCTGA
TGAGCAGTTGAAATCTGGAACTGCCTCTGTTGTGTGCCTGCTGAATAACTTCTATCCCAGAG
AGGCCAAAGTACAGTGGAAGGTGGATAACGCCCTCCAATCGGGG**TAA**CTCCCAGGAGAGT
GTCACAGAGCAGGACAGCAAGGACAGCACCTACAGCCTCAGCAGCACCCTGACGCTGAGC
AAAGCAGACTACGAGAAACACAAAGTCTACGCCTGCGAAGTCACCCATCAGGGCCTGAGCT
CGCCCGTCACAAAGAGCTTCAACAGGGGAGAGTGTTAG

Nucleotide sequence of normal *IgK* gene and *IgK* gene in IgK KO cell clones. The orange represents the *variable* (*VJ*) region and green the *constant* (*C*) region. The underlined nucleotides represent where the gRNA sequence used in the Clustered Regularly Interspaced Short Palindromic Repeats (CRISPR)/Cas9 assay, bound to the DNA. **A.** Normal *IgK* gene sequence based on sequencing from former master's student Roy Abhijeet. This sequence was seen in both IgK control clones. **B.** Altered *IgK* sequence from IgK KO cell clones from

sequencing after Zero Blunt PCR Cloning. The inserted G (marked as red) was seen in all IgK KO cell clones and resulted in an early stop codon.

8.7 Previously obtained results on SQSTM1 dependent free IgK secretion in INA-6 cells

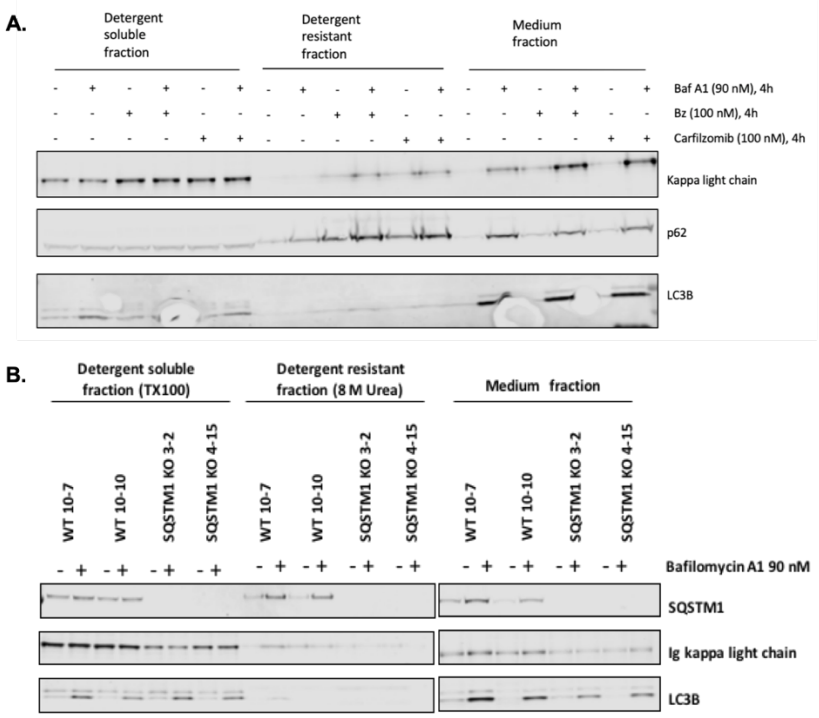

Previously obtained results on SQSTM1/p62 dependent free IgK secretion in INA-6 cell lines. Both assays have used the protein-fraction protocol, as described in Materials and Methods. **A.** INA-6 cell lines treated with CFZ (100 nM) and BZ (100 nM) with and without BafA1 (90 nM) for 4 h. **B.** SQSTM1 KO cell lines and WT cell lines treated with BafA1 (90 nM) for 4 h.

8.8 Preliminary results from the myeloma group on PI adapted INA-6 cells and autophagy inhibition

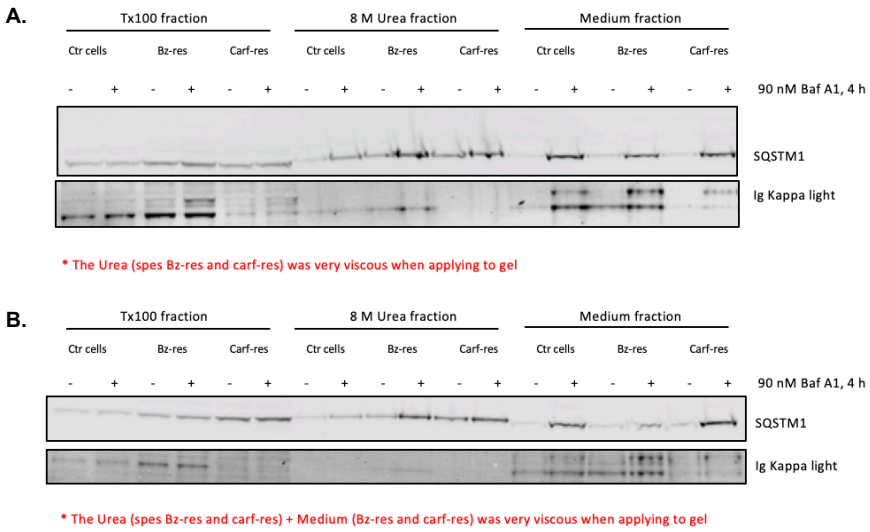

Preliminary results of protein aggregation and secretion in PI adapted INA-6 cell lines. **A.** and **B.** represent two independent replicas of the same assay where INA-6-WT, INA-6-BZR and INA-6-CFZR have been stimulated with BafA1 (90 nM) for 4 h before making different protein fractions using the protein-fraction assay as describes in Materials and Methods.

8.9 ER-stress in Multiple Myeloma cell lines

8.9.1 ER-stress in INA-6 cells after PI drug treatment

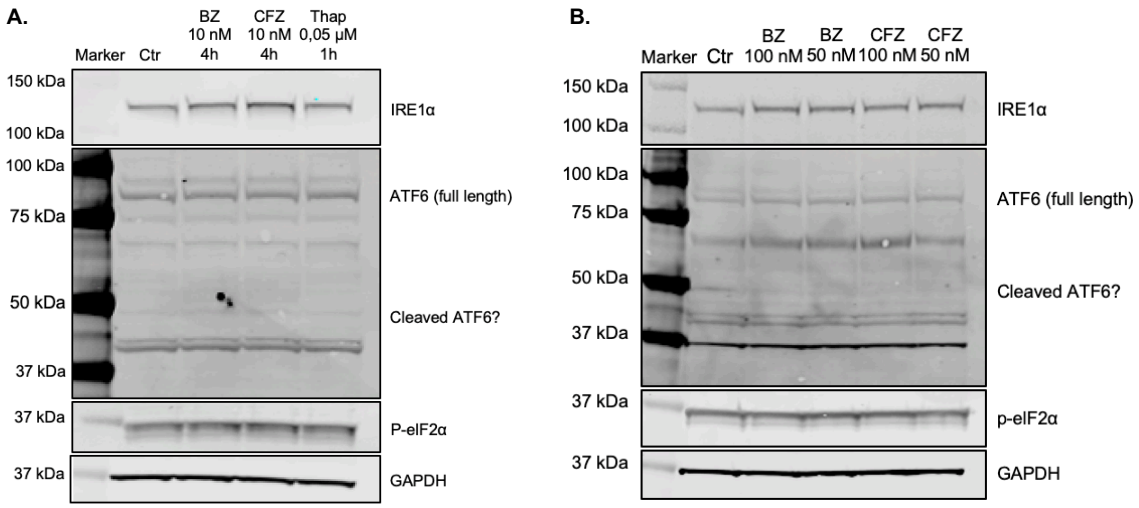

Detection of ER-stress upon PI stimulation in INA-6. INA-6 sells were seeded (2 million cells/condition) and stimulated with **A.** BZ (10 nM), CFZ (10 nM) and Thapsigargin (0,05

μM) for 1 h/4 h and **B.** BZ (100 nM, 50 nM) and CFZ (100 nM, 50 nM) for 4 h. Thapsigargin, which inhibits a calcium pump in the cell membrane hence introducing ER-stress [101] was used as a positive control for ER-stress. When harvested, INA-6 cells were lysed in 8 M Urea lysis buffer before loading 60 μg protein onto the gel. After protein separation by gel electrophoresis, IRE1α-, ATF6-, p-elF2α-levels were detected by immunoblotting. GAPDH was used as a loading control for both membranes.

8.9.2 ER-stress in INA-6 IgK KO clones versus IgK control clones

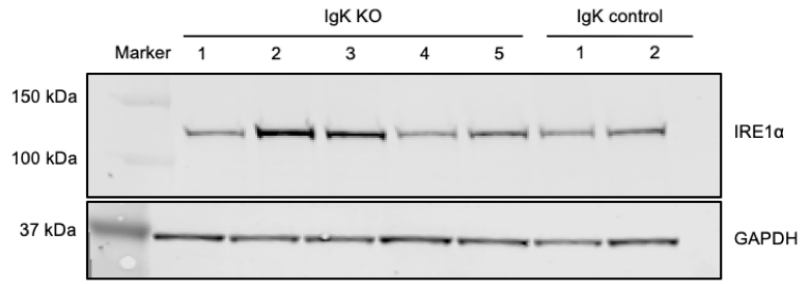

WB of basal protein extracts detecting levels of IRE1α in IgK KO cell clones and IgK controls. Basal cell pellets (1 million cells per pellet) were lysed in 8 M Urea lysis buffer and 35 μg protein was loaded onto gel. After protein separation by gel electrophoresis, levels of IRE1α was detected by immunoblotting. GAPDH was detected as a loading control.

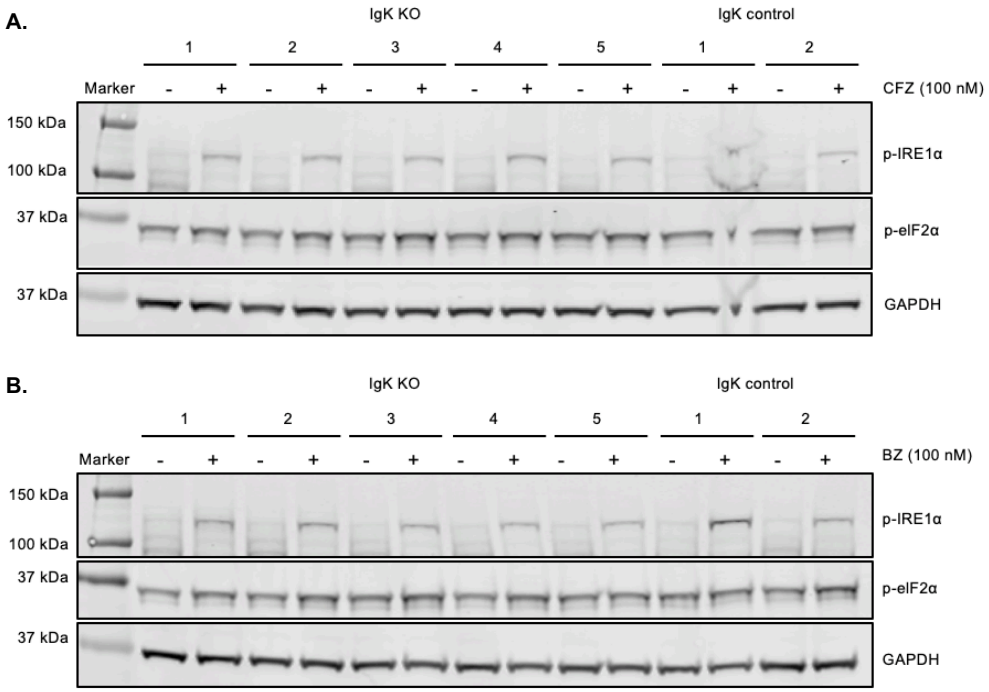

WB of IgK KO INA-6 cell clones and control cell clones and detection of ER-stress upon PI stimulation. The INA-6 IgK KO clones and IgK controls were seeded (2 million cells/condition) and incubated for 4 h after stimulation with **A.** CFZ (100 nM) **B.** BZ (100 nM). When harvested, cells were lysed in 8 M Urea lysis buffer and 60 µg protein was loaded onto the gel. After protein separation by gel electrophoresis, p-IRE1α-, p-elF2α-levels were detected by immunoblotting. GAPDH was detected as a loading control for both membranes.

8.9.3 Basal level detection of ER-stress in PI adapted AMO-1 cell lines

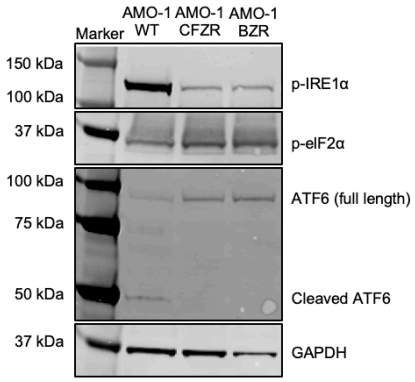

WB of basal protein extracts detecting levels of ER-stress proteins in PI adapted AMO-1 cell lines. Basal cell pellets (2 million cells per pellet) were lysed in TX100 lysis buffer and 60 µg protein was loaded onto gel. After protein separation by gel electrophoresis, p-IRE1α-, p-elF2α- and ATF6-levels were detected by immunoblotting. GAPDH was detected as a loading control. The results are representative of three independent experiments.

Kamilla Isaksen Stortjønnli

NTNU
Norwegian University of
Science and Technology